ANALYSIS OF SHIP HULL AND PLATE VIBRATIONS CAUSED BY WAVE FORCES

by

Fnu Lakitosh

A Dissertation Submitted to the Faculty of

College of Engineering and Computer Science

in Partial Fulfillment of the Requirements for the Degree of

Doctor of Philosophy

Florida Atlantic University

Boca Raton, FL

May 2012

ANALYSIS OF SHIP HULL AND PLATE VIBRATIONS CAUSED

BY WAVE FORCES

by

Fnu Lakitosh

This dissertation was prepared under the direction of the candidate's dissertation advisor, Dr. Palaniswamy Ananthakrishnan, Department of Ocean and Mechanical Engineering, and has been approved by the members of his supervisory committee. It was submitted to the faculty of the College of Engineering and Computer Science and was accepted in partial fulfillment of the requirements for the degree of Doctor of Philosophy.

SUPERVISORY COMMITTEE:

Palaniswamy Ananthakrishnan, Ph.D.
Dissertation Advisor

Manhar Dhanak, Ph.D.

Hassan Mahfuz, Ph.D.

Francisco Presuel-Moreno, Ph.D.

Javad Hashemi, Ph.D.
Chair, Department of Ocean and Mechanical Engineering

Mohammad Ilyas, Ph.D.
Interim Dean, The College of Engineering and Computer Science

Barry T. Rosson, Ph.D
Dean, Graduate College

April 5, 2012
Date

ACKNOWLEDGEMENTS

This work is carried out under the supervision of Dr. Palaniswamy Ananthakrishnan, Associate Professor, Department of Ocean and Mechanical Engineering at Florida Atlantic University. I would like to thank him for his extraordinary guidance, constant support, and ideas based on his deep insight into the field of hydrodynamics. Support of my dissertation committee members, Dr. Manhar Dhanak, Dr. Hassan Mahfuz and Dr. Francisco Presuel-Moreno, and their useful suggestions during the semester meetings are also highly appreciated.

I am grateful to the financial support provided by US Office of Naval Research in the form of research assistantship through the grant N00014-98-1-0151 (Program manager: Ms. Kelly Cooper). I also want to thank the Florida Atlantic University staff for providing me with necessary help to resolve various problems through the years and making sure that I fulfill all my requirements for the degree in a timely manner.

A special thanks to my parents, Balbir Singh and Usha, and my wife, Baishali, for their love and wishes. Without their help and support, this accomplishment wouldn't have been possible. The support and understanding of all my friends are also greatly appreciated.

ABSTRACT

Author: Fnu Lakitosh

Title: Analysis of Ship Hull and Plate Vibrations Caused by Wave Forces

Institution: Florida Atlantic University

Dissertation Advisor: Dr. P. Ananthakrishnan

Degree: Doctor of Philosophy

Year: 2012

In the present dissertation, the hydrodynamic and hydro-elastic characteristics of ship hull and plate vibrations are analyzed using theoretical and numerical methods. The wave forces are determined using a suite of methods which include the Froude-Krylov method for incident wave forces, Wagner's method and ABS rules for the slamming wave force, and numerical methods for nonlinear wave radiation forces. Finite difference methods are developed to determine the wave forced vibrations of ship hull plates which are modeled using a range of plate theories including nonlinear plate theory with and without material damping and orthotropic plate theory for stiffened hull plates. For small amplitude deformation of thin plates, a semi-theoretical superposition method is used to determine the free and forced vibrations. The transient ship hull vibration due to whipping is also analyzed using the finite difference method. Results, in the form of deformations and stress distributions, are obtained for a range of scantling and wave parameters to identify key parameters to consider in ship structural design.

DEDICATION

To *maa, papa* and *biwi*

ANALYSIS OF SHIP HULL AND PLATE VIBRATIONS CAUSED

BY WAVE FORCES

LIST OF TABLES

LIST OF FIGURES

NOMENCLATURE

a	Length of the plate
A	Wave amplitude
A_{22}	Heave added mass
A_w	Water plane area
b	Breadth of the plate
B	Beam of the ship
B_{22}	Heave damping coefficient
B_{cl}	Distance between hull centerlines
B_w	Waterline beam of one hull
$c(t)$	Wetted length (in the Wagner's Theory)
C_b	Block coefficient
D	Modulus of rigidity
D_t	Rigidity of torsion
D_x	Rigidity of the plate in x-direction
D_y	Rigidity of the plate in y-direction
E	Modulus of elasticity
E_{1m}	Unknown corresponds to the first block
E_{2m}	Unknown corresponds to the second block

E_{3m}	Unknown corresponds to the third block
E_{4m}	Unknown corresponds to the fourth block
E_{5m}	Unknown corresponds to the fifth block
E_x	Modulus of elasticity in x-direction
E_y	Modulus of elasticity in y-direction
F	Airy stress function, wave force per unit length
F_{wave}	Total wave force per unit length
g	Gravity acceleration
G(P, Q)	Green's function (for linear wave-body interaction problem)
G_A	Vertical distance of wet-deck from lightest waterline
h	Thickness of the plate
H	Wave height as well as for $(\nu_y D_x + \nu_x D_y + 4D_t)/2$ of plates.
h(t)	Instantaneous depth of immersion in the wedge-entry problem
H_s	Significant wave height
I	Cross-sectional moment of inertia of hull plates and hull girder
k	Wave number
l	Length of stiffeners
L	Length of the ship
L_w	Waterline length
L_{wd}	Length of the wet-deck of catamaran crafts
m	Mass per unit length of the ship hull girder
M_x	Longitudinal plate bending moment

M_{xy}	Plate shearing moment
M_y	Transverse plate bending moment
n	normal at the free/body surface
N_h	Number of hulls
N_x	Internal normal stress in x-direction
N_{xy}	Internal shear stress on the xy plane
N_y	Internal normal stress in y-direction
P, p	pressure
P_{exc}	Wave excitation pressure
$P_{radiation}$	Radiation wave pressure
P_{wd}	Slamming wave pressure on the wet-deck of a twin hull craft.
R	Radius of free-surface paraboloid (in Wagner's theory)
r(P, Q)	Distance between field and source points, P and Q
s	Spacing between plate stiffeners
S(ω)	Sea-state spectrum
S_B	Body boundary (in wave-body interaction formulation)
S_F	Free surface (in wave-body interaction formulation)
S_Σ	Far field boundary (in wave-body interaction formulation)
$S_{\Sigma B}$	Bottom boundary (in wave-body interaction formulation)
t	Time
T_P	Spectrum peak period
$\vec{U}$	Fluid velocity

V	Body velocity
V_r	Relative velocity between body and fluid
V_x	Shear force in x-direction
V_{xy}	Shear force on xy plane
V_y	Shear force in y-direction
$W(x,y)$	Plate deflection
W_1	Deflection of first block (in the superposition theory)
W_2	Deflection of second block (in the superposition theory)
W_3	Deflection of third block (in the superposition theory)
W_4	Deflection of fourth block (in the superposition theory)
W_5	Deflection of fifth block (in the superposition theory)
W_{wd}	Width of wet-deck of a twin-hull ship
Z	Vertical hip-hull response
Z_E	Flexural response of the ship hull
Z_R	Rigid body response
α	Angle of intersection between the hull and the free surface
β	Dead-rise angle of the ship wedge
$\delta(t)$	jet thickness (in the wedge entry problem)
Δ	Ship displacement
$\delta\omega$	wave frequency band width
ε_x	normal strain in x-direction
ε_y	normal strain in y-direction

γ_d	material viscous damping ratio
γ_{xy}	shear strain
η_b	Contact ave profile (in the Wagner's theory)
η	wave elevation; non-dimensional y parameter in plate theory
κ	plate aspect ratio
λ	non-dimensional frequency parameter
λ_{zz}	wave damping per unit length of the ship hull
μ_{zz}	added mass per unit length of the ship hull
ν	Poisson's ratio
ω	wave frequency
φ	Velocity potential
ρ	fluid density
ρ_p	plate mass per unit area
σ_a	Yield stress
σ_x	normal stress in x-direction
σ_y	normal stress in y-direction
τ_{xy}	shear stress
ξ	non-dimensional x parameter in plate theory

1. INTRODUCTION

1.1 Significance and Motivation of the Problem

Large floating platforms and naval ships are often required to operate all the year round, including in high seas. Such structures are prone to both capsizing and structural failure under the action of large amplitude wave forces. Efficient design of the lines to improve the sea-keeping performance of the structural scantlings while avoiding structural failure, require an accurate estimation of wave forces and the determination of ensuing rigid-body as well as flexural response of the platforms and ships to the wave loads in different sea states.

In order to determine the hydro-elastic response of the ships, a thorough knowledge of the hydrodynamic forces is essential, especially impact loading caused by the relative motion between the ship hull and ocean surface waves, extreme case of which is known as wave slamming. In the present study, a special focus is on the wave slamming, which creates a large impact pressure on the hull over a short period of time. Wave slamming can not only cause local deformation of the hull structure but can also set up vibrations along the entire hull structure, known as the whipping effect of the slamming force. A ship or platform in high seas can undergo several wave-slamming cycles, which can cause failure of the hull structure. For example, in the extreme cases wave slamming could damage entire bow sections and these cases of ship structural failure

point to the need for better structural design, which in turn require accurate means and methods to determine the wave loads and structural deformation. The underlying physics of large deformations and motions is usually nonlinear making the analysis extremely difficult. Therefore, ship structural designs have to often depend on experimental findings and empirical data, which for most times tend to be cost-wise prohibitive. The purpose of this dissertation is to contribute to the development of the theoretical models and numerical methods to analyze structural response of ship hull subject to large amplitude wave forces. Results obtained will also shed light on specific mechanisms governing the structural deformations, and therefore possible failure modes, as a function of scantling structural geometry and sea states.

Briefly, in the present research, analytical methods and algorithms are developed based on the beam theory and nonlinear plate theories for structural vibration of ship hull and hull plates subject to wave loading. To determine the slamming wave loads, a suite of methods such as a modified Wagner theory and classification society rules are used. Regular wave loads on the oscillating body are determined using the finite difference algorithm developed by Ananthakrishnan [33]. Nonlinear boundary-integral algorithm has also been discussed to obtain the slamming loads on a ship bow modeled as wedge-entry problem.

1.2 Literature Review

The literature review covers the following areas involved in the present research; namely, (1) determination of the wave forces on stationary bodies, (2) determination of the rigid-body response to waves, (3) structural periodic (springing-types) vibrations of large structures and hull girders subject to the wave loading, (4) determination of the

wave impact loads (slamming) due to the large relative motion between a ship hull and waves and (5) determination of whipping and local plate deformation response due to wave slamming loads. The review covers both classical and recent research works on these topics.

1.2.1 Review of Related Landmark Works

The present dissertation on hydro-elasticity of surface ships deals with two classical subjects, namely wave hydrodynamics and solid/structural mechanics. Some of the problems that have been solved in wave hydrodynamics, decades, if not centuries, ago include (i) Cauchy-Poisson solution to transient wave motions (1815), (ii) Michel's thin ship theory (1898) for wave resistance, (iii) Stokes solution to linear and weakly-nonlinear water wave problems, (iv) Ursell's analysis of wave diffraction over a submerged cylinder, and (v) John's investigation of existence and uniqueness of solutions to linear wave-body interaction problems. The reader may find these topics addressed in, for example, Lamb [1], Stoker [2], Wehausen and Laiton [3], Ursell [4] and Whitham [5]. In water-wave mechanics, including mechanics of submerged or floating bodies, the governing linear potential flow problem, for the most part, is considered to be solved and fully understood. For geometries that are simple, closed form analytical solutions have been obtained using methods such as separation of variables, perturbation techniques, and matched asymptotics. A thorough discussion on these analytical solutions can be found for linear wave body interaction in Wehausen and Laiton [3]. Other methods and theories, such as strip theory (Salvesen et al [6]), Newman-Kelvin approach (Doctors and Beck [7]), and Galerkin methods (Yeung [16]), have also been

developed to obtain the solution for linear wave body interaction. For complex shapes, boundary integral methods based on Greens functions have been developed for analysis, both in the frequency domain (Frank [8] and Yeung [9]) and in the time domain (King [10], Clement [11] and Beck & Liapis [12]). Hard to believe, but a fact, is that there are still some open problems even in the linear analysis of wave-body interactions; for example, it has been recently found that solutions may not exist or may be unique for certain geometries which can support 'trapped waves' which are non-trivial solutions to the homogeneous problem as shown by McIver [13] and [14]. One may find these and other similar works in wave and wave-body hydrodynamics discussed in review articles such as Annual Review of Fluid Mechanics, Wehausen [15] and Yeung [16]; and Advances in Applied Mechanics, Wehausen [17] and Ogilvie [18].

Of particular relevance to the present dissertation, are the numerical methods developed for the analysis of wave-body interactions. For linear inviscid interaction problems, one may use boundary integral methods based on the Greens function (Wehausen and Laiton [3]) in which only boundary involved in the analysis is that of the body (or) boundary integral method based on simple source distribution (Yeung [9] and [16]) analysis of which involves all the boundaries and therefore allows for example irregular sea-bottom boundary. Using these methods a wide range of linear wave-body interaction problems have been solved over the years (eg.,Newman [21]; Yeung [22]).

Next, in the field of solid/structural mechanics, several classical theories and analysis have been carried to determine static and dynamic deformations of elastic bodies. Bernoulli's beam theory, von Karman plate theory, etc are some classic examples which one may find discussed in texts such as Timoshenko [26] and Ventsal

[27] etc. For linear dynamic deformations of simple geometries, analytical solutions have been obtained both for beam and plate deformations (Vladimir [28] and Gorman [29]). In the present dissertation, which also deals with large deformations of ship structural elements resulting from large wave slamming loads, nonlinear plate and beam theories have to be used and numerical methods need to be developed for the solution of the nonlinear equations(as will be discussed in later chapters). Some of the plate and beam theories considered in the present research include (i) thin isotropic plate theory [26] which can be used for small deformation of plates subject to small-amplitude and non-resonant wave loads (ii) orthotropic plate theory [27] used to model stiffened plates, [iii] nonlinear damped plate theory [27] used to study large deformation of ship structural elements resulting from slamming loads. These theories and methods of solution are presented in later chapters of this dissertation.

1.2.2 Review of Recent Works

(i) Wave Hydrodynamics and Computational Methods

In the recent years, much effort has gone in to tackling nonlinear wave-body interactions including viscosity and turbulence. The viscosity effect is of course significant in the resistance problems and, in the case of wave-body oscillation problems, at large Keulegan-Carpenter number (Dean and Dalrymple [19]).

Viscous wave-body interaction problems can be solved by using methods like Reynolds Averaged Navier-Stokes (RANS) [30], large eddy simulation (LES) [31] smooth particle hydrodynamic (SPH) [32], and finite-difference methods based on boundary-fitted coordinates Ananthakrishnan ([20] and [34]) and volume of fluid (VOF)

Nicholas et al ([36] and [37]) techniques . Although these methods provide accurate results for viscous fluid-structure interaction problems, these methods tend to be computationally intensive requiring large amount of time for simulation. This makes them unsuitable in many wave-body interaction problems as the one considered here.

Methods based on inviscid fluid-structure problems are easier to handle and computationally effective, and the cases in which the effect of viscosity is not significant, valuable solution can be provided without much loss in accuracy. In such cases, inviscid solutions match well with the results of viscous solutions (example, Ananthakrishnan [34] and [35]). In this dissertation, the effect of viscosity has been neglected since we deal with inertia dominated wave and wave impact forces. It should be noted that material damping has been taken into consideration in the hydro-elasticity analysis of large deformations and will be discussed in later sections.

For the analysis of fully-nonlinear inviscid wave-body interaction problems, the mixed Eulerian-Lagrangian formulation, which was originally developed by Longuet-Higgins and Cokelet [23], is widely used. In this time-domain method, one integrates the Lagrangian form of the exact free-surface conditions to determine the free-surface elevation and velocity potential on the free surface at each time step. The Greens theorem is then solved for unknown potential (or potential gradients) on the solid (or free) boundaries. This mixed Eulerian-Lagrangian (MEL) approach has been used to solve several fully nonlinear inviscid wave body interactions (Dommermuth [24] and Grosenbaugh [25]). The MEL has also been implemented in field-discretization methods as in Ananthakrishnan [20]. In the present dissertation, the MEL method is used to

determine wave impact loads on the ship hulls. The details of this method are presented in a later chapter.

Wave-Body interaction problems can be broadly categorized into three cases according to the body position and motion: (1) fluid and submerged body interactions, (2) surface piercing body and wave interaction, and (3) transient entry of wedge-type bodies from the atmosphere into the water. As discussed earlier, analytical solutions for linear submerged body problem are available. Numerical methods, such as the boundary element method (BEM) and finite-difference method, have been developed for nonlinear wave-body interaction analysis. For example, Puaut [38] used the BEM with MEL [23] to analyze the linear and nonlinear 3D fluid and submerged-vehicle interaction with free surface effects. In the work of Puaut [38], hydrodynamic coefficients were found for an autonomous underwater vehicle. Similar approach of BEM was used by Olivier [39] to examine stability of near-surface vehicles and by Vimal [40] to solve nonlinear diffraction over a submerged body. In [39], Olivier calculated the hydrodynamic stability coefficients for forced maneuvers of AUV and their effect on the dynamic stability of the body. Vimal used the BEM approach to determine the nonlinear diffraction forces acted on submerged bodies. Koo and Kim [41] studied the hydrodynamics of the dual submerged cylinders in a numerical tank. BEM with MEL approach is used to find the wave deformation and forces on submerged cylinders. It was also found that the effect of the viscosity becomes important only for higher Keulegan-Carpenter (KC) numbers, which confirms theoretical finding based on order-of-magnitude comparison (Dean and Dalrymple [19]).

In problems dealing with surface-piercing bodies, one often encounters problems such as the singularity of the solution at the intersection of the body and the free surface, and the instabilities related to numerical algorithms. In [42] and [43], Koo and Kim studied the interaction of the surface waves with a stationary single body, in [42] and a stationary double body, in [43]. Harmonic wave loads were determined and results showed that effect of nonlinearity and higher order forces become more significant at resonant frequency corresponding to sloshing wave modes and that the gap between the bodies affects the first-order vertical and horizontal forces on the body. Tarafdar and Suzuki [44] used potential based BEM for hydrodynamic analysis of Wigley hulls. Wave interference effects between the hulls, were studied and an optimum range of Froude's number was found for better sea-keeping. In [45], they used the modified Rankine source panel method with linear boundary conditions, to solve wave-body interaction of Series-60 hulls. Wave Profile due to the motion of the ship was studied and the results were promising except at the bow section due to the high nonlinear behavior of the surface wave at the bow.

As an extension of the single hull floating body, multiple body wave interaction also involves some interesting physics. Initial interest in this field was mainly focused on the scattering and radiation of the incident waves due to an array of the fixed/floating cylinders. Various analytical methods have been developed to estimate the drift forces on the fixed/floating array of the cylinders. McIver and Evans [46] developed an analytical method for calculating the potential based on the assumption of plane diffracted waves and sufficiently large gap between the cylinders. Linton and Evan [47] provided a much simpler analytical method based on the work of Spring and Monkmeyer [48], which was

able to capture the far field wave amplitude of the diffracted waves. Later, the focus of the study of multi body wave interaction was on the estimation of the trapped modes of the wave oscillations between the cylinders. Evans and Porter [49], Maniar and Newman [50], Newman [51], and McIver and McIver [52] studied the phenomenon of the trapped waves between the cylinders. It was found that wave of same wave number exhibits a much higher intensity of the load on the large array of cylinders as compared to a single cylinder, which is mainly due to the trapped waves between the cylinders. Forced motion or multihull structure and effect of the trapping modes is discussed in the work of McIver, McIver and Zhang [53], where both asymptotic and numerical methods were used to show the generation of the resonant waves due to forced oscillation of the body. Later, the effect of viscosity was also analyzed by Ananthakrishnan [55]. It was seen that the effect of the viscosity is negligible for the small amplitude of the oscillation but significant difference was noticed in hydrodynamic forces due to high amplitude body oscillation.

Now moving to the review of wedge dropping and slamming problems in the literature, which is more relevant to the dissertation, we find that there are several methods, such as FEM, Wagner's theory [56], BEM and asymptotic method etc., developed to solve the nonlinear problem. Sun and Faltinsen [57] used BEM to analyze the water flow during the water entry of a circular object. Flow near the body surface was solved analytically and the results were compared with Wagner's theory [56] and experimental analysis. Results match well at the initial impact time span but not at later stage, because at the later stage, flow separation and ventilation effects become important which were ignored in the BEM.

Wu et al., in [58], [59], [60] and [61], studied the wedge water entry problem for different cases such as single wedge, twin wedge and asymmetrical wedge water entry problems. In [58], BEM was used to obtain time domain solution of the free surface elevation, pressure distribution and the acceleration of the body. Results were matched with the experimental studies at the initial time but not for large time due to the assumption that aircushion effect is negligible (especially for the smaller dead-rise angles). In [60], they studied the water entry problem for asymmetric wedge using the same approach. It was observed that the wave elevation and pressure distribution was higher on the side with smaller dead-rise angle. The need of applying Kutta condition [62] was also observed due to the formation of negative pressure at the tip of the wedge which could be a possible reason for the air entrapment at the tip of the wedge. In [61], they demonstrated the effect of vertical velocity, horizontal velocity and rotational velocity on the wedge water entry problem. The wave elevations and pressure distributions were determined for different combinations of symmetric and asymmetric wedge drops with vertical, horizontal and rotational velocities.

In [63], Korobkin and Iafrati studied the abrupt (impulse) starting of a floating body's motion, using asymptotic method and the results were compared with the numerical ones. It was observed that this method can be coupled with numerical methods to determine initial and large-time solutions. In Korobkin, Gueret and Malencia [64] Wagner's theory is used to compute the hydrodynamic loads; it is coupled with a finite-element model to determine the structural response to slamming. Even though the effect of the body deformation on the fluid was ignored in this study, results were reasonable for engineering purposes.

To briefly summarize, we have thus far discussed several numerical as well as theoretical methods to tackle the non-linear problems of wave-single body/multi body interaction. In this dissertation, hydrodynamic loads obtained in Ananthakrishnan [55] for multi-hull body oscillations at different frequencies including sloshing resonance frequency, are used. An algorithm, based on BEM [16] along with MEL [23], is also presented to compute the nonlinear hydrodynamic loads for the wedge water entry case. Wagner's theory [56] and ABS rules for the high-speed vehicles [65] are also used to compute the slamming forces. The literature related to the structural mechanics and hydro-elasticity is next discussed in the following section.

(ii) On Structural Mechanics and Hydro-Elastic Analysis of Ship Hull and Plates

This section is mainly focused towards structural mechanics and hydroelasticity of both the plate panels modeled as isotropic and orthotropic plates and the hull girder modeled as a beam. Different plate theories, such as those corresponding to (i) small deflection of isotropic plates, (ii) orthotropic plates and (iii) large nonlinear damped vibrations of plate, have been used to model the hull plate panels. There are several approaches to solve these plate equations, such as analytical methods, finite element method (FEM), finite difference method (FDM) and superposition methods etc. For simply supported plate boundary conditions analytical solutions can be obtained using the method of separation of variables (Timoshenko [26] and Ventsel [27]). For other types of boundary conditions, such as clamped end conditions, it is not straightforward to obtain the analytical solution. For the linear dynamic structural analysis of the isotropic plates with different boundary conditions, the superposition method was introduced by Gorman [66]. Gorman, in [67] and [68], showed the applicability of superposition

method to determine the free vibrations of rectangular plates. Eigenvalues for different modes of vibration were computed which matched satisfactorily with results from other known works. Yu [69] obtained the analytical solution of free and forced vibrations of a cantilever plate by using the superposition method and modal summation. The scheme used to calculate the eigenvalues for vibrations were found to be accurate when matched with the other known results.

Several works have also been carried out on the response of the structure subject to the wave loading. For example, Andrianov ([70] and [71]) obtained linear theoretical solution to floating platform deformed by surface waves. The floating platform was modeled as a thin plate with modified free-surface dynamic condition. The deformations of semi-infinite and circular plates are obtained using a Green's function method. Senjanovic et al. ([72], [73], [74] and [75]) investigated the ship structures using FEM. In [72], free vibration analysis of 1D rectangular barge beam model was carried out for both uncoupled and coupled horizontal-torsional vibrations. Modal coupling of the free vibrations was carried out to investigate the horizontal bending RAO and torsional bending RAO in irregular waves generated by JONSWAP spectra, Lewis [84]. Numerical simulation results matched well with the experimental results, especially at the resonant frequencies. In [73], a similar approach, same as [72], was applied to obtain the free coupled vibration modes of a 7800 TEU container ship vessel. The vessel was considered as an elastic beam and the governing equation for the coupled vibrations was solved by using energy method [27]. Overall, results matched well with the complex 3D FEM model of the same ship. In [74], the beam model was fully coupled with the hydrodynamic model, where the pressure forces were determined using the Bernoulli's

equation [21] based on potential theory. In [75] RAOs of horizontal and torsional bending moment were determined for a range of encounter frequencies. Elastic model was compared with the rigid body model and it was found that elastic model behaved like a rigid-body model at low frequencies (long waves). At high frequency range it was observed that the resonance between the encounter frequency and the dry natural vibration frequency of the model gave higher values of RAOs than that predicted by rigid-body model.

The local analysis of hydroelastcity of plates due to the impact is as important as the global hydroelastic analysis of the ship hull girder. Lu et al [77] used BEM along with FEM to solve fully coupled wedge water entry problem. In this work, hydrodynamic impact pressure is estimated by using BEM with the cutting of jet flow approximation. This pressure was then applied to the FEM model of the V-shaped wedge and the deformation of the wedge was determined at every time step using the beam model. Korbkin [78] solved the similar problem of wedge water entry by using the theoretical approach of generalized Wagner's theory. The response of the wedge to the slamming load was obtained by using FEM beam model and then compared with the results determined using modal analysis. Maki et al [79] used open source CFD library OpenFOAM along with the dynamic FEM to predict the hydro-elastic response of a wedge shaped body. Initially, the wedge was assumed to be rigid in order to determine the slamming pressure; subsequently, taking elasticity of the body into consideration hydroelastic response due to the impact pressure was determined. Luo et al [80] obtained the slamming pressure on the wedge by experimental study. This slamming pressure was applied on a stiffened panel and solved by using design software ANSYS. The study has

provided valuable experimental results which can be used to validate results from theoretical and numerical analyses.

1.3 Scope and Contributions of the Dissertation

From above literature review, that wave mechanics and structural mechanics are classical fields with numerous works carried out on theoretical and practical aspects of ship dynamics and hull vibrations caused by wave forces. Since the exact equations governing the problem of wave and structure interactions problems, particularly in the cases such as capsizing and structural failures, are highly nonlinear and coupled, analyses have to make assumptions of one sort or another to tackle the ship dynamics hydro-elasticity problems. The present work would make similar such assumptions as needed but focus on an accurate determination of ship hull plate vibrations due to wave and slamming forces. Specifically, the present research develops an accurate and robust hydro-elasticity model to solve for both time-harmonic and transient response of ocean structures subject to large wave loads. For determining nonlinear wave forces, for a finite-difference method based on the mixed Eulerian-Lagrangian (MEL) boundary integral method ([17], [18], [19], [35]) is used. The primary rigid-body response is determined by solving equations governing heave motions. Wagner's theory [56] and ABS rules for high speed vehicles [65] are used to determine the wave impact loading caused by the relative motion of a ship with respect to waves. The primary structural elastic response of the hull is determined using the finite difference scheme, in which the hull is taken as a beam with variable moment of inertia and mass along the length of the hull. For determining the ship hull plate vibrations, isotropic plate theory is used for the

case of small structural deformations and governing equations are solved using methods based on the superposition method [66]. For the case of stiffened plate, the orthotropic plate theory is used and governing equations are solved using the finite difference method. Large nonlinear deformation of the plate structures as that might occur in the case of large magnitude wave slamming is also tackled using the finite difference method including material damping. The methods developed in the present dissertation are validated through comparisons with theoretical and experimental results found in the literature. Results, in the form of stresses and deformations, for both hull girder and plate vibrations are then obtained for a range of parameters and examined against yield stress and failure criteria to identify key parameters to consider for hull and structural scantling design.

The main contributions of the dissertation are (i) modeling hydro-elastic deformation of ship hull plates due to both regular and slamming wave forces, (ii) modeling of slamming wave force (iii) determination of springing and whipping of ship hull beam due to wave and impact forces, (iv) development of numerical methods for nonlinear deformation of hull plates including the effects of material damping and plate stiffeners and (v) the results which can be used to determine possible structural failure due to yield by transient slamming loads and fatigue caused by wave forces. As a future endeavor, the present algorithms may be integrated into other models, for example as that used in finite-element models (such as that of Maki et al [79] and Ma [92]), used for ship structural and wave interactions.

2. MATHEMATICAL FORMULATION OF WAVE FORCES

In this chapter, different mathematical formulations are presented to determine wave loads. These formulations are categorized into several methods to tackle different problems of interest in the wave-structure interaction problem. These include the determination of (i) slamming pressure on the water entering wedge, (ii) slamming pressure on the wet-deck of the twin hull ship, (iii) regular/resonant pressure on the surface piercing twin hull under oscillatory motion and (iv) pressure due to incident and body-motion generated radiating waves. In the first two cases, the loading is transient, in the third case, the loading is due to forced oscillation and in case (iv), loading is caused by both the incident and radiating waves.

An algorithm based on 2D Boundary Element Method (BEM) is presented to determine the slamming pressure on the water entering wedge. Wagner's wave slamming theory [56] and ABS rules for high speed ships [65] are used to determine wave impact pressure on the wet-deck of a twin hull ship. Pressure on the bottom of oscillating twin hull is taken from the work of Ananthakrishanan [54]. Apart from the above analyses, Froude-Krylov theory [21] is presented to determine the incident wave forces at different sea states which will then be used for the springing analysis of the ship hull girder and vibration analysis of the hull plates.

2.1 Formulation of the wedge entry problem

A V-shaped wedge is assumed to enter in the initially calm 2D fluid domain with a constant downward velocity $\vec{V} = -V\hat{j}$. The fluid is assumed to be inviscid, incompressible and irrotational. Therefore, the fluid velocity $\vec{U}$ can be described in terms of velocity potential ϕ [21];

$$\vec{U} = \nabla\phi \tag{2.1}$$

With velocity potential in the equation of continuity, one obtains the Laplace equation [21]:

$$\nabla.\vec{U} = \nabla^2\phi = 0 \tag{2.2}$$

The Euler's equation of motion, which is based on the balance of linear momentum of an inviscid fluid, is given by

$$\rho\frac{D\vec{U}}{Dt} = -\rho g - \nabla p \tag{2.3}$$

where, ρ is the fluid density, g is gravity acceleration and p is the pressure.

On integrating Eqn. 2.3 in space and removing the time integral constant by refining the potential, one can obtain the following Euler's integral which is also referred to as unsteady Bernoulli's equation:

$$\rho\left(\frac{\partial\phi}{\partial t} + \frac{1}{2}|\nabla\phi|^2 + gy\right) + p = 0 \tag{2.4}$$

In the present work, the Laplace equation Eqn. 2.2 is solved using the Boundary Element Method (BEM) for the rigid wedge entering in the fluid domain with a constant velocity V. The formulation of BEM requires a domain boundary, which can be part Neumann type and part Dirichlet type of boundaries. Neumann boundary consists of the

body boundary S_B, where the gradient of velocity potential is known or specified and Dirichelt boundary consists of the free surface S_F and far field boundaries, $S_{\sum B}$ and $S_{\sum}$, as shown in Fig. 2.1, on which the velocity potential is given. The mathematical expressions for both these boundaries are given as follows:

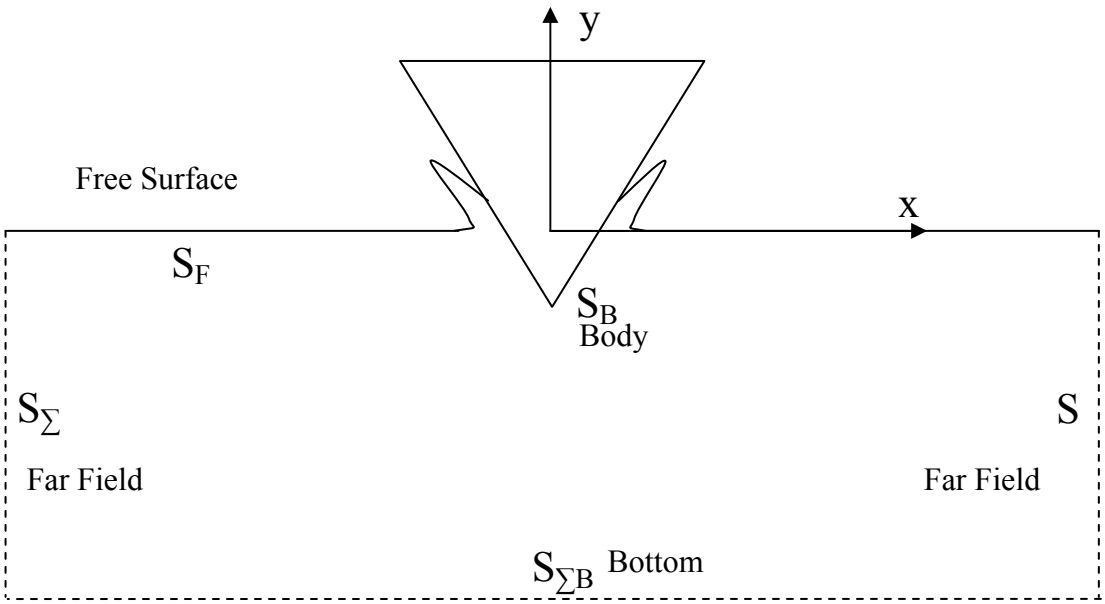

Figure 2.1: V-shaped wedge falling on the initially calm water surface

2.1.1 Boundary Conditions: Neumann's Boundary (Body: S_B)

On the Neumann's boundary S_B, by no-flux or impermeability of the fluid we have

$$\frac{\partial \phi}{\partial n} = V.n \tag{2.5}$$

where, **n** is the normal on the body surface coming out of the fluid domain.

2.1.2 Boundary Conditions: Dirichlet's Boundary (Free Surface: S_F)

The free surface S_F is governed by two conditions: (i) kinematic, and (ii) dynamic boundary conditions. Nonlinear 2D free surface kinematic boundary condition can be

obtained by treating free surface as a material surface, i.e. the water particles do not leave the surface at any time. The free surface dynamic boundary condition is obtained by using the Euler's integral and setting the fluid pressure equal to the atmospheric pressure at the surface. The Lagrangian form of the kinematic and dynamic boundary conditions is given by:

$$\frac{dy}{dt} = \frac{\partial \phi}{\partial y}, \quad \frac{dx}{dt} = \frac{\partial \phi}{\partial x} \tag{2.6}$$

$$\frac{d\phi}{dt} = \frac{1}{2}|\nabla \phi|^2 - gy \tag{2.7}$$

where, $\boldsymbol{\frac{d}{dt}}$ is total derivative and $\boldsymbol{g}$ is the gravity acceleration. The dynamic condition on the free surface shows that the pressure remains constant on the free surface. Thus, the formulation of air-cavity between the body and water surface is not modeled in this formulation.

2.1.3 Boundary Conditions: Dirichlet's Boundaries (Bottom/Far-field: $S_{\sum B}$ and $S_{\sum}$)

Bottom and far-field boundaries are kept at sufficiently large distance from the body so the flow may be negligible during the entire time duration of simulation. Therefore, the boundary condition applied on far field $S_{\sum B}$ and $S_{\sum}$ is given as:

$$\phi = 0 \tag{2.8}$$

2.2 Boundary Element Method

Defining the domain boundary conditions, Laplace equation can be solved using the Boundary Element Method (BEM). The solution method is based on the Green's second identity by which the potential at any field point *P* on a surface is written as;

$$\alpha\phi(P) = \int_S \phi(Q)\frac{\partial G(P,Q)}{\partial n_Q} dS_Q - \int_S G(P,Q)\frac{\partial \phi(Q)}{\partial n_Q} dS_Q \tag{2.9}$$

where, *G(P,Q)=ln(r(P,Q))*. *r(P,Q)* is the distance between field point *P* and a source point *Q*. The velocity potential is computed on the free surface through integration of the dynamic condition and the open boundary $\phi = 0$. The normal gradient of the potential is known on the body surface based on the "no flux" condition. Singularity occurs when field point *P* coincides with the source point *Q* and this singularity can be excluded by a small region. In the limit of the small excluded region vanishing, there is a finite contribution for "dipole" term (refer to Newman [21] for details) and trivial contribution from the source term. In the final form, the Green's theorem can be written as

$$\alpha\phi(P) = \int_{S_B} \phi(Q)\frac{\partial G(P,Q)}{\partial n_Q} dS_{BQ} + \int_{S_F} \phi(Q)\frac{\partial G(P,Q)}{\partial n_Q} dS_{FQ} + \tag{2.10}$$

$$\int_{S_\Sigma} \phi(Q)\frac{\partial G(P,Q)}{\partial n_Q} dS_{\Sigma Q} + \int_{S_{\Sigma B}} \phi(Q)\frac{\partial G(P,Q)}{\partial n_Q} dS_{\Sigma BQ} -$$

$$\int_{S_B} G(P,Q)\frac{\partial \phi(Q)}{\partial n_Q} dS_{BQ} - \int_{S_F} G(P,Q)\frac{\partial \phi(Q)}{\partial n_Q} dS_{FQ} -$$

$$\int_{S_\Sigma} G(P,Q)\frac{\partial \phi(Q)}{\partial n_Q} dS_{\Sigma Q} - \int_{S_{\Sigma B}} G(P,Q)\frac{\partial \phi(Q)}{\partial n_Q} dS_{\Sigma BQ}$$

By discritizing the boundary into N elements, integral equation Eqn. 2.10 can be transformed into a set of N algebraic equations, as shown in Eqns. 2.11 and 2.13.

$$\alpha\phi(P) = \sum_{Q=1}^{N} H_{PQ}\phi_Q - \sum_{Q=1}^{N} G_{PQ}\frac{\partial \phi}{\partial n_Q} \tag{2.11}$$

where, H_{PQ} are the coefficients of velocity potential ϕ and G_{PQ} are the coefficients of normal derivative of velocity potential $\frac{\partial \phi}{\partial n}$. Angle α can be taken as π for smooth boundaries but near the impact region, the surface boundary doesn't remain smooth. To overcome this irregularity, Beskos [76] provided a direct calculation of diagonal elements using other elements in the row.

$$H_{PP} = -\sum_{\substack{Q=1 \\ Q \neq P}}^{N} H_{PQ} \tag{2.12}$$

Initially, on the free surface S_F velocity potential ϕ is assumed to be zero and on the far-fields $S_{\sum B}$ & $S_{\sum}$, velocity potential ϕ is always kept zero assuming that the impact generated flow does not reach the far field during the entire time of simulation. Keeping unknown terms on the left side and known terms on the right side, Eqn. 2.11 can be written as;

$$\begin{bmatrix} H^B & -G^F & -G^{\Sigma B+\Sigma} \end{bmatrix} \begin{Bmatrix} \phi_B \\ \frac{\partial \phi}{\partial n_F} \\ \frac{\partial \phi}{\partial n_{\Sigma B+\Sigma}} \end{Bmatrix} = \begin{bmatrix} G^B & -H^F & -H^{\Sigma B+\Sigma} \end{bmatrix} \begin{Bmatrix} \frac{\partial \phi}{\partial n_B} \\ \phi_F \\ \phi_{\Sigma B+\Sigma} \end{Bmatrix} \tag{2.13}$$

Superscripts on the coefficients and subscripts on ϕ and $\frac{\partial \phi}{\partial n}$ correspond to the respective boundaries. Eqn. 2.13 is solved for every time step and free surface is updated by using Mixed Eluerian-Lagrangian (MEL) [23] formulation. The detailed algorithm of MEL is in the following section.

2.2.1 Mixed Eulerian-Lagrangian (MEL) Method

The mixed Eulerian- Lagrangian (MEL) formulation for the solution of nonlinear wave-body interaction problem was introduced by Longuet-Higgins and Cocklet [23].

MEL consists of two steps, (i) Eulerian step and (ii) Lagrangian step. Solving the Laplace equation using BEM Eqn. 2.13 is called the Eulerian step. Time integration of the free-surface conditions to determine the free-surface elevation and the velocity potential on the free surface is referred to as the Lagrangian step of the MEL formulation. This process is repeated to get the advance the solution in time.

2.2.2 Numerical Instabilities and proposed solutions

In implementing the MEL based BEM, one may encounter two types of instabilities, (i) jet formation which is physical, and (ii) the corner instability, occurring at the intersection of the body surface and free surface, because of the mismatch of free-surface and solid-boundary conditions. Other instabilities, such as saw-tooth instability and time integration instability, can be removed easily as compared to the former two main instabilities. Saw-tooth instability can be removed by re-gridding the free surface and time integration instability can be removed by choosing stable time marching scheme (4^{th} order Runge-Kutta) and selecting a proper time-step size.

2.2.2.1 Truncation of the jet

In the wedge water entry problem, a thin jet develops at the intersection of the free surface and the body surface which moves quickly in the upward direction. Numerically, it is extremely difficult to capture the jet because of the rapid increase in the computation domain.

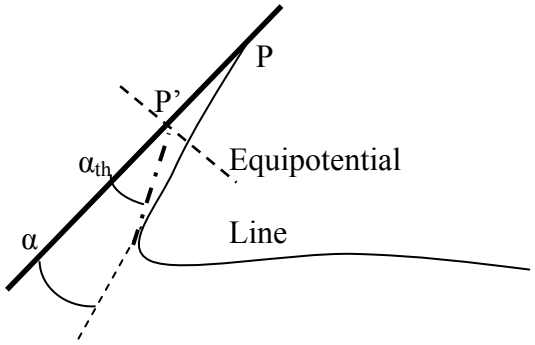

Figure 2.2: Jet cutting model

This cutting model for the jet is based on the theory provided by Kihara [85], which suggests that the interior contact angle between the free surface and the body remains under a threshold value. The value of the threshold angle α_{th} can be taken between $\pi/15$ and $\pi/9$. If the contact angle α drops beyond this limit then a new position of the intersection point P changes to a new position P'. The gradient of velocity potential at new location is known from the body boundary condition and the new velocity potential is determined using the interpolation technique, since it needs to be continuous. An equipotential line, perpendicular to body surface, is assumed to be passing through the old element and new location of intersection point P'. This determines the new velocity potential at P'.

2.2.2.2 Treatment of corner instability

The corner instability occurs due to the surface discontinuity and the confluence of two different boundary conditions (Neumann and Dirichlet) at the intersection point. A double-node technique, e.g. Dommermuth and Yue [24], gives an excellent treatment of this type of discontinuity.

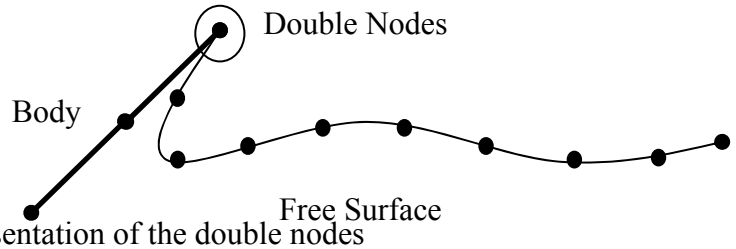

Figure 2.3: Representation of the double nodes

In double node technique, coinciding nodes are treated with their respective boundary conditions. In the system of double node, one node "NB" represents the body element and other "NF" represents the free surface element.

Node related to body element (NB)	ϕ unknown and $\frac{\partial \phi}{\partial n}$ known
Node related to free surface element (NF)	ϕ known and $\frac{\partial \phi}{\partial n}$ unknown

From the above table it can be deduced that there are two unknowns in the double node system. One unknown can be removed by assuming the continuity of the velocity potential that there cannot be jump in the value of ϕ. Hence the velocity potential ϕ at NB is known from the velocity potential ϕ at NF. By taking the above assumption, the collocation of the double node in BEM provides only one equation for one unknown i.e. $\frac{\partial \phi}{\partial n}$ on the free surface.

2.2.2.3 Time stepping and free surface re-gridding

After solving the Laplace equation using BEM, the kinematic and dynamic free surface boundary conditions are integrated numerically. To improve the stability and robustness, 4th order Runge-Kutta scheme has been used to determine free surface's new

position and new velocity potential at every time step. Due to the high flow gradients near the wave body impact region, clustering of the nodes and saw-tooth instability can occur. Continuous re-gridding of the free surface, based on for example cubic-spline method, seems to overcome these instabilities

Apart from the above procedure, it is also necessary to track the intersection point. If not properly handled, the intersection point can go inside the body surface which is not physically possible and lead to the numerical instability of the scheme. Then, the intersection point is forced to move along the tangential line of the body boundary. This and other such fine details of the numerical aspects of the method can be found in [91].

2.2.3 Determination of Pressure

The pressure on the body surface can be determined at each time instant, by using the Bernoulli's equation. The expression for the dynamic pressure on the body surface is given as;

$$\frac{p}{\rho} + \frac{\partial \phi}{\partial t} + \frac{1}{2}|\nabla \phi|^2 + gy = 0 \xrightarrow{yields} \frac{p}{\rho} \tag{2.12}$$

$$= -\left(\frac{\partial \phi}{\partial t} + \frac{1}{2}|\nabla \phi|^2 - gy\right)$$

In the nonlinear analysis, local time derivative of the velocity potential $\frac{\partial \phi}{\partial t}$ does not provide the accurate estimation of the pressure because of the continuous motion and re-gridding of the body surface. Hence, the total time derivative of potential $\frac{d\phi}{dt} = \frac{\partial \phi}{\partial t} + |\nabla \phi|^2$ is required to get the accurate pressure on the body, because total time derivative

follows the fluid particle. On replacing the partial time derivative with the total derivative, Eqn. 2.12 becomes;

$$\frac{p}{\rho} = -\frac{d\phi}{dt} + \frac{1}{2}|\nabla\phi|^2 - gy \tag{2.13}$$

2.3 Wagner's Slamming Model

This section discusses two types of wave slamming, (i) slamming on a water entering wedge, and (ii) wet-deck slamming. Wave slamming loads are different from the regular wave loads, such that in the event of wave slamming, high pressure is localized in small time and space. Hence, the local study of the hull plating behavior becomes important along with the global response of the structure. In this study, the structure is assumed to be rigid while determining the slamming pressure while the elasticity is considered to determine the structural deformation of the plate due to the slamming pressure.

2.3.1 Wedge water entry problem

To determine the pressure on a water entering body with a constant velocity, Wagner's approach has been followed. When a wedge enters in initially calm water, it creates a water rise up and a jet spray along the body and above the water surface.

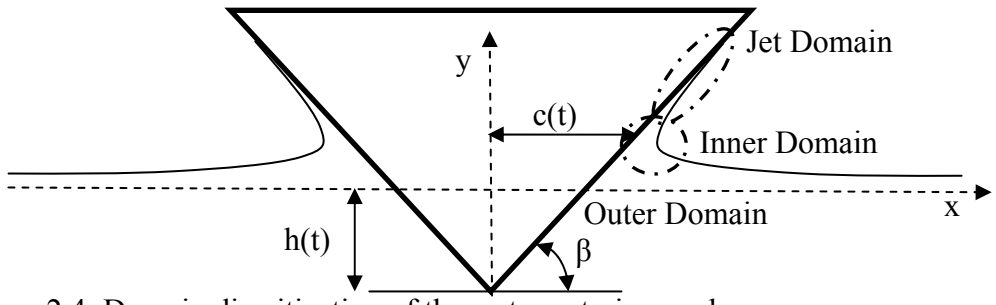

Figure 2.4: Domain discritization of the water entering wedge

The flow is characterized into three domains, (i) outer domain, which is the section of the body below the spray root $x < c(t)$, (ii) inner domain, location where the flow overturns to create a jet, $x \geq c(t)$, and (iii) jet domain, the effect of this domain is neglected because it is observed that it does not provide any significant pressure variation on the body.

For a wedge of dead-rise angle β and a constant water entering velocity *V*, the pressure for outer domain is given by Wagner, which can be found in [54].

$$p_{outer} = \rho V \frac{c(t)}{\sqrt{c(t)^2 - x^2}} \frac{dc(t)}{dt} \tag{2.14}$$

where, $c(t)$ is the half wetted length in x-direction and it can be expressed in terms of water entering velocity *V,* dead-rise angle β and depth of immersion $h(t) = Vt$ as:

$$c(t) = \frac{\pi h(t)}{2tan\beta} \tag{2.15}$$

The inner domain pressure solution is given in Peseux et al [87], which depends on the jet thickness. The expressions for jet thickness and inner domain pressure are as follows:

$$\delta(t) = \frac{\pi V^2 c(t)}{8\dot{c}(t)^2} \tag{2.16}$$

and

$$p_{inner} = \rho \frac{\dot{c}(t)}{2} \left[1 - \left(\frac{1-u}{1+u}\right)^2\right] \tag{2.17}$$

where, $\dot{c}(t)$ is time derivative of $c(t)$ and u is known as the stretching transformation, which can be expressed as;

$$x - c(t) = \frac{\delta(t)}{\pi}(-2\ln u - 4u - u^2 + 5) \tag{2.18}$$

Maximum pressure occurs when $x = c(t)$ i.e. $u = 1$. The matching of both, inner and outer domain, solutions has been carried out by Zhao and Faltinsen [88]. The solution for the common pressure is;

$$p_{common} = \rho \frac{Vc(t)\dot{c}(t)}{\sqrt{2c(t)(c(t) - x)}} \tag{2.19}$$

The final expression of the pressure on rigid body can be written as the combination of inner and outer pressure solution with the exclusion of the common pressure.

$$p_{rigid} = p_{outer} + p_{inner} - p_{common} \tag{2.20}$$

2.3.2 Wet-Deck Slamming

Next, let us consider the slamming pressure on the wet-deck, the cross structure which connects two demi-hulls of a twin hull ship. Frontal area of the wet-deck is more prone to wave slamming, because it has the direct exposure to incoming waves and more downward velocity due to the pitch motion. The procedure to determine the wave slamming forces is based on the Wagner's slamming model with some modifications. In this section, two types of cases of wave/wet-deck interaction are discussed. Fig. 2.5 depicts the phenomenon in which the wave hit the frontal part of the twin hull ship and

Fig. 2.6 illustrates the occurrence of slamming due to relative motion between a plate and wave surface.

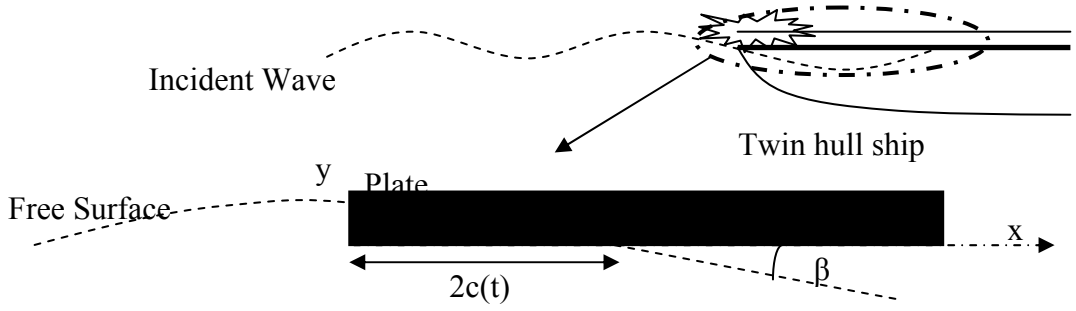

Figure 2.5: Wave hitting the frontal part of twin hull ship

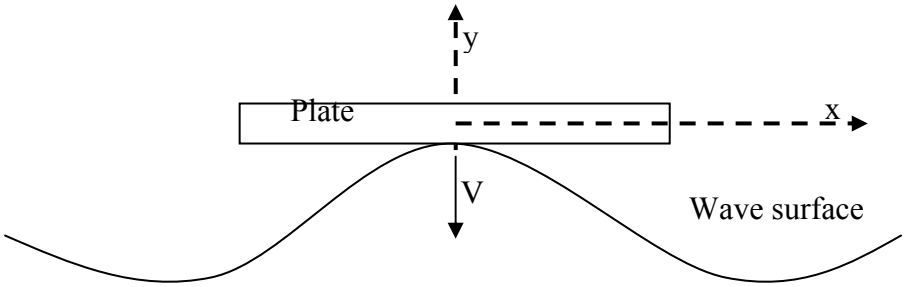

Figure 2.6: Plate hitting surface wave

Wet-deck slamming can produce negative effects locally on the plate as well as globally, commonly known as whipping. In this section, we will focus on the determination of the slamming pressure on the plate panels which can be used in global analysis of the ship hull structure.

Case 1: As in Fig. 2.5, consider a wave is hitting on the front part of the wet-deck. As shown in Faltinsen et al. [87], the expression of the slamming pressure can be obtained

analytically with some assumptions. The effect of the jet formation and entrapment of air are not considered in the formulation. It is assumed that the wet-deck is having a constant downward velocity *V* and free surface makes angle β with the bottom of the plate. With these assumptions, the velocity potential on the wetted part of the wet-deck can be written as follows;

$$\phi = -V\sqrt{x(2c(t) - x)} \tag{2.21}$$

where, $2c(t)$ is the wetted length of the wet-deck. The pressure on the wetted part can be written using the linear form of Eqn. 2.13.

$$p = -\rho V \frac{\dot{c}(t)}{\sqrt{x(2c(t) - x)}} \tag{2.22}$$

where, $c(t)$ is defined as;

$$c(t) = \frac{2Vt}{3\tan\beta} \tag{2.23}$$

Case 2: As in Fig. 2.6 consider a plate is falling on a wave profile with a constant velocity *V*. At time instant t=0, the wetted area on the plate is zero and it increases with the time. The modeling here follows the Wagner's slamming model [54], in which slamming model is presented as a 2-D model. In this dissertation, it is assumed that wave slamming occurs on an area of plate, which depends on the wave profile which is taken to be paraboloid or some other realistic form of the wave profile.

(i) Paraboloid form: From Wagner's 2-D slamming model, the relative vertical velocity between the fluid particles on the free surface and the body, is;

$$V_r = \frac{\partial \phi}{\partial y} + V \tag{2.24}$$

When the fluid particle intersects the body surface, then body moves a vertical distance with respect to the initial contact. That vertical distance can be expressed as,

$$\eta_b(x,y) = \int_0^t \frac{V\left|\sqrt{x^2+y^2}\right|}{\sqrt{x^2+y^2-c^2(t)}}dt \tag{2.25}$$

where, *c(t)* is wetted radial length. Assuming that the wave profile is of paraboloid form $\eta_b(x,y) = 0.5\frac{x^2+y^2}{R}$ and on considering that the wetted length varies from *0* to *R,* then Eqn. 2.25 can be written as;

$$\eta_b(x,y) = \int_0^R \frac{x\mu(c)}{\sqrt{x^2+y^2-c^2}}dc \tag{2.26}$$

where,

$$\mu(c)dc = Vdt \tag{2.27}$$

To obtain an approximate solution, $\mu(c)$ is expressed as;

$$\mu(c) = A + Bc \tag{2.28}$$

using the assumed profile and performing the integration, one can find the expression of wetted length as;

$$c = 2\sqrt{VtR} \tag{2.29}$$

Now the slamming pressure can be expressed as [37],

$$p - p_a = \rho V \frac{c}{\sqrt{c^2-(x^2+y^2)}}\frac{dc}{dt} \tag{2.30}$$

for *c(t)* as in Eqn. (2.29), Pressure can be defined as;

$$p - p_a = \rho \frac{2RV^2}{\sqrt{4RVt-(x^2+y^2)}} \tag{2.31}$$

(ii) Real wave form: In this case, a long crested real wave profile is chosen for the slamming pressure analysis. After integrating Eqn. 2.26, following expression can be obtained [56];

$$\eta_b(x) = A\frac{\pi}{2}x + Bx^2 \tag{2.32}$$

Assuming $\eta_b(x) = \frac{H}{2}\sin kx$, and applying the Taylor expansion, constants *A* and *B* can be obtained as $A = \frac{kH}{\pi}$ and *B=0*. where, *H* is the wave height and *k* is the wave number of the incident wave. The expression of the wetted length can be written as;

$$c = \frac{\pi V t}{kH} \tag{2.33}$$

Subsequently, the slamming pressure can be determined using Eqn. 2.30

2.4 ABS Slamming Formula

The study and the results are based on the ABS: Rules for Building and Classing High-Speed Craft. Design slamming pressure, longitudinal stiffeners spacing, transverse stiffeners spacing and the plate thickness etc. are obtained using the ABS Rules [65] .Design slamming pressure is required to determine the wet-deck plate thickness and scantling. The design slamming pressure depends mainly on displacement, waterline length, waterline beam, number of hulls, width of the wet-deck between hull sides, vertical distance from lightest waterline and significant wave height. Per ABS rules, the design pressure is given as [65]

$$P_{wd} = N_1\left[\frac{\Delta}{0.332(L_w N_h B_w + L_{wd}W_{wd}}\right]\left[H_b + \eta_{xx}\right]\left[1 - \frac{G_A}{H_w}\right]F_D$$

where,

N_1=0.1

B_w= waterline beam of one hull in m

N_h= number of hulls

L_{wd}= Length of wet-deck, overall, in m

W_{wd}=width of wet-deck between hull sides in m

H_b= 1 for catamarans

G_A=vertical distance of wet-deck from lightest waterline in m

H_w=H_s

L_w= waterline length in m

Δ = displacement at design waterline in kgs

η_{xx} =parameter depends on craft speed, vertical acceleration provided in reference [65]

Second step is to find the longitudinal and transverse spacing in order to get the wet-deck plate thickness. Spacing calculations require design stress and respective section modulus. Followings are the respective expressions per ABS rules:

Design Stress

$$\sigma_d = 0.9\sigma_a$$

where,

σ_a = yield stress i.e. 250 MPa for steel

Longitudinal Section Modulus

$$SM_L = C_1 C_2 L^2 B(C_b + 0.7) K_3 K_4 CQ \quad cm^2 m$$

where, C_1=6.40

C_2=0.01

L= length of the craft

B= Breadth of the craft

C_b= Block Coefficient

$$K_3 = 0.7 + 0.3\left[\frac{\frac{V}{\sqrt{L}} + 1.2}{3.64}\right]$$

K_4= 1.0

C= 1.0 for steel craft

Q= 1.0 for steel

V= maximum speed in knots

Transverse Section Modulus

$$SM_T = M_T / \sigma_d$$

where, $M_T = K_1 \Delta B_{cl} n$

K_1= 0.255

Δ = displacement at design waterline in kg

B_{cl}= distance between hull centerlines in m

n= vertical acceleration at the craft's center of gravity

Spacing

$$s = \frac{SM * \sigma_d}{83.3 * p * l^2}$$

where, l= length of the longitudinal/transverse girder in m

Spacing and design pressure (determined earlier using ABS rules) are used to determine the thickness of the plate and the expression for the thickness is as follows;

Thickness of the Plate

$$h = s\sqrt{\frac{pk}{1000\sigma_d}}$$

where,

s= spacing in mm

p= design pressure in kN/m^2

k= plate panel aspect ratio facto 0.3-0.5

σ_d = design stress in N/mm^2

2.5 Regular wave forces in different sea states

This section provides the formulation of the dynamic pressure of the incident waves on the floating structure. Incident waves can be categorized into two wave systems, (i) regular wave system, this system provides a sinusoidal expression for the wave elevation, and (ii) irregular wave system, this type of system is of particular interest which matches with the actual ocean environment. But, irregular system can also be expressed as a combination of different sinusoidal terms which makes it easier to tackle, theoretically. The derivation and details are already given in many textbooks such as Newman [21] and Edward [84]. In this section, an overview is presented on both of the wave systems, which is as follows;

2.5.1 Regular wave system

By taking the fact in consideration that regular wave system is sinusoidal, Free surface elevation can be written as;

$$\eta = A\cos(kx - \omega t) \tag{2.35}$$

where, A is the wave amplitude, k is wave number and ω is the wave frequency. From the free surface kinematic and linearized dynamic conditions, Eqns. 2.6 and 2.7, the free surface elevation can be written as;

$$\eta = -\frac{1}{g}\frac{\partial \phi}{\partial t} \tag{2.36}$$

where, ϕ is the velocity potential which satisfies the Laplace equation Eqn. 2.2. An expression of velocity potential can be obtained by solving the Laplace equation and Eqn. 2.36, which is as follows;

$$\phi = \frac{gA}{\omega} e^{ky} \sin(kx - \omega t) \tag{2.37}$$

This expression for velocity potential is for deep water case and a dispersion relation, relating the wave number and the frequency, can be written as;

$$k = \frac{\omega^2}{g} \tag{2.38}$$

Through the use of Euler's integral, the expression for linear dynamic pressure can be obtained, which is given by;

$$P = -\rho\frac{\partial \phi}{\partial t} \tag{2.39}$$

2.5.2 Irregular wave system

Irregular ocean wave system can be represented by combination of many sinusoidal waves. These wave components can be also be expressed in terms of variance spectrum *S(ω)*. This spectrum is also known as sea-state spectrum and has many mathematical formulations. Here, we are following ISSC spectrum or modified Pierson-Moskowitz spectrum, which can be expressed as;

$$S(\omega) = \frac{5}{16}\left(\frac{2\pi}{T_p}\right)^4 \frac{H_s^2}{\omega^5} exp\left[-\frac{5}{4}\left(\frac{2\pi}{T_P\omega}\right)^4\right] \tag{2.40}$$

This wave spectrum represented the fully developed sea state, where, H_s is the significant wave height and T_P is the spectrum peak period $T_P = 1.408T_Z$. T_Z is average wave period of a given sea state. This sea spectrum is made of many wave components and the amplitude of any wave component can be expressed in terms of frequency band width $\delta\omega$ with ω_i as the center of the band.

$$\bar{A}_i = \sqrt{2S(\omega)\delta\omega} \tag{2.40}$$

where, A_i is the amplitude of a wave component in a given sea state. Upon taking the unidirectional spectrum, the total ocean wave system can be written as;

$$\eta(x,t) = \sum_{i=1}^{N} A_i \cos(k_i x - \omega_i t) \tag{2.41}$$

The velocity potential of this wave system also satisfies the Laplace equation and can be expressed as;

$$\phi = \sum_{i=1}^{N} \frac{gA_i}{\omega_i} e^{k_i y} \sin(k_i x - \omega_i t) \tag{2.42}$$

Dynamic pressure due to the ocean wave system, Eqn. 2.41, can be determined by using Eqn. 2.39.

These regular wave pressure and slamming pressures are applied on the hull plates to determine their response. Flexural deflection and von Mises stress of the plates are determined for each and combination of above hydrodynamic loadings. The formulation of the structural mechanics is discussed in the next chapter.

3. MATHEMATICAL FORMULATION OF SHIP STRUCTURAL MECHANICS

In this chapter, we present theories and formulations for the determination of structural deformation of ship hull and plates, subject to hydrodynamic loadings theory which was presented in the earlier chapter. Structural analysis can be categorized into two parts, (i) global analysis and (ii) local analysis. Here, we will present the methods to evaluate the deflection, stress and strain on the hull structure as well on the plate panels due to the applied wave loading. Hull of the ship is modeled as a beam which follows Euler-Bernoulli beam theory, and for the analysis of the plates, different types of plate theories such as linear isotropic plate theory, non-linear isotropic plate theory and orthotropic plate theories are used. For the frequency domain analysis, a semi-analytical method known as the superposition method [64] is used and for the time domain, finite difference method [27] is used.

3.1 Analysis of the ship hull girder

The term global analysis of the ship hull indicates the springing and whipping analysis of the ship hull girder subject to regular and slamming wave loading, respectively. Euler-Bernoulli beam theory [79] is used to model the ship hull in order to determine stress distribution over a range of frequencies in the linear frequency domain

analysis as well as for the transient time domain analysis for a range of load amplitudes. The governing equation of beam vibration [81] is as follows.

$$(m + \mu_{zz})\frac{\partial^2 Z}{\partial t^2} + \lambda_{zz}\frac{\partial Z}{\partial t} + \frac{\partial^2}{\partial x^2}\left(EI(x)\frac{\partial^2 Z}{\partial x^2}\right) + \rho g A_w Z = F_{wave} \tag{3.1}$$

where,

m = mass per unit length

μ_{zz} = added mass coefficient per unit length

Z = structural response

λ_{zz} = wave damping coefficient per unit length

E = elastic modulus of the hull material

$I(x)$ = second moment of structural cross section area about neutral axis

ρ = water density

g = gravity acceleration

A_w = water plane area

F_{wave} = total wave force

The structural response can be decomposed into (i) rigid body response, and (ii) elastic response, significance of each of which depends on the wave frequency. For a typical ship, rigid body response is of low frequency while the structural response is of high frequency. In a given sea state wave spectrum, low frequencies will therefore excite rigid-body motions while the high frequency content excite structural vibrations. If the overlap between the two modes is negligible, then Equation (3.1) can be split into the following equations:

(i) For rigid body response

$$(m+\mu_{zz})\frac{\partial^2 Z_R}{\partial t^2}+\lambda_{zz}\frac{\partial Z_R}{\partial t}+\rho g A_w Z_R = F \tag{3.3}$$

(ii) For elastic body response

$$(m+\mu_{zz})\frac{\partial^2 Z_E}{\partial t^2}+\frac{\partial^2}{\partial x^2}\left(EI(x)\frac{\partial^2 Z_E}{\partial x^2}\right) = F \tag{3.4}$$

The response spectrum corresponding to Eqn. (3.1) will exhibit peaks at two regimes, one corresponding to rigid-body modes and the other to structural modes and higher harmonics in the case of nonlinear wave loading.

3.1.1 Rigid Body Analysis

Assuming $Z_R = Z_R^* e^{i\sigma t}$ and $F = Fe^{i\sigma t}$, one can write the Eqn. 3.3 as

$$Z_R^* = \frac{F}{\rho g A_w + i\sigma\lambda_{zz} - (m+\mu_{zz})\omega^2} \tag{3.6}$$

where, Z_R^* is the rigid body response and *F* is the wave exciting force determined using Froude-Krylov method (if diffraction and drag forces can be neglected), as discussed in Chapter 2. From above, one can note that the maximum resonant response will be at damped natural frequency $\omega = \sqrt{\frac{\rho g A_w}{m+\mu_{zz}}}$. This response comes out as a complex number because of the wave damping force and it can be expressed as;

$$Z_R^* = Z_{R(real)} + iZ_{R(img)} \tag{3.7}$$

The absolute response function and phase difference can be written as;

$$|Z_R^*| = \sqrt{Z_{R(real)}^2 + Z_{R(img)}^2},$$

$$\theta = \tan^{-1}\left(\frac{Z_{R(img)}}{Z_{R(real)}}\right)$$

3.1.2 Elastic Analysis of the ship model

Eqn. 3.4 shows the governing equation for the beam vibrations with variable moment of inertia *I(x)*. If "*I*" is taken as a constant along the ship length and assuming $Z_E = Z_E^* e^{i\sigma t}$ and $F = F^* e^{i\omega t}$, the equation (3.4) can be re-written as;

$$-(m + \mu_{zz})\omega^2 Z_E^* + EI\frac{\partial^4 Z_E^*}{\partial x^4} = F^* \tag{3.8}$$

Above Eqn. 3.8 can be solved easily for example, Kling [60] has carried out the elastic analysis of a rectangular barge model using the Green's function method Mei [83].

The governing equation for the beam vibrations with non uniform moment of inertia can be expressed in the frequency domain as:

$$-(m + \mu_{zz})\omega^2 Z_E^* + \frac{\partial^2}{\partial x^2}\left(EI\frac{\partial^2 Z_E^*}{\partial x^2}\right) + \rho g A_w Z_E^* = F^* \tag{3.9}$$

For the time domain analysis of rigid-body response and structural vibration, Eqn. 3.4 and 3.9 are solved using finite difference method which is presented in Appendix A.

3.2 Local Analysis of Ship Hull's Plate Panels

In this section, we consider vibration of hull plates on (i) the bottom plate element of the hull, and (ii) wet-deck/cross structure of twin hull ship because of

slamming loads. The plate theories considered for modeling include (i) linear isotropic plate theory, (ii) nonlinear isotropic plate theory, and (iii) orthotropic plate theory. The governing equations for the linear plate vibrations are solved using a semi-theoretical method known as the superposition method [64] and non-linear plate vibrations are solved using the finite difference scheme in the time domain.

3.2.1 Analysis of thin isotropic plates the superposition method

In this dissertation, two theories are used to determine the isotropic plate vibrations (i) small deflection plate theory and (ii) large deflection plate theory. The development of the governing differential equation for the plate vibrations is as follows:

3.2.1.1 Isotropic small deflection thin plate theory

Small deflection thin plate theory is based on the Kirchhoff's plate theory [26]. The fundamental assumptions in the linear elastic and small deflection theory are as follows, [26] and [27]:

1. The material of the plate is elastic, homogeneous, and isotropic.
2. The plate is initially flat.
3. The deflection of the mid plane is small compared with the thickness of the plate. The slope of the deflected surface is therefore very small and the square of the slope is a negligible quantity in comparison with the unity.
4. The straight lines, initially normal to the middle plane remain straight and normal to the middle surface during the deformation, and the length of such elements is not altered. This means that the vertical shear strains are negligible and the normal strain may also be omitted. This assumption is referred to as the "*hypothesis of straight normals"*.

5. Since the displacements of a plate are small, it is assumed that the middle surface remains unstrained after bending.

The development of the governing equations of this model proceeds as follows. Considering an elastic body subject to the external loads, the stress developed on an element due to the applied load can be expressed as Fig. 3.1.

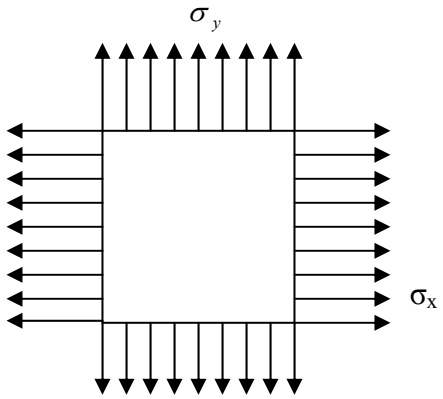

Figure 3.1: Plate Element subjected to normal Stresses

where, σ_x is the normal stress in x-direction and σ_y is the normal stress in y-direction.

Longitudinal strains in x and y-directions due to these stresses can be written as [26];

$$\varepsilon_x = \frac{\sigma_x - \nu\sigma_y}{E}, \quad \varepsilon_y = \frac{\sigma_y - \nu\sigma_x}{E} \tag{3.10}$$

where, E is the Young's modulus and ν the Poisson's ratio. On rearranging the terms in Eqn. 3.1, stress components can be written in terms of the strains;

$$\sigma_x = \frac{E(\varepsilon_x + \nu\varepsilon_y)}{1-\nu^2}, \quad \sigma_y = \frac{E(\varepsilon_y + \nu\varepsilon_x)}{1-\nu^2}, \quad \tau_{xy} = G\gamma_{xy} \tag{3.11}$$

From the assumption that the displacements vary linearly over a plate thickness, the strain displacement relation can be written as;

$$\varepsilon_x = -z\frac{\partial^2 W(x,y)}{\partial x^2}, \varepsilon_y = -z\frac{\partial^2 W(x,y)}{\partial y^2}$$
$$\gamma_{xy} = -2z\frac{\partial^2 W(x,y)}{\partial x \partial y} \tag{3.12}$$

In the above equations, it is implicit that the plate is on x-y plane and z is positive upwards and *W* is the plate deflection in z-direction. Using the above strain terms with in Eqn. 3.11, we get

$$\sigma_x = -Ez\left\{\frac{\frac{\partial^2 W(x,y)}{\partial x^2} + \nu\frac{\partial^2 W(x,y)}{\partial y^2}}{1-\nu^2}\right\}$$
$$\sigma_y = -Ez\left\{\frac{\frac{\partial^2 W(x,y)}{\partial y^2} + \nu\frac{\partial^2 W(x,y)}{\partial x^2}}{1-\nu^2}\right\} \tag{3.13}$$
$$\tau_{xy} = -Ez\left\{\frac{\frac{\partial^2 W(x,y)}{\partial x \partial y}}{1-\nu}\right\}$$

Integrating Eqn. 3.13 over the thickness of the plate, expressions for bending moment can be achieved and expressed as follows;

$$M_x = -D\left\{\frac{\partial^2 W(x,y)}{\partial x^2} + \nu\frac{\partial^2 W(x,y)}{\partial y^2}\right\}$$
$$M_y = -D\left\{\frac{\partial^2 W(x,y)}{\partial y^2} + \nu\frac{\partial^2 W(x,y)}{\partial x^2}\right\} \tag{3.14}$$
$$M_{xy} = -D(1-\nu)\frac{\partial^2 W(x,y)}{\partial x \partial y}$$

where, $D = \frac{Eh^3}{12(1-\nu)}$ and h is the plate thickness. Shear forces can also be expressed in terms of lateral displacement.

$$V_x = -D\left\{\frac{\partial^3 W(x,y)}{\partial x^3} + (2-\nu)\frac{\partial^3 W(x,y)}{\partial x \partial y^2}\right\}$$
$$V_y = -D\left\{\frac{\partial^3 W(x,y)}{\partial y^3} + (2-\nu)\frac{\partial^3 W(x,y)}{\partial y \partial x^2}\right\} \quad (3.15)$$

Using $\xi = x/a$, $\eta = y/b$ and $\kappa = b/a$, as non-dimensional parameters, equations (3.14) becomes;

$$-\frac{M_\xi a}{D} = \frac{\partial^2 W(\xi,\eta)}{\partial \xi^2} + \nu\kappa^{-2}\frac{\partial^2 W(\xi,\eta)}{\partial \eta^2}$$
$$-\frac{M_\xi b\kappa}{D} = \frac{\partial^2 W(\xi,\eta)}{\partial \eta^2} + \nu\kappa^{2}\frac{\partial^2 W(\xi,\eta)}{\partial \xi^2} \quad (3.16)$$

3.2.1.3 Governing Differential Equation for vibration of isotropic plate

Using the expression for the bending moment obtained in 3.16 in the equilibrium condition [26], we get

$$\frac{\partial^2 M_x}{\partial x^2} + \frac{\partial^2 M_y}{\partial y^2} - 2\frac{\partial^2 M_{xy}}{\partial x \partial y} = q(x,y) \quad (3.17)$$

where, *q(x, y)* represents static or dynamic loading; note, in the latter case the inertia term will be also in *q(x, y)*. Using the bending moment equations (3.14) and introducing the inertial force term into equation (3.17);

$$\frac{\partial^4 W(x,y,t)}{\partial x^4} + 2\frac{\partial^4 W(x,y,t)}{\partial x^2 \partial y^2} + \frac{\partial^4 W(x,y,t)}{\partial y^4}$$
$$-\frac{\rho_p}{D}\frac{\partial^2 W(x,y,t)}{\partial t^2} = q(x,y) \quad (3.18)$$

where, ρ_p is the mass of the plate per unit area. In the frequency domain and changing into dimensionless form, with frequency parameter $\lambda^2 = \omega a^2 \sqrt{\frac{\rho_p}{D}}$ and q^* as non-dimensional pressure, equation (3.18) can be expressed for the free vibrations analysis as;

$$\frac{\partial^4 W(\xi,\eta)}{\partial \eta^4} + \frac{2}{\kappa^2}\frac{\partial^4 W(\xi,\eta)}{\partial \xi^2 \partial \eta^2} + \frac{1}{\kappa^4}\frac{\partial^4 W(\xi,\eta)}{\partial \xi^4} - \lambda^4 W(\xi,\eta) = q^* \qquad (3.19)$$

which is the well-known Kirchoff's plate equation in the frequency domain.

3.2.1.4 Free Vibration Analysis of Clamped Plate using Superposition Method

Equation 3.19 can be solved for simply supported rectangular plate using the method of separation of variables. For other forms of boundary conditions, the solution is not so straightforward. Gorman introduced a technique to solve the plate equation with other forms of boundary conditions. Gorman's superposition method is based on the principle of boundary decomposition. The fourth order differential equation for the plate vibrations, Eqn. 3.19, has a direct solution for simply supported boundary conditions, but when the boundary conditions are not simply supported then it is hard to obtain an analytical solution for Eqn. 3.19. Thus, the plate vibration problem can be divided into two parts, (i) when at least two opposite sides have simply supported boundary conditions, Eqn. 3.19 can be solved analytically and (ii) when plates are not bounded with a pair of simply supported boundary conditions on opposite sides, Eqn. 3.19 does not have any direct solution but it can be solved by using the superposition method [66].

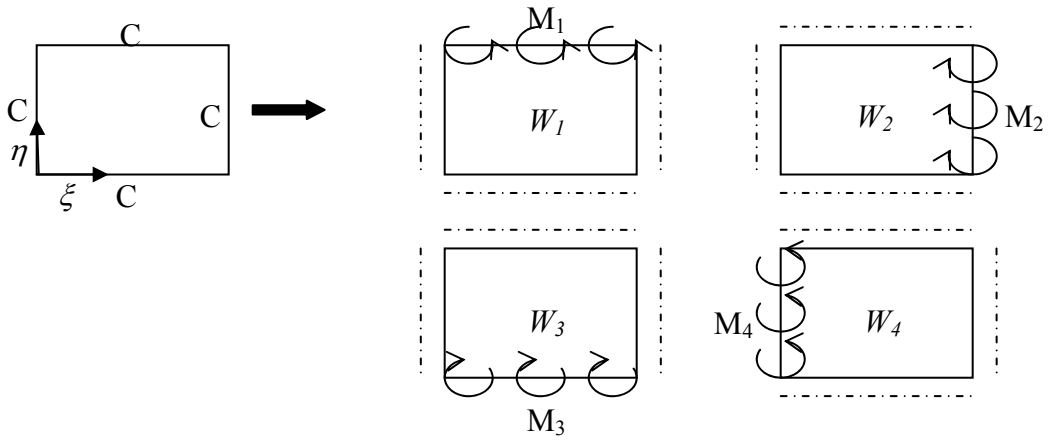

Figure 3.2: Buliding blocks to obtain solution for clamped plate vibrations using superposition method

In the superposition method, original boundary conditions are decomposed into the simply supported and the slip-shear boundary conditions. As per slip-shear boundary condition, transverse shear force and slope are zero at the boundary.

The boundary conditions for the present ship-hull plate vibration problem are taken as clamped boundary conditions. It is then assumed that the hull plate is fixed between the hull girders. Superposition method is applied to the Eqn. 3.19 to solve for the plate vibrations.

Fig. 3.2 shows that the plate is dissembled into four different blocks. Each block has one driving edge, which has zero lateral displacement and an assigned moment, which depends on the other boundary conditions. Remaining three clamped edges are converted into the simply supported edges. Every block is solved individually and the results from each block are superimposed to get the deflection and the stress distribution over the clamped plate.

(a) Free vibrations analysis for the first block

As we can observe in Fig. 3.2 that the first block has simply supported boundary conditions on the edges $\xi = 0$, $\xi = 1$ and $\eta = 0$. Levy's type solution [64] is expressed in Eqn. 3.20, which is based on the boundary-conditions along the edges $\xi = 0$ and $\xi = 1$,

$$W_1(\xi, \eta) = \sum_{m=1}^{M} Y_m(\eta) \sin(m\pi\xi) \tag{3.20}$$

where, M is the number of terms in the solution series. Upon substituting the above expression in the governing differential equation of plate vibrations Eqn. 3.19, one can obtain the following ordinary differential equation for $Y_m(\eta)$. The solution of the ordinary differential equation is given by [64]

if $m^2\pi^2 > \lambda^2$

$$Y_m(\eta) = A_m \cosh(\beta_{1m}\eta) + B_m \sinh(\beta_{1m}\eta) + C_m \cosh(\gamma_{1m}\eta) + D_m \sinh(\gamma_{1m}\eta) \tag{3.21a}$$

and if $m^2\pi^2 < \lambda^2$

$$Y_m(\eta) = A_m \cosh(\beta_{1m}\eta) + B_m \sinh(\beta_{1m}\eta) + C_m \cos(\gamma_{1m}\eta) + D_m \sin(\gamma_{1m}\eta) \tag{3.21b}$$

where, $\beta_{1m}^2 = (\kappa m\pi)^2 + \kappa^2\lambda^2$ and $\gamma_{1m}^2 = (\kappa m\pi)^2 - \kappa^2\lambda^2$ or $\gamma_{1m}^2 = \kappa^2\lambda^2 - (\kappa m\pi)^2$

On applying all the boundary conditions for the simply supported edges, we obtain an expression of $Y_m(\eta)$ as,

if $m^2\pi^2 > \lambda^2$

$$Y_m(\eta) = C_m\left(-\frac{\sinh\gamma_{1m}}{\sinh\beta_{1m}}\sinh(\beta_{1m}\,\eta) + \sinh(\gamma_{1m}\,\eta)\right) \tag{3.22a}$$

and if $m^2\pi^2 < \lambda^2$

$$Y_m(\eta) = C_m\left(-\frac{\sin\gamma_{1m}}{\sinh\beta_{1m}}\sinh(\beta_{1m}\,\eta) + \sin(\gamma_{1m}\,\eta)\right) \tag{3.22b}$$

Noting that the fourth edge, with boundary condition as $\eta = 1$, has zero lateral displacement and one driving bending moment. The moment expression, Eqn. 3.16, for this edge can be written in terms of $\sin(m\pi\xi)$ as follows,

$$\left.\frac{M_\eta \kappa b}{D}\right|_{\eta=1} = \sum_{m=1}^{M} E_{1m}\sin(m\pi\xi) \tag{3.23}$$

where, E_{1m} are the coefficients of the series.

Using Eqns. 3.22 and 3.23, the displacement for the first block can be expressed as follows;

if $m^2\pi^2 > \lambda^2$

$$W_1 = \sum_{m=1}^{M}\frac{E_{1m}}{(\beta_{1m}^2 - \gamma_{1m}^2)}\left(-\frac{\sinh(\beta_{1m}\,\eta)}{\sinh\beta_{1m}} + \frac{\sinh(\gamma_{1m}\eta)}{\sinh\gamma_{1m}}\right)\sin(m\pi\xi) \tag{3.24a}$$

and if $m^2\pi^2 < \lambda^2$

$$W_1 = \sum_{m=1}^{M}\frac{E_{1m}}{(\beta_{1m}^2 + \gamma_{1m}^2)}\left(-\frac{\sinh(\beta_{1m}\,\eta)}{\sinh\beta_{1m}} + \frac{\sin(\gamma_{1m}\eta)}{\sin\gamma_{1m}}\right)\sin(m\pi\xi) \tag{3.24b}$$

(b)Second block analysis

Similar to first block, second block has simply supported boundary conditions on the edges $\eta = 0$, $\eta = 1$ and $\xi = 0$. Based on the edges $\eta = 0$ and $\eta = 1$, the Levy's type solution will be;

$$W_2(\xi, \eta) = \sum_{m=1}^{M} X_m(\xi) \sin(m\pi\eta) \tag{3.25}$$

where, *M* is the number of terms in the series.

As done for the first block the above expression is substituted in the governing differential equation of plate vibrations to obtain an ordinary differential equation for $X_m(\xi)$ solution of which is;

if $\frac{m^2\pi^2}{\kappa^2} > \lambda^2$

$$X_m(\xi) = A_m \cosh(\beta_{2m}\xi) + B_m \sinh(\beta_{2m}\xi) + C_m \cosh(\gamma_{2m}\xi) + D_m \sinh(\gamma_{2m}\xi) \tag{3.26a}$$

and if $\frac{m^2\pi^2}{\kappa^2} < \lambda^2$

$$X_m(\xi) = A_m \cosh(\beta_{2m}\xi) + B_m \sinh(\beta_{2m}\xi) + C_m \cos(\gamma_{2m}\xi) + D_m \sin(\gamma_{2m}\xi) \tag{3.26b}$$

where, $\beta_{2m}^2 = \left(\frac{m\pi}{\kappa}\right)^2 + \lambda^2$ and $\gamma_{2m}^2 = \left(\frac{m\pi}{\kappa}\right)^2 - \lambda^2$ or $\gamma_{2m}^2 = \lambda^2 - \left(\frac{m\pi}{\kappa}\right)^2$

On applying all the boundary conditions for the simply supported edges, we obtain an expression of $X_m(\xi)$ as,

if $\frac{m^2\pi^2}{\kappa^2} > \lambda^2$

$$X_m(\xi) = C_m\left(-\frac{\sinh\gamma_{2m}}{\sinh\beta_{2m}}\sinh(\beta_{2m}\,\xi) + \sinh(\gamma_{2m}\,\xi)\right) \tag{3.27a}$$

and if $\frac{m^2\pi^2}{\kappa^2} < \lambda^2$

$$X_m(\xi) = C_m\left(-\frac{\sin\gamma_{2m}}{\sinh\beta_{2m}}\sinh(\beta_{2m}\,\xi) + \sin(\gamma_{2m}\,\xi)\right) \tag{3.22b}$$

Similar to the solution of the first block, the fourth edge of the second block, with boundary condition as $\xi = 1$, has zero lateral displacement and one driving bending moment. Using the Fourier series expansion, the moment, Eqn. 3.16, for this edge can be written in terms of $\sin(m\pi\eta)$ as follows,

$$\left.\frac{M_\xi a}{D}\right|_{\xi=1} = \sum_{m=1}^{M} E_{2m}\sin(m\pi\eta) \tag{3.28}$$

where, E_{2m} are the coefficients of the series.

Using Eqns. 3.27 and 3.28, the displacement for the second block can be expressed as follows;

if $\frac{m^2\pi^2}{\kappa^2} > \lambda^2$

$$W_2 = \sum_{m=1}^{M}\frac{E_{2m}}{(\beta_{2m}^2 - \gamma_{2m}^2)}\left(-\frac{\sinh(\beta_{2m}\xi)}{\sinh\beta_{2m}} + \frac{\sinh(\gamma_{2m}\xi)}{\sinh\gamma_{2m}}\right)\sin(m\pi\eta) \tag{3.29a}$$

and if $\frac{m^2\pi^2}{\kappa^2} < \lambda^2$

$$W_2 = \sum_{m=1}^{M}\frac{E_{2m}}{(\beta_{2m}^2 + \gamma_{2m}^2)}\left(-\frac{\sinh(\beta_{2m}\,\xi)}{\sinh\beta_{2m}} + \frac{\sin(\gamma_{2m}\xi)}{\sin\gamma_{2m}}\right)\sin(m\pi\eta) \tag{3.29b}$$

(c) Third block analysis

The third block lateral displacement is similar to the first block, Fig. 3.2. The solution can be written in terms of that of the first block analysis simply by shifting the origin to (0, 1). In term of a new parameter $\eta^* = 1 - \eta$ and the expression for the lateral displacement can be expressed as;

if $m^2\pi^2 > \lambda^2$

$$W_3 = \sum_{m=1}^{M} \frac{E_{3m}}{(\beta_{1m}^2 - \gamma_{1m}^2)} \left(-\frac{\sinh(\beta_{1m}\,\eta^*)}{\sinh \beta_{1m}} + \frac{\sinh(\gamma_{1m}\eta^*)}{\sinh \gamma_{1m}} \right) \sin(m\pi\xi) \tag{3.30a}$$

and if $m^2\pi^2 < \lambda^2$

$$W_3 = \sum_{m=1}^{M} \frac{E_{3m}}{(\beta_{1m}^2 + \gamma_{1m}^2)} \left(-\frac{\sinh(\beta_{1m}\,\eta^*)}{\sinh \beta_{1m}} + \frac{\sin(\gamma_{1m}\eta^*)}{\sin \gamma_{1m}} \right) \sin(m\pi\xi) \tag{3.30b}$$

(d) Fourth block analysis

The fourth block lateral displacement is similar to the second block. The solution can be written in terms of that of the first block analysis simply by shifting the origin to (1, 0). In term of a new parameter $\xi^* = 1 - \xi$ and the expression for the lateral displacement can be written as

if $\frac{m^2\pi^2}{\kappa^2} > \lambda^2$

$$W_4 = \sum_{m=1}^{M} \frac{E_{4m}}{(\beta_{2m}^2 - \gamma_{2m}^2)} \left(-\frac{\sinh(\beta_{2m}\xi^*)}{\sinh \beta_{2m}} + \frac{\sinh(\gamma_{2m}\xi^*)}{\sinh \gamma_{2m}} \right) \sin(m\pi\eta) \tag{3.31a}$$

and if $\frac{m^2\pi^2}{\kappa^2} < \lambda^2$

$$W_4 = \sum_{m=1}^{M} \frac{E_{4m}}{(\beta_{2m}^2 + \gamma_{2m}^2)} \left(-\frac{\sinh(\beta_{2m}\,\xi^*)}{\sinh \beta_{2m}} + \frac{\sin(\gamma_{2m}\xi^*)}{\sin \gamma_{2m}} \right) \sin(m\pi\eta) \tag{3.31b}$$

3.2.1.5 The Superimposition of the blocks

Having the solution for the four blocks, the solution for the fully clamped plate can be obtained by superimposing the blocks' solutions. The superimposed solution for the fully clamped plate can be written as

$$W(\xi, \eta) = \sum_{j=1}^{4} W_j(\xi, \eta) \tag{3.32}$$

The superimposed solution also satisfies the governing differential equation, Eqn. 3.16 and remaining one of the two boundary conditions (slope along the edges is zero) along each edge. The superimposed solution has *4M* unknown constants which can be determined by imposing the second boundary condition along all the edges. The zero lateral displacement boundary condition is already satisfied along all the edges. The remaining boundary condition for the clamped boundaries i.e. the slope normal to the edges which happens to be zero, is applied to the superimposed solution, Eqn. 3.32. The expression for the remaining boundary condition on all the four boundaries can be written as;

$$\begin{aligned} &\frac{\partial}{\partial \xi}\left(\sum_{j=1}^{4} W_j(\xi, \eta)\right)_{\xi=0} = 0, \frac{\partial}{\partial \xi}\left(\sum_{j=1}^{4} W_j(\xi, \eta)\right)_{\xi=1} = 0 \\ &\frac{\partial}{\partial \eta}\left(\sum_{j=1}^{4} W_j(\xi, \eta)\right)_{\eta=0} = 0, \frac{\partial}{\partial \eta}\left(\sum_{j=1}^{4} W_j(\xi, \eta)\right)_{\eta=1} = 0 \end{aligned} \tag{3.33}$$

There four boundary conditions, Eqns. 3.33, provide *4*M* algebraic equations with *4*M* unknowns E_{jm}. These algebraic equations which will be of the form *AX=B* can be solved using a matrix inversion method. In case of the free vibrations, determinant of matrix *A* can be used to determine the eigen-frequencies of free vibrations, by setting it equal to zero and determining the roots of the characteristic equation.

3.2.1.6 Forced Vibrations of clamped isotropic plate

From the principle of superposition method, in addition to four blocks, Fig. 3.2, a fifth block can be introduced to model the loading. This block, assumed to be under the simply supported boundary conditions for all the edges and loading can be applied as a point loading or as distributed loading.

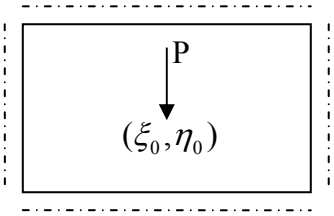

Figure 3.3: Fifth building block in addition to figure (3.2) for pulsating force P

A force is assumed to be applied as a point pulsating load with frequency ω_p at point (ξ_0, η_0). Then, the governing differential equation for the plate vibrations Eqn. 3.16 can be modified for the fifth block as;

$$\frac{\partial^4 W(\xi,\eta)}{\partial \eta^4} + 2\kappa^2 \frac{\partial^4 W(\xi,\eta)}{\partial \xi^2 \partial \eta^2} + \kappa^4 \frac{\partial^4 W(\xi,\eta)}{\partial \xi^4} - \kappa^2 \lambda^4 W(\xi,\eta) = \frac{P}{Dh} \kappa^4 a^4 \delta(\xi - \xi_0)\delta(\eta - \eta_0) \tag{3.34}$$

The solution of Eqn. 3.34 can be shown as;

$$W_5 = \sum_{m=1}^{M}\sum_{n=1}^{M} E_{5mn}\sin(m\pi\xi)\sin(n\pi\eta) \tag{3.35}$$

The boundary conditions for the fifth block edges are simply supported. Hence, the deflection and moment becomes zero on the edges and Eqn. 3.35 satisfies all the boundary conditions. Based on the orthogonality of sine and cosine functions and the property of delta function, the expression of $E_{5,mn}$ can be obtained by solving governing differential equation Eqn. 3.34 with Eqn. 3.35,

$$E_{5mn} = \frac{4P\kappa^4 a^4 \sin(m\pi\xi_0)\sin(n\pi\eta_0)}{Dh\left(m^4\pi^4\kappa^4 + 2\kappa^4 m^2 n^2\pi^4 + n^4\pi^4 - \frac{\rho}{D}\omega_p^2\kappa^4 a^4\right)}$$

To obtain the solution for fully clamped plate vibration, fifth building block solution is also superimposed to the remaining four building block solutions and the total deformation takes the following form;

$$W(\xi,\eta) = \sum_{j=1}^{5} W_j(\xi,\eta) \tag{3.36}$$

3.2.2 Damped nonlinear Vibrations of the Isotropic Plate

In plate vibrations, the large-amplitude nonlinear theory is referred to as the von Karman nonlinear theory. In the case of large deformations, certain additional terms will be presented related to the strain of the mid-plane [27], Specifically, these additional forces depend not only on the external forces but also on the strain of the middle plane of the plate caused due to bending.

The governing differential equation for the large deformation can be modified in the following manner [27]:

$$D\left(\frac{\partial^4 W}{\partial x^4}+2\frac{\partial^4 W}{\partial x^2\partial y^2}+\frac{\partial^4 W}{\partial y^4}\right)+\rho\frac{\partial^2 W}{\partial t^2}+2\rho\gamma_d\frac{\partial W}{\partial t} = q+N_x\frac{\partial^2 W}{\partial x^2}+N_y\frac{\partial^2 W}{\partial y^2}+2N_{xy}\frac{\partial^2 W}{\partial x\partial y} \tag{3.37}$$

where, γ_d is the material damping and N_x, N_y and N_{xy} are the internal stress developed on the plate element. Assuming that there is only lateral force acting on the plate, the equation of equilibrium on a plate element can be written as [22],

$$\frac{\partial N_x}{\partial x}+\frac{\partial N_{xy}}{\partial x}=0 \; and \; \frac{\partial N_{xy}}{\partial x}+\frac{\partial N_y}{\partial x}=0 \tag{3.38}$$

and the corresponding strain components are,

$$\varepsilon_x=\frac{\partial u}{\partial x}+\frac{1}{2}\left(\frac{\partial W}{\partial x}\right)^2 \; and \; \varepsilon_y=\frac{\partial v}{\partial y}+\frac{1}{2}\left(\frac{\partial W}{\partial y}\right)^2 \qquad \gamma_{xy}=\frac{\partial u}{\partial y}+\frac{\partial v}{\partial x}+\frac{\partial W}{\partial x}\frac{\partial W}{\partial y} \tag{3.39}$$

Using the Airy's stress function F [26] , the internal loads can be expressed as,

$$N_x=h\frac{\partial^2 F}{\partial y^2}, \qquad N_y=h\frac{\partial^2 F}{\partial x^2}, \qquad N_{xy}=-h\frac{\partial^2 F}{\partial x\partial y} \tag{3.40}$$

Strain components (3.39) can also be shown in terms of the stress function F

$$\varepsilon_x=\frac{1}{E}\left(\frac{\partial^2 F}{\partial y^2}-\nu\frac{\partial^2 F}{\partial x^2}\right) \; and \; \varepsilon_y=\frac{1}{E}\left(\frac{\partial^2 F}{\partial x^2}-\nu\frac{\partial^2 F}{\partial y^2}\right) \qquad \gamma_{xy}=-\frac{2(1+\nu)}{E}\frac{\partial^2 F}{\partial x\partial y} \tag{3.41}$$

By using the above strain equations (3.41) and governing differential equation (3.37), we get the following two equations to govern the deflection and Airy stress function,

$$D\left(\frac{\partial^4 W}{\partial x^4}+2\frac{\partial^4 W}{\partial x^2\partial y^2}+\frac{\partial^4 W}{\partial y^4}\right)+\rho\frac{\partial^2 W}{\partial t^2}+2\rho\gamma_d\frac{\partial W}{\partial t}$$

$$=q+h\frac{\partial^2 F}{\partial y^2}\frac{\partial^2 W}{\partial x^2}+h\frac{\partial^2 F}{\partial x^2}\frac{\partial^2 W}{\partial y^2}-2h\frac{\partial^2 F}{\partial x\partial y}\frac{\partial^2 W}{\partial x\partial y} \quad (3.42)$$

$$\frac{\partial^4 F}{\partial x^4}+2\frac{\partial^4 F}{\partial x^2\partial y^2}+\frac{\partial^4 F}{\partial y^4}=E\left[\left\{\frac{\partial^2 W}{\partial x\partial y}\right\}^2-\frac{\partial^2 W}{\partial x^2}\frac{\partial^2 W}{\partial y^2}\right]$$

Lateral Deflection W and Airy stress function F can be determined by solving these two equations, Eqn. 3.42, simultaneously. In order to solve these equations, one needs to specify the boundary conditions for Airy stress function too. For a clamped plate, following are the boundary conditions for displacement and the stress function:

$$W=0,\quad \frac{\partial W}{\partial x}=0,\quad \frac{\partial^2 F}{\partial y^2}=0,\quad \frac{\partial^2 F}{\partial x\partial y}=0\ at\ x=0,a$$

$$W=0,\quad \frac{\partial W}{\partial y}=0,\quad \frac{\partial^2 F}{\partial x^2}=0,\quad \frac{\partial^2 F}{\partial x\partial y}=0\ at\ y=0,b$$

3.2.2 Orthotropic Plates: Theory and Problem Formulation

Orthotropic plates can be used to model the stiffened plates of the hull due to the different elastic properties in orthogonal directions (x & y- direction). Isotropic plates have homogeneous material properties, like the modulus of elasticity E and Poisson's ratio ν, same in every direction, whereas orthotropic plates have two modulus of

elasticity E_x, E_y and two Poisson's ratios ν_x, ν_y in orthogonal directions x and y respectively.

According to the Betti's principle, [26] and [27], these material properties of orthotropic plates can be related to each other as follows;

$$\frac{\nu_x}{\nu_y} = \frac{E_x}{E_y} \tag{3.43}$$

3.2.2.1 Development of moments and shear force terms

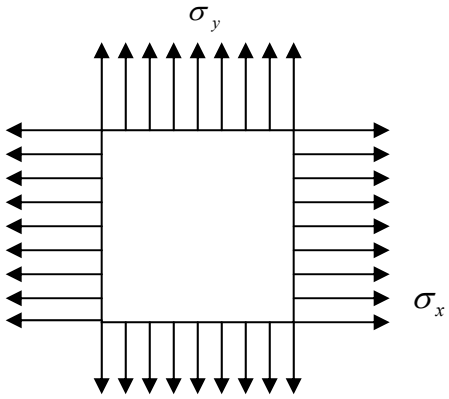

Figure 3.4: Schematic representation of an orthotropic plate element

Longitudinal strains in x and y direction,

$$\varepsilon_x = \frac{\sigma_x}{E_x} - \frac{\nu_y \sigma_y}{E_y}, \quad \varepsilon_y = \frac{\sigma_y}{E_y} - \frac{\nu_x \sigma_x}{E_x} \tag{3.44}$$

As shown in [21] and [22], the bending moment can be written as;

$$M_x = -D_x \left\{ \frac{\partial^2 W(x,y)}{\partial x^2} + \nu_y \frac{\partial^2 W(x,y)}{\partial y^2} \right\}$$

$$M_y = -D_y \left\{ \frac{\partial^2 W(x,y)}{\partial y^2} + \nu_x \frac{\partial^2 W(x,y)}{\partial x^2} \right\} \tag{3.45}$$

$$M_{xy} = 2D_t \frac{\partial^2 W(x,y)}{\partial x \partial y}$$

where, $D_x = \frac{E_x h^3}{12(1-\nu_x \nu_y)}$,$D_y = \frac{E_y h^3}{12(1-\nu_x \nu_y)}$, and $D_t = \frac{G_{xy} h^3}{12}$

Using non-dimensionlized variables, $\xi = x/a$, $\eta = y/b$ and $\kappa = b/a$, (where a and b are the plate dimensions in the x and y direction, respectively) the bending moments can be written in the dimensionless form:

$$\begin{aligned} -\frac{M_\xi a}{D_x} &= \frac{\partial^2 W(\xi,\eta)}{\partial \xi^2} + \nu_y \kappa^{-2} \frac{\partial^2 W(\xi,\eta)}{\partial \eta^2} \\ -\frac{M_\eta b^2}{a D_y} &= \frac{\partial^2 W(\xi,\eta)}{\partial \eta^2} + \nu_x \kappa^2 \frac{\partial^2 W(\xi,\eta)}{\partial \xi^2} \end{aligned} \tag{3.46}$$

3.2.2.2 Governing Differential Equation for vibration of orthotropic plates

From the equilibrium condition [26], we have

$$\frac{\partial^2 M_x}{\partial x^2} + \frac{\partial^2 M_y}{\partial y^2} - 2\frac{\partial^2 M_{xy}}{\partial x \partial y} = q(x,y) \tag{3.47}$$

where, *q(x, y)* represents the dynamic or static loading. Using the bending moment equations, Eqn. 3.45, and introducing the inertial force term into Eqn. 3.47, the governing differential equation for the plate vibrations can be written as;

$$\begin{aligned} D_x \frac{\partial^4 W(x,y,t)}{\partial x^4} + 2H \frac{\partial^4 W(x,y,t)}{\partial x^2 \partial y^2} + D_y \frac{\partial^4 W(x,y,t)}{\partial y^4} \\ -\rho_p \frac{\partial^2 W(x,y,t)}{\partial t^2} = q(x,y) \end{aligned} \tag{3.48}$$

where, ρ_p is the mass of the plate per unit area and $2H = \nu_y D_x + \nu_x D_y + 4D_t$.

For the solution of the time-domain equations, particularly of nonlinear, damped and orthotropic theories, the finite-difference method is used. Briefly, in the finite-

difference algorithms second-order central differencing is used to discretize the time- and spatial-derivative terms. The time step size is determined based on accuracy and stability criteria [39]. The details of the algorithms are given in Appendix A.

3.3 The von Mises Yield Stress Criterion

This yield criterion is also known as shear or distortion strain energy criterion, which was established by von Mises and Hencky. It is based on the principle of strain energy which suggests that the failure of the structure occurs when the maximum distortion energy per unit volume becomes more than the maximum distortion energy per unit volume required to cause yield.

Maximum distortion energy required for yield can be expressed in terms on principal stresses, σ_1 and σ_2, which are shown below in terms of body element stress in x-y directions;

$$\sigma_1 = \frac{\sigma_x + \sigma_y}{2} + \sqrt{\left(\frac{\sigma_x - \sigma_y}{2}\right)^2 + \tau_{xy}^2} \qquad (3.47)$$

$$\sigma_2 = \frac{\sigma_x + \sigma_y}{2} - \sqrt{\left(\frac{\sigma_x - \sigma_y}{2}\right)^2 + \tau_{xy}^2}$$

The strain energy per unit volume can be written in terms of the principal stress [26];

$$U_s = \frac{1}{12G}[(\sigma_1 - \sigma_1)^2 + \sigma_1^2 + \sigma_2^2] \qquad (3.48)$$

According to the distortion energy theory, strain energy per unit volume can be written as follows;

$$U_s = \frac{\sigma_{VM}^2}{6G} \tag{3.48}$$

where, σ_{VM} is the von Mises stress. As discussed above, the strain energies per unit volume, shown in Eqn. 3.48 and 3.49, should be equal to each other at the yielding point. Hence the expression for vonMises yield stress can be written as;

$$\sigma_{VM}^2 = \frac{1}{2}[(\sigma_1 - \sigma_1)^2 + \sigma_1^2 + \sigma_2^2] \tag{3.50}$$

The various beam and plate theories and formulations presented in this chapter are considered for modeling the elastic deformation of ship hull and its plate structures. Specific theory or formulation to be used in an analysis would depend on the nature and magnitude of wave forces and structural design. Also, through comparison of results, we determine the contributions and effects of, for example, plate nonlinearity, material damping and plate stiffeners.

4. RESULTS: VIBRATIONS OF ISOTROPIC PLATE

This chapter presents the free vibrations and forced vibrations of a rectangular plate, in both frequency domain and time domain. Frequency domain linear analysis of the isotropic plates was carried out using the superposition method, while the time domain analysis for both linear and non-linear vibrations of isotropic plates was performed with the use of finite difference method. An overview of the results to be presented is given below:

1. **Linear vibration analysis of isotropic plates in frequency domain:** Free and forced vibrations are obtained. The mode shapes are compared with the published free vibrations results, Wu et al [84].
2. **Linear vibration analysis of isotropic plates in time domain:** The time histories of mid-point deflection and stress are obtained under the time varying pressure applied on a patch or as a point load on the plate.
3. **Nonlinear vibration analysis of isotropic plates in time domain:** Nonlinear vibration characteristics are studied and compared with that of small-amplitude linear vibrations of an isotropic plate.

4.1 Linear Vibration Analysis of Isotropic Plates in Frequency Domain

An isotropic plate made of steel, with modulus of Elasticity as 200 *GPa*, is considered for the numerical analysis. As given in Chapter 3 by Eqn. 3.19, the linear equation of isotropic plate vibration is given by:

$$\frac{\partial^4 W(\xi,\eta)}{\partial \eta^4} + \frac{2}{\kappa^2}\frac{\partial^4 W(\xi,\eta)}{\partial \xi^2 \partial \eta^2} + \frac{1}{\kappa^4}\frac{\partial^4 W(\xi,\eta)}{\partial \xi^4} - \lambda^4 W(\xi,\eta) = 0 \qquad (4.1)$$

where, $\xi = x/a$, $\eta = y/b$, $\kappa = b/a$ and $\lambda^2 = \omega a^2 \sqrt{\frac{\rho_p}{D}}$. a and b are the plate length and breadth, respectively.

Different values of non-dimensional frequency parameter λ are obtained for the different modes of the free vibrations. These values are enlisted in the Table 4.1.

Mode	**Present Research**	**Wu et al [84]**
1	5.805	5.906
2	8.243	8.347
3	9.245	9.197

Table 4.1: Free vibration frequencies of clamped isotropic plate with aspect ratio 1

Wu et al [86] used Bessel function method to solve for linear free vibration of the isotropic plate. As can be observed from the values given in the above table, the comparison between the results show that the results from the presented research is good with a difference of only about 10%. We present the mode shapes in Figs. 4.1 and 4.2 for two representative cases: λ= 5.805 and λ= 12.855 and on the same figures the results of Wu et al; the results compare well.

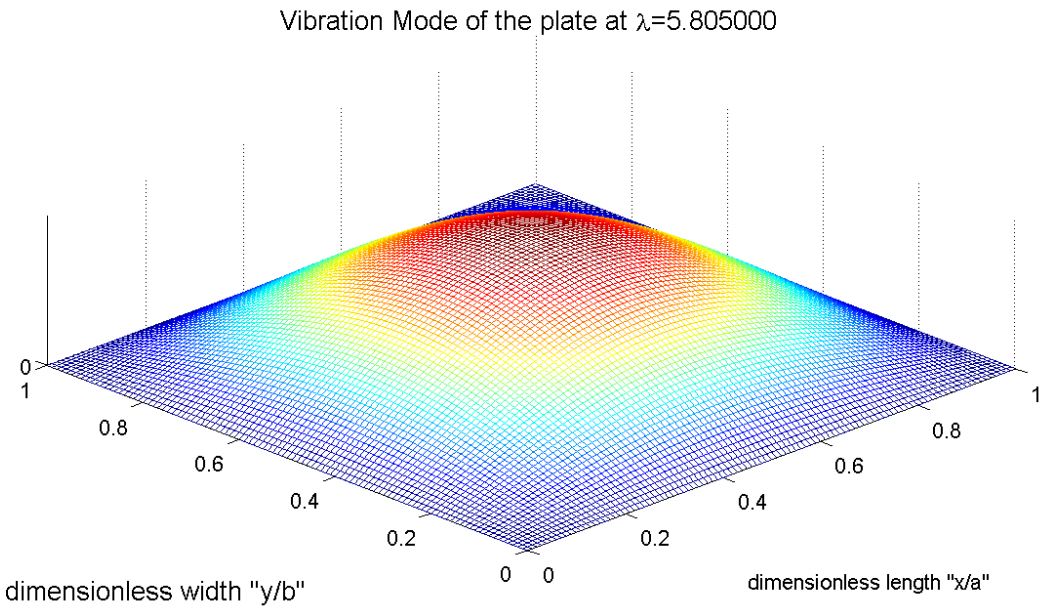

Figure 4.1: Free vibration mode of the clamped isotropic plate at non-dimensional frequency $\lambda = 5.805$. Aspect ratio of the plate $\kappa = 1$, length of the plate a = 1m, breadth of the plate b = 1m, and thickness h = 1 cm

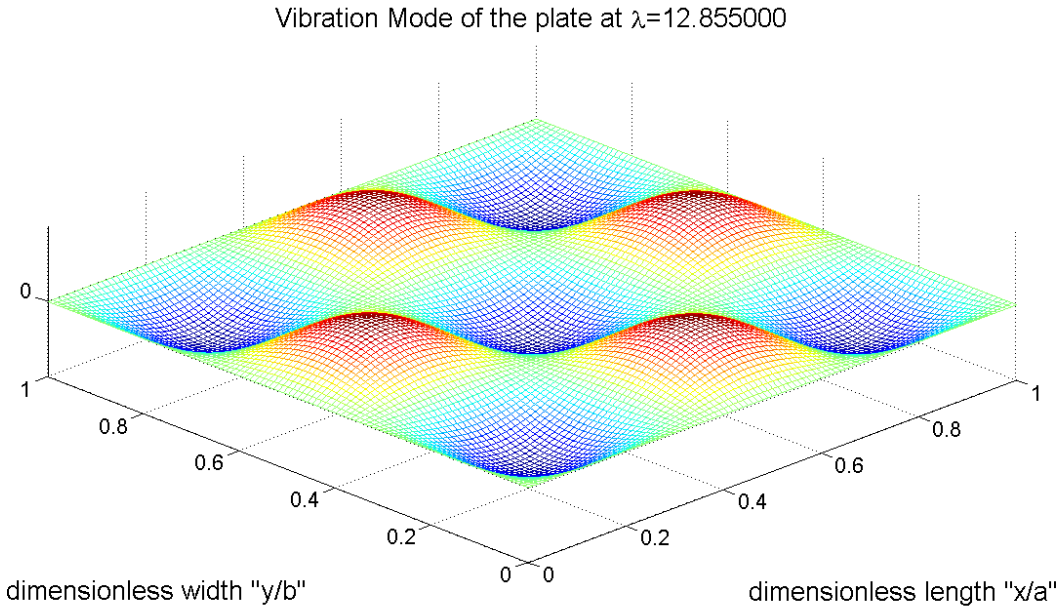

Figure 4.2: Free vibration mode of the clamped isotropic plate at non-dimensional frequency $\lambda = 12.855$. Aspect ratio of the plate $\kappa = 1$, length of the plate a = 1m, breadth of the plate b = 1m, and thickness h = 1 cm

For the forced vibration analysis, Eqn. 3.19 can be solved using the method of superposition by introducing one more superposition block in addition to the four blocks shown in Fig. 3.2 and as discussed in Chapter 3. This fifth block considered here, as shown in Fig. 4.3, has its boundaries defined as simply supported and the load as a point pulsating load at various locations of the plate.

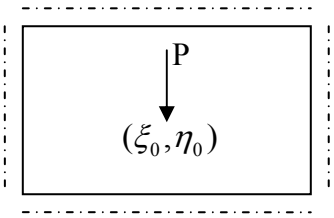

Figure 4.3: fifth block in addition of the four blocks showed in Fig. 3.2. A point pulsating load P is acting on the point (ξ_0, η_0)

Eqn. (3.19) can be rewritten in a way more specific to the point pulsating load problem as;

$$\frac{\partial^4 W(\xi,\eta)}{\partial \eta^4} + \frac{2}{\kappa^2}\frac{\partial^4 W(\xi,\eta)}{\partial \xi^2 \partial \eta^2} + \frac{1}{\kappa^4}\frac{\partial^4 W(\xi,\eta)}{\partial \xi^4} - \lambda^4 W(\xi,\eta) \tag{4.2}$$

$$= \frac{P}{Dh}\kappa^4 a^4 \delta(\xi - \xi_0)\delta(\eta - \eta_0)$$

where, P is the amplitude of the load and (ξ_0, η_0) is the location of the impact on the plate and δ is the delta function representing the point loading. The solution for the simply supported plate can be expressed as [26] and [27];

$$W_5(\xi,\eta) = \sum_{m=1}^{K}\sum_{n=1}^{K} E_{mn} Sin(m\pi\xi) Sin(n\pi\eta) \tag{4.3}$$

where, K is the number of *sine* terms in the series. Using the orthogonal property of trigonometric functions and property of delta function, the unknown E_{mn} can be expressed in terms of pressure amplitude P, and can be written as;

$$E_{mn} = \frac{4P\kappa^4 a^4 Sin(m\pi\xi_0)Sin(n\pi\eta_0)}{Dh(m^4\pi^4\kappa^4 + 2m^2n^2\pi^4\kappa^2 + n^4\pi^4 - \kappa^4)} \tag{4.4}$$

To obtain the solution for clamped plate vibrations, fifth block solution for the deflection is added to the Eqn. 3.32. Expression for the deflection can be written as;

$$W(\xi,\eta) = \sum_{j=1}^{5} W_j(\xi,\eta) \tag{4.5}$$

First four blocks denoting the homogenous solution and the fifth block in the particular solution corresponding to the point loading. The unknowns in the above expression can be determined by applying the boundary conditions, as given by Eqn. 3.33 in Chapter 3, and by using a matrix inversion.

Case 1: Plate's geometric and material characteristics: plate length a = 1m, plate breadth b = 1m, plate aspect ratio b/a = 1, plate thickness h = 1cm, modulus of elasticity E = 200 GPa, pressure amplitude = 70 kPa, point loading location: ξ = 0.5, η=0.5.

Figs. 4.4, 4.5 and 4.6 show the plate deformation modes at different forcing frequencies which are close to the free vibration frequencies of the clamped plate. For example, in Fig. 4.4, It can be seen that if the forcing frequency is close to the fundamental frequency of the free vibrations of the clamped isotropic plate, the plate deflection reaches to a very large value because of the resonance. Theoretically, deflection of the plate at resonant frequency should reach to infinity but it's not possible to depict such responses.

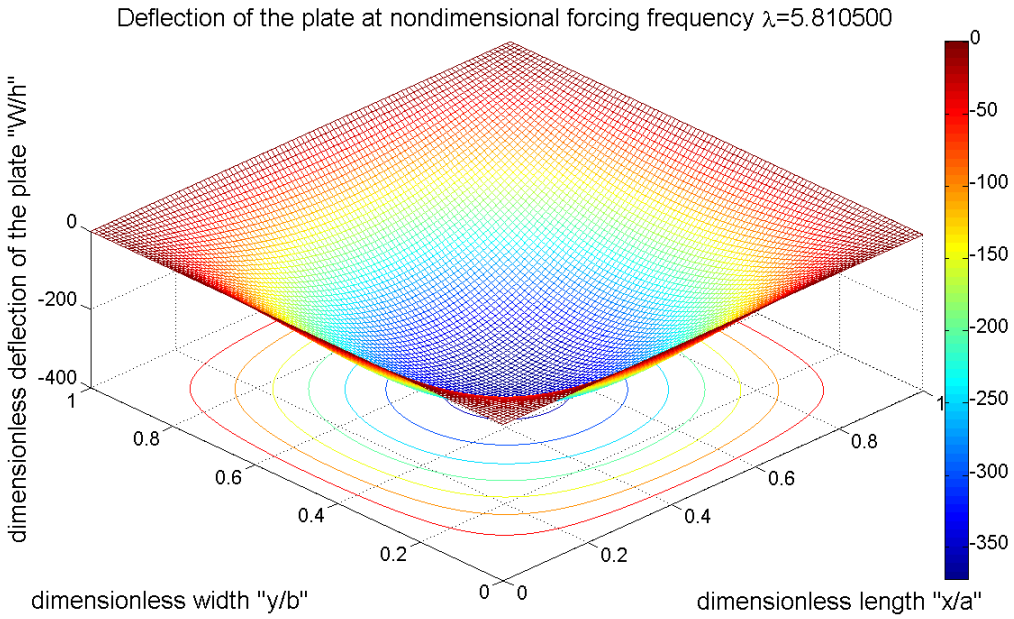

Figure 4.4: Plate deflection mode at non-dimensional forcing frequency λ = 5.805. Maximum pressure amplitude P = 70 kPa, plate aspect ratio b/a= 1, plate length a=1 m, plate breadth b=1m, plate thickness =1 cm, location of point load = (0.5, 0.5)

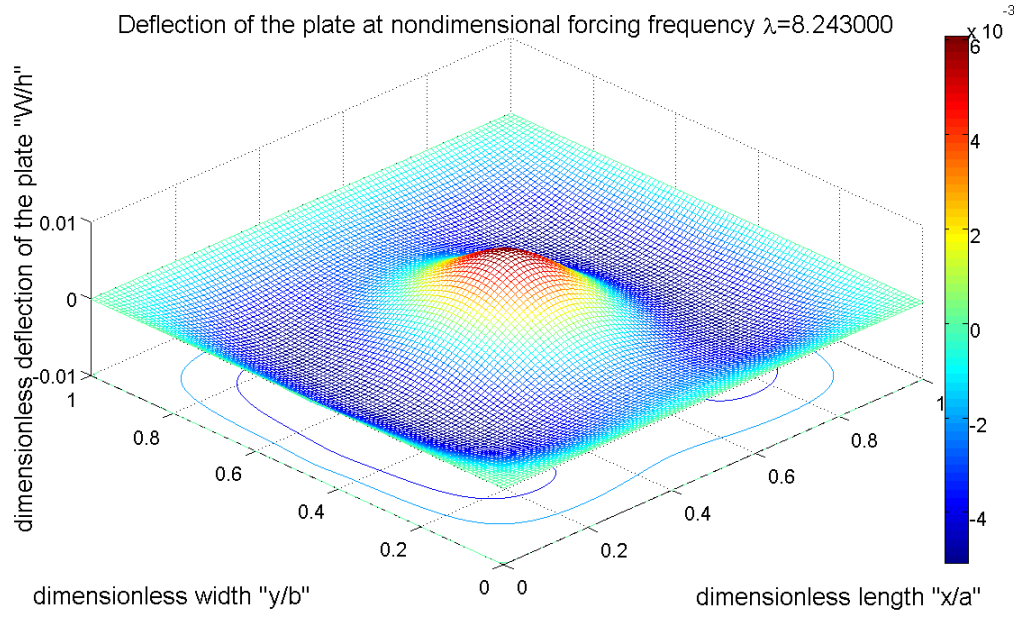

Figure 4.5: Plate deflection mode at non-dimensional forcing frequency λ = 8.243. Maximum pressure amplitude P = 70 kPa, plate aspect ratio b/a= 1, plate length a=1 m, plate breadth b=1m, plate thickness =1 cm, location of point load = (0.5, 0.5)

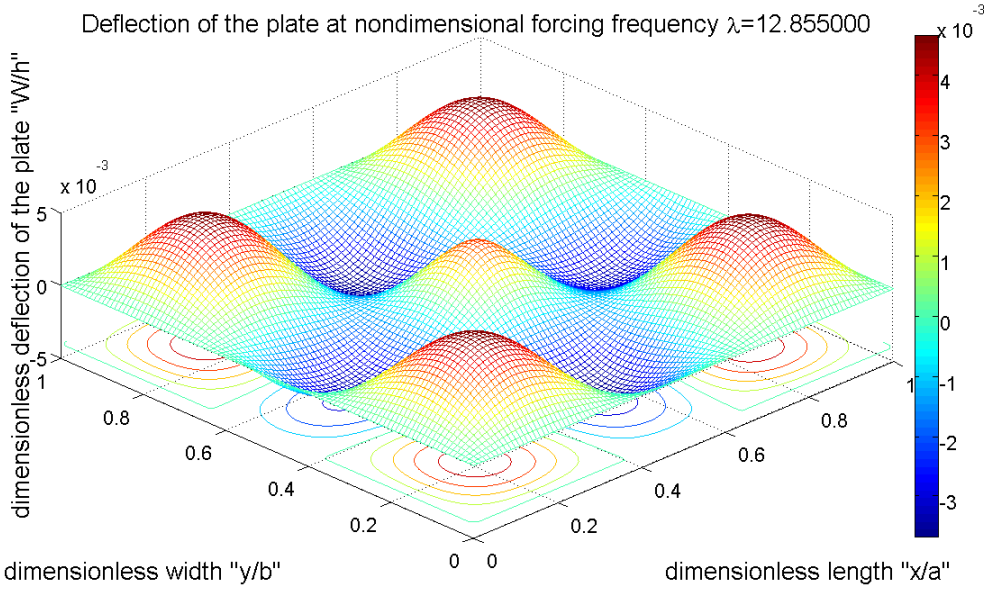

Figure 4.6: Plate deflection mode at non-dimensional forcing frequency λ = 12.855. Maximum pressure amplitude P = 70 kPa, plate aspect ratio b/a= 1, plate length a=1 m, plate breadth b=1m, plate thickness =1 cm, location of point load = (0.5, 0.5)

*Case2***:** Plate's geometric and material characteristics: plate length a = 1m, plate breadth b = 1m, plate aspect ratio b/a = 1, plate thickness h = 1cm, modulus of elasticity E = 200 GPa, pressure amplitude = 70 kPa, location = ($\xi = 0.25, \eta = 0.25$).

Figs. 4.7, 4.8 and 4.9 show the plate's modes of deflections under three different frequencies applied at different locations, as specified above. As we have seen before, if the forcing frequency falls in the proximity of the fundamental frequency of the free vibrations of the plate, larger deflection of the plate is observed, Fig. 4.7, and the location of the point of impact also does not matter in this case. In Figs. 4.8 and 4.9, it can be seen that the location of the applied load gives unsymmetrical small deformations when forcing frequency doesn't match or is not in the proximity.

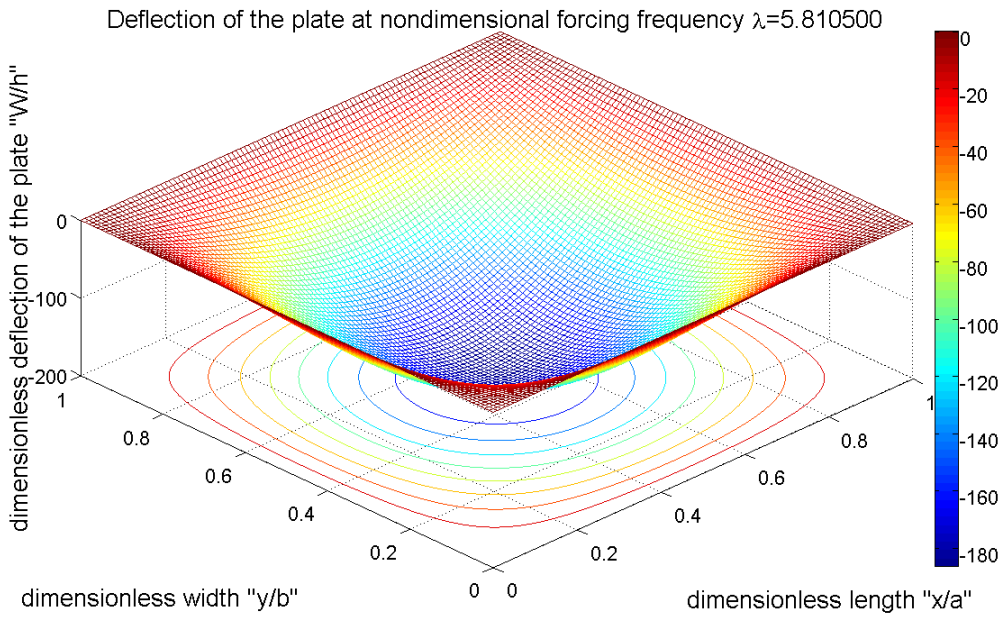

Figure 4.7: Plate deflection mode at non-dimensional forcing frequency λ = 5.8105. Maximum pressure amplitude P = 70 kPa, plate aspect ratio b/a= 1, plate length a=1 m, plate breadth b=1m, plate thickness =1 cm, location of point load = (0.25, 0.25)

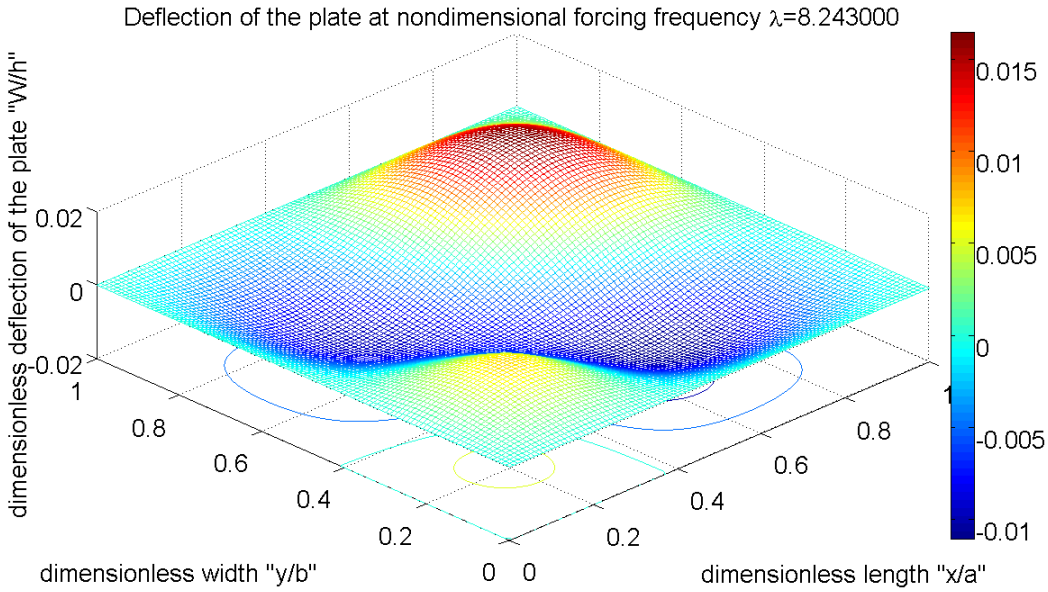

Figure 4.8: Plate deflection mode at non-dimensional forcing frequency λ = 8.243. Maximum pressure amplitude P = 70 kPa, plate aspect ratio b/a= 1, plate length a=1 m, plate breadth b=1m, plate thickness =1 cm, location of point load = (0.25, 0.25)

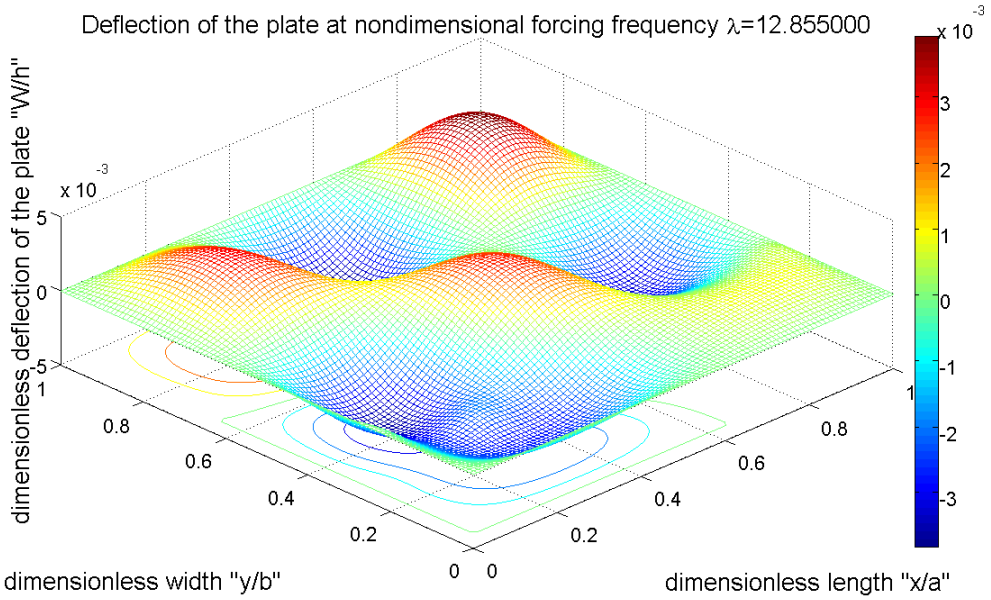

Figure 4.9: Plate deflection mode at non-dimensional forcing frequency λ = 12.855. Maximum pressure amplitude P = 70 kPa, plate aspect ratio b/a= 1, plate length a=1 m, plate breadth b=1m, plate thickness =1 cm, location of point load = (0.25, 0.25)

Case 3: Plate's geometric and material characteristics: plate length a = 2m, plate breadth b = 1m, plate aspect ratio b/a = 0.5, plate thickness h = 1cm, modulus of elasticity E = 200 GPa, pressure amplitude = 70 kPa, location at ($\xi = 0.5$, $\eta = 0.5$). Figs. 4.10, 4.11 and 4.12 illustrate the forced vibration mode of a rectangular plate with aspect ratio *b/a=0.5*. As expected, the long crested vibrations are developed on the longer side of the plate and because the loading is concentrated at the center, the vibrations are symmetrical.

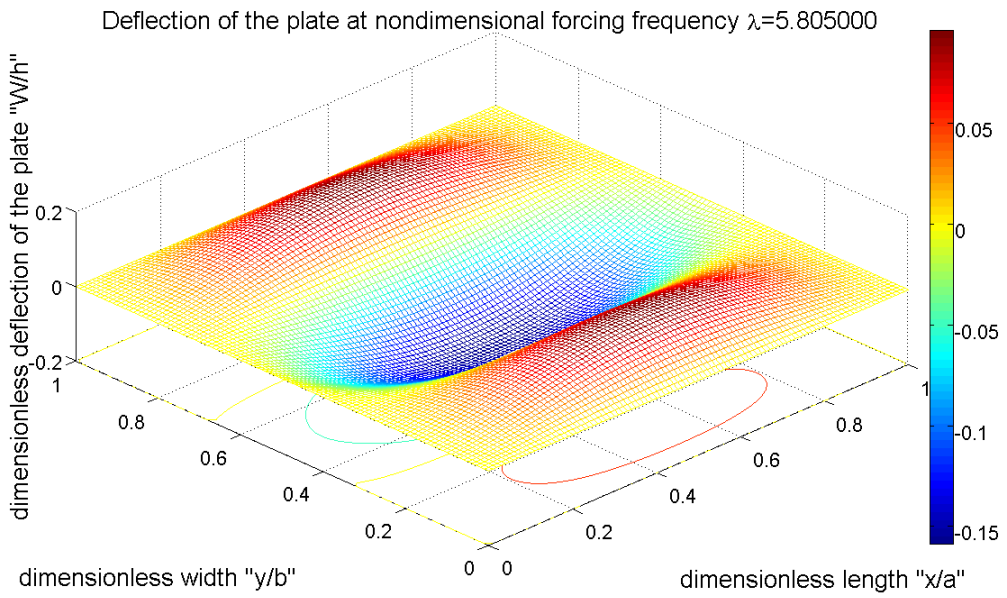

Figure 4.10: Plate deflection mode at non-dimensional forcing frequency λ = 5.805. Maximum pressure amplitude P=70 kPa, plate aspect ratio b/a=0.5, plate length a=2 m, plate breadth b=1 m, plate thickness =1 cm, location of point load=(0.5, 0.5)

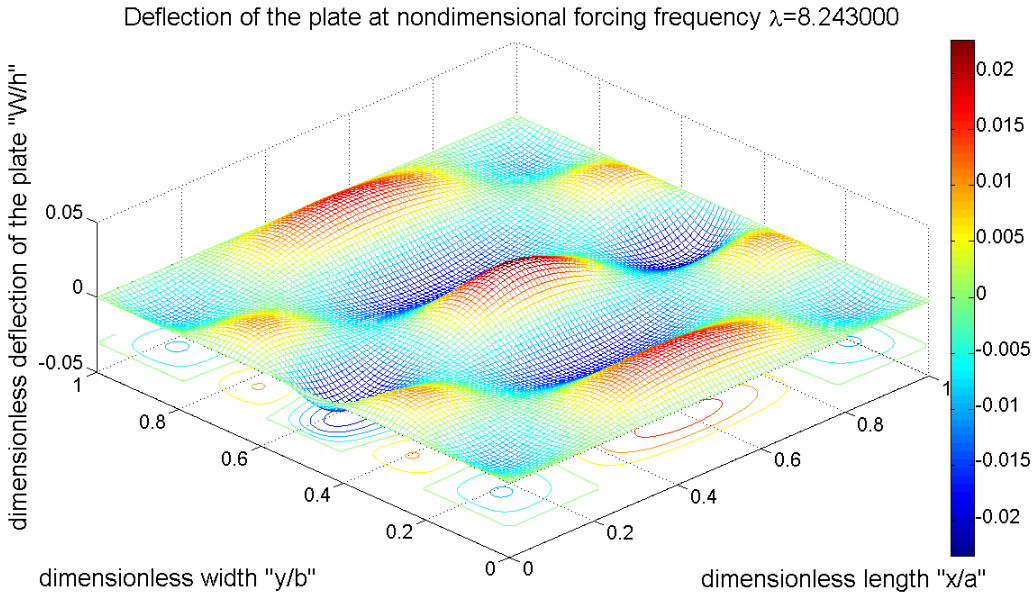

Figure 4.11: Plate deflection mode at non-dimensional forcing frequency λ = 8.243. Maximum pressure amplitude P=70 kPa, plate aspect ratio b/a=0.5, plate length a=2 m, plate breadth b=1 m, plate thickness =1 cm, location of point load=(0.5, 0.5)

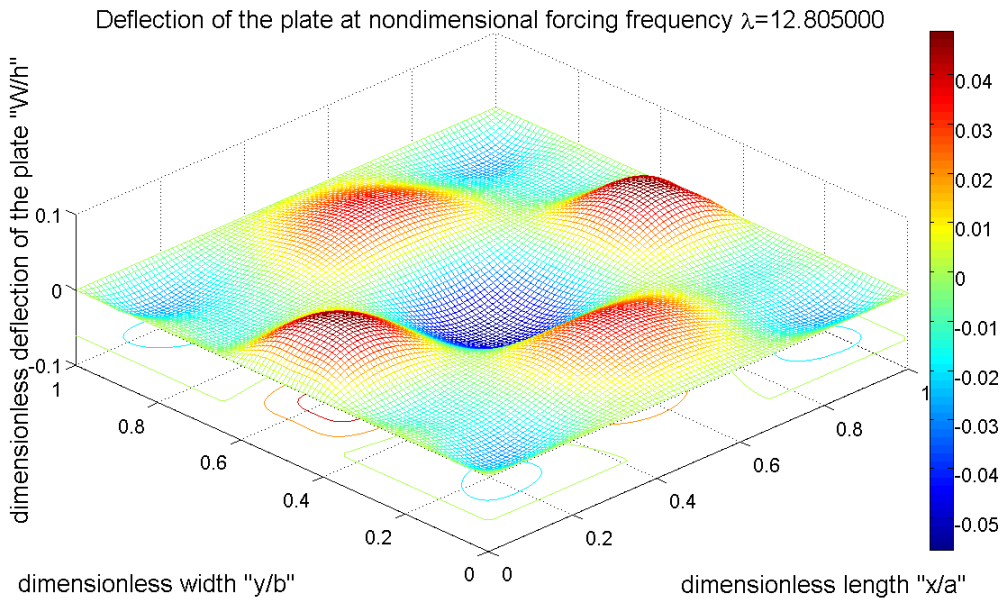

Figure 4.12: Plate deflection mode at non-dimensional forcing frequency λ = 12.805. Maximum pressure amplitude P=70 kPa, plate aspect ratio b/a=0.5, plate length a=2 m, plate breadth b=1 m, plate thickness =1 cm, location of point load=(0.5, 0.5)

Case 4: Plate's geometric and material characteristics: plate length a = 2m, plate breadth b = 1m, plate aspect ratio b/a = 0.5, plate thickness h = 1cm, modulus of elasticity E = 200 GPa, pressure amplitude = 70 kPa, location at ($\xi = 0.25, \eta = 0.25$). Following Figs. 4.13, 4.14 and 4.15 depicts the last case of forced plate vibrations of isotropic plates in the frequency domain. In these forced modes, the point load is applied to the location specified above.

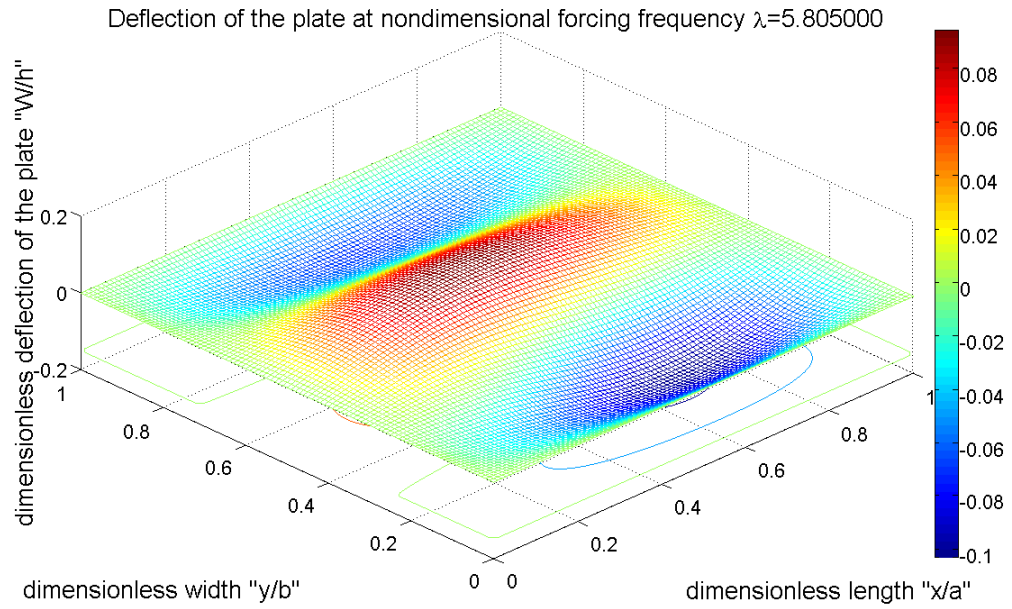

Figure 4.13: Plate deflection mode at non-dimensional forcing frequency λ = 5.805. Maximum pressure amplitude P=70 kPa, plate aspect ratio b/a=0.5, plate length a=2 m, plate breadth b=1 m, plate thickness =1 cm, location of point load=(0.25, 0.25)

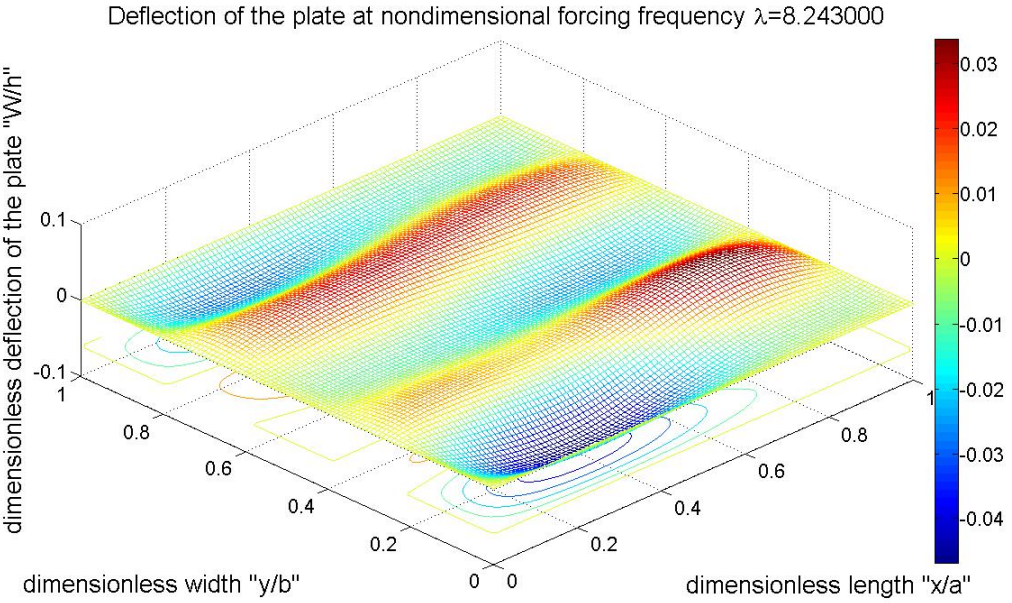

Figure 4.14: Plate deflection mode at non-dimensional forcing frequency λ = 8.243. Maximum pressure amplitude P=70 kPa, plate aspect ratio b/a=0.5, plate length a=2 m, plate breadth b=1 m, plate thickness =1 cm, location of point load=(0.25, 0.25)

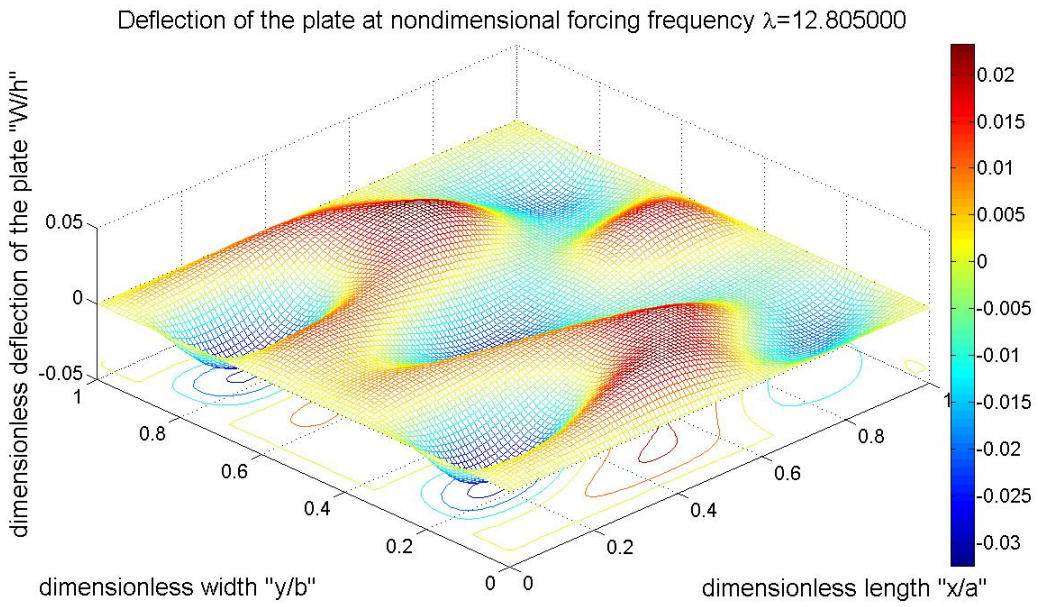

Figure 4.15: Plate deflection mode at non-dimensional forcing frequency λ = 8.243. Maximum pressure amplitude P=70 kPa, plate aspect ratio b/a=0.5, plate length a=2 m, plate breadth b=1 m, plate thickness =1 cm, location of point load=(0.25, 0.25)

4.2 Linear Vibration Analysis of Isotropic Plates in Time Domain

In the time domain, linear vibration analysis of the isotropic plates has been done for different kinds of pressure variations such as Froude Krylov pressure, slamming pressure using Wagner's theory, Slamming pressure using ABS rules with assumed time profile and the pressure obtained from the work of Ananthakrishnan [53]. Obtained results are categorized in to several sections according to the type of pressure variation as follows;

4.2.1 Froude-Krylov pressure

In this section, time domain analysis for the linear isotropic plate vibrations has been done carried out with the fluid loading taken to be that of the Froude-Krylov force only. The results are obtained for 3 different sea states, and deflection and stresses at the

center of the plate are plotted over a span of time. The draft of the plate is kept as 1m. The plate is assumed to be made of steel with length = 1m, breadth=1m and the thickness=1cm. Modulus of elasticity for the steel plate is taken as 200GPa and the yield stress for the steel plate is known i.e. 250MPa.

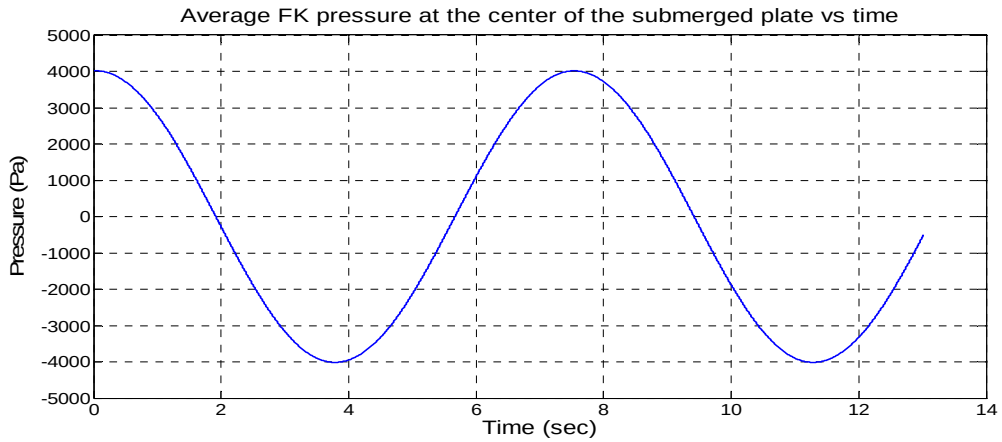

Figure 4.16: Froude-Krylov pressure at the center of the plate for sea-state 3

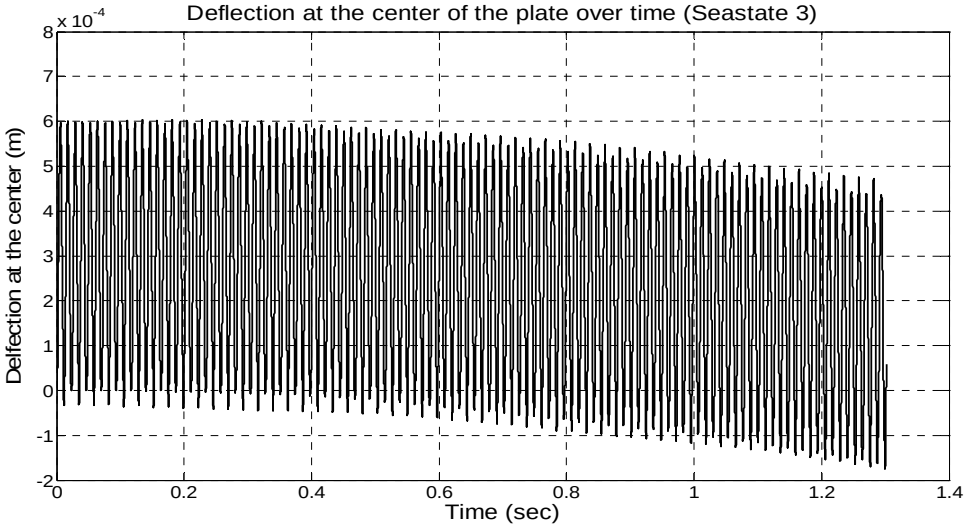

Figure 4.17: Deflection at the center of the plate under Froude-Krylov pressure. Sea State 3: Wave height = 0.88m, time period=7.5sec, length of the plate=1m, breadth of the plate=1m, thickness=1cm

Fig. 4.16 shows the Froude-Krylov pressure at the center of the isotropic plate. The pressure is determined using the average wave height and the average zero crossing wave period, Edwards [84].

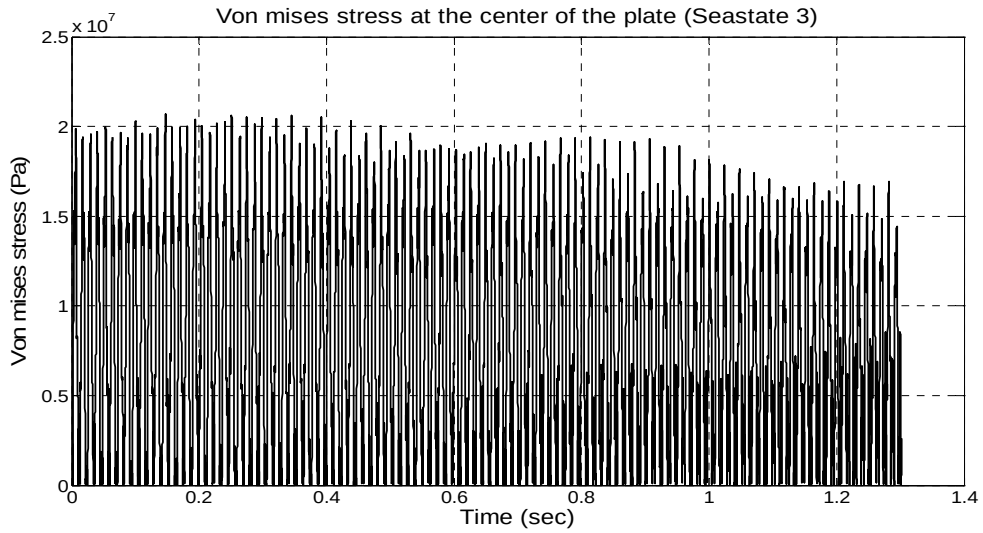

Figure 4.18: Stress at the center of the plate under Froude-Krylov pressure. Sea State 3: Wave height = 0.88m, time period=7.5sec, length of the plate=1m, breadth of the plate=1m, thickness=1cm

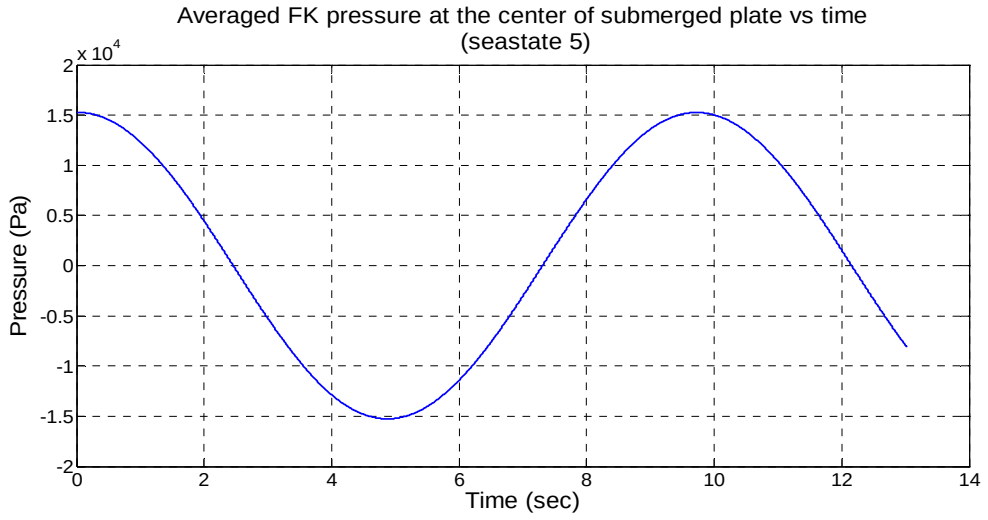

Figure 4.19: Froude-Krylov Pressure at the center of the plate vs. time for sea state 5

Fig. 4.17 and 4.18 show the defelction and the von Mises stress at the center of the plate for seastate 3 Froude-Krylov pressure. Stress at the center of the plate, Fig. 4.18, remains under the yield stress limit.

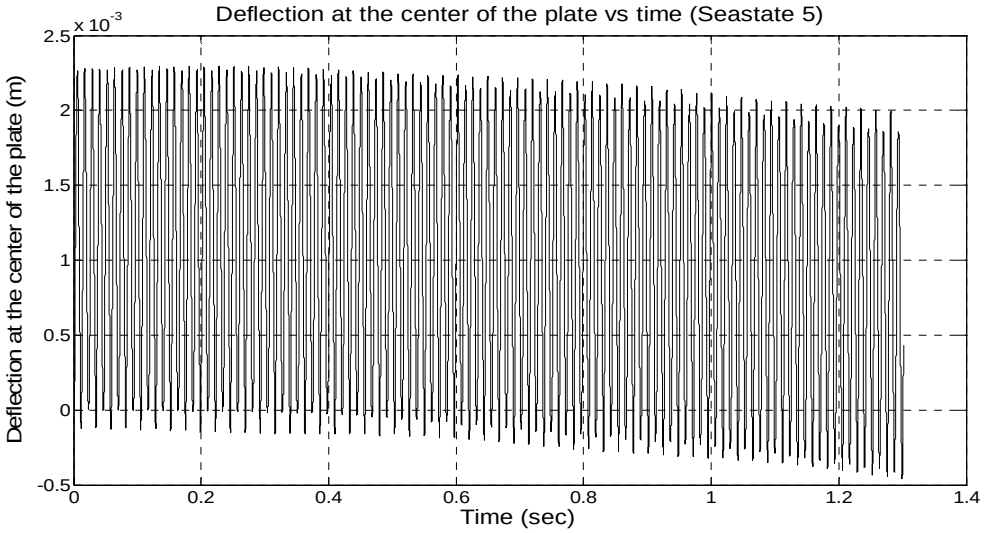

Figure 4.20: Deflection at the center of the plate under Froude-Krylov pressure. Sea State 5: Wave height = 3.25m, time period=9.7sec, length of the plate=1m, breadth of the plate=1m, thickness=1cm

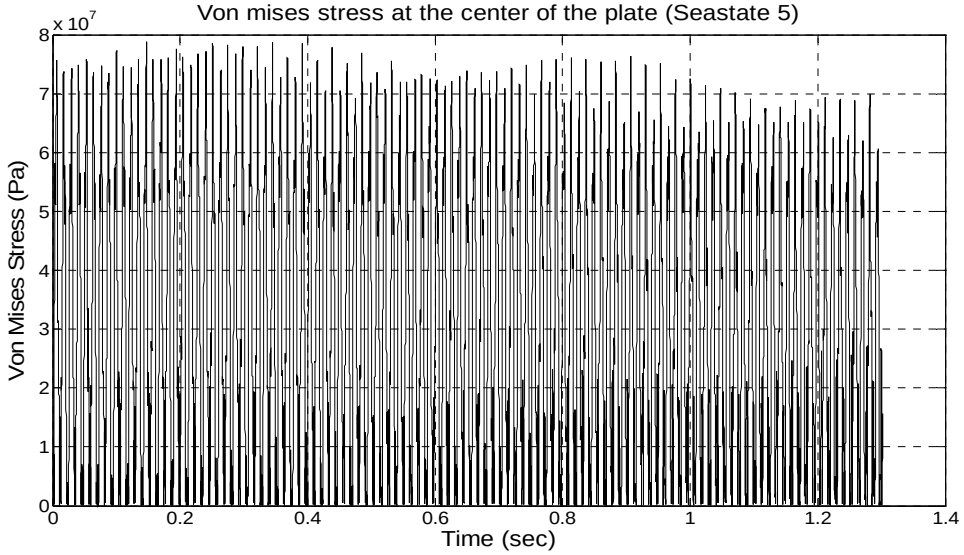

Figure 4.21: Stress at the center of the plate under Froude-Krylov pressure. Sea State 5: Wave height = 3.25m, time period=9.7sec, length of the plate=1m, breadth of the plate=1m, thickness=1cm

Fig. 4.19 depicts the pressure variation over time at the center of the plate under seastate 5. It can be observed from Fig. 4.21 that the von Mises stress has increased as compared to the seastate 3 case but still remains under the yield stress limit. Fig. 4.20 gives the time profile of the deflection of the plate.

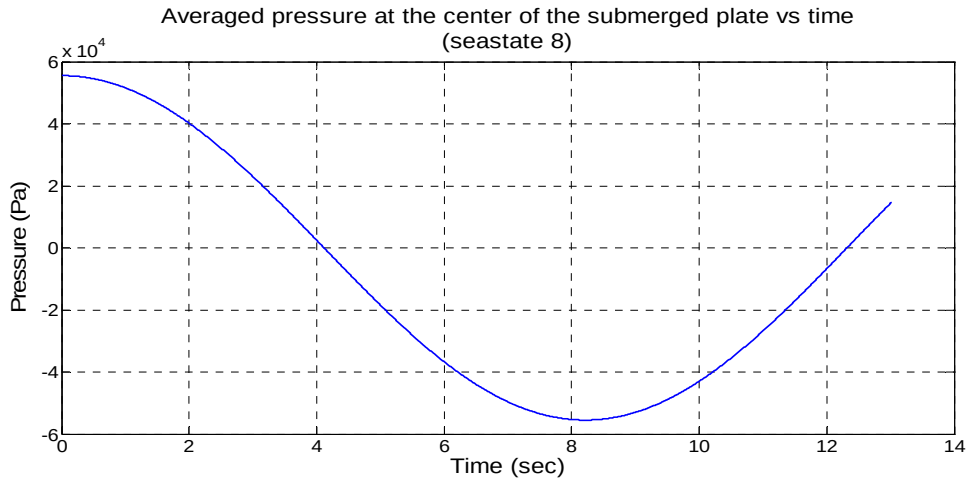

Figure 4.22: Froude-Krylov Pressure at the center of the plate vs. time for sea state 8

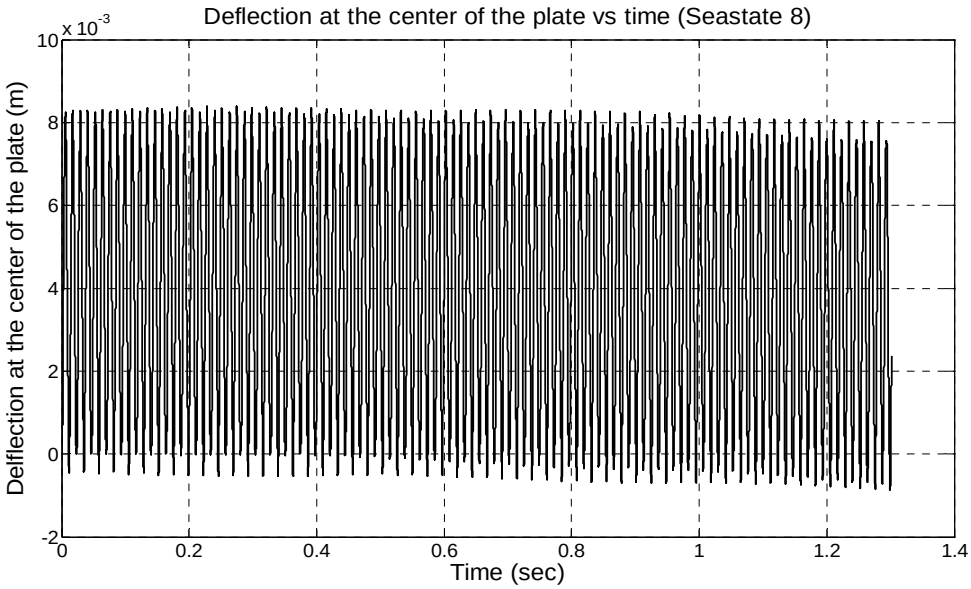

Figure 4.23: Deflection at the center of the plate under Froude-Krylov pressure. Sea State 8: Wave height = 11.5m, time period=16.4sec, length of the plate=1m, breadth of the plate=1m, thickness=1cm

Fig. 4.22 illustrates the Froude-Krylov pressure at the center of submerged plate at sea state 8. It can be seen that as the sea-state level increases, amplitude of the pressure increases.

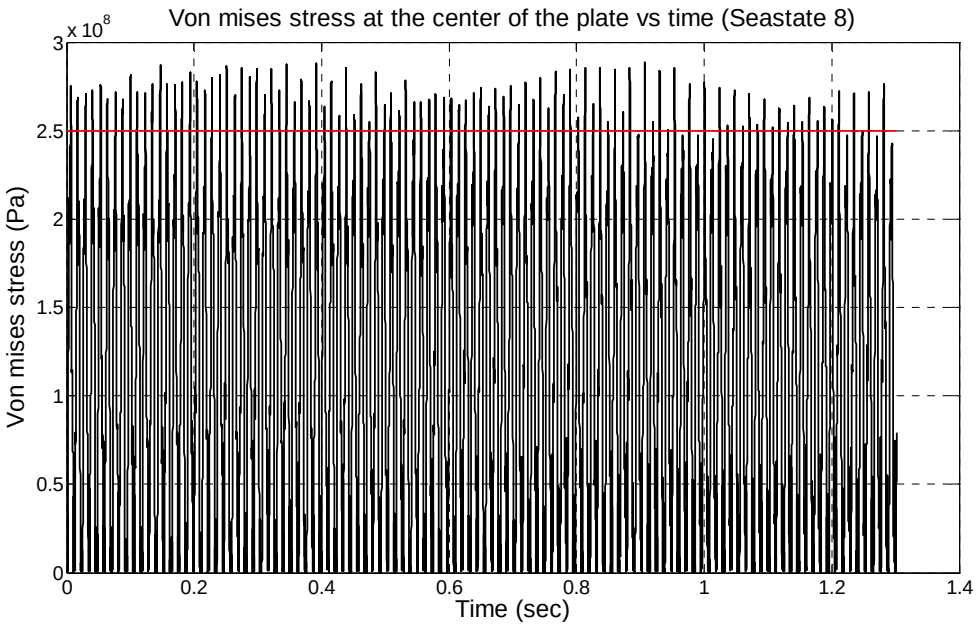

Figure 4.24: Stress at the center of the plate under Froude-Krylov pressure. Sea State 8: Wave height = 11.5m, time period=16.4sec, length of the plate=1m, breadth of the plate=1m, thickness=1cm

Fig. 4.23 shows the deflection of the center of the plate over time and Fig. 4.24 illustrates von Mises stress which is developed at the center of the plate due to the periodic loading. It can be seen that at the higher sea state level stresses can surpass the yield stress but remain under the ultimate stress limit of the steel i.e. 400 MPa.

4.2.2 Slamming Pressure using ABS rules

Design slamming pressure is obtained using an empirical formula given in ABS rules for high-speed marine vehicles. Empirical formulas provide the static slamming

pressure, so two time profiles have been chosen to determine the plate response, (i) $f(t) = \frac{1}{\sqrt{t}}$, which is based on Wagner's theory, and (ii) periodic spike function, which is based on the experimental nature of wave slamming event. The spatial distribution considered is also of two types, (i) pressure concentrated at a point, and (ii) pressure distributed over an area. Following results are presented to show the effect of these slamming loading on the ship hull plate panels.

(i) Wagner's type profile

Plate dimensions and material properties are kept same, i.e., length of the plate a = 1m, breadth of the plate b = 1m, thickness of the plate h = 1cm, and modulus of elasticity E = 200GPa. The time variation profile $f(t) = \frac{1}{\sqrt{t}}$ for the design slamming pressure is shown in Fig. 4.25 and the spatial distribution of the slamming pressure is depicted in Fig. 4.27. Fig. 4.26 (a) shows that the pressure is concentrated at the center of the plate whereas Fig. 4.26 (b) shows that the slamming pressure is distributed over an area of the isotropic plate.

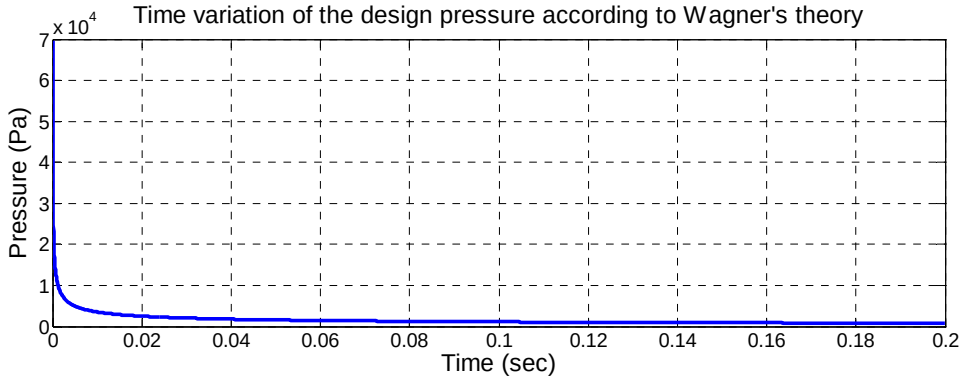

Figure 4.25: Time variation of the design pressure similar to Wagner's slamming pressure profile

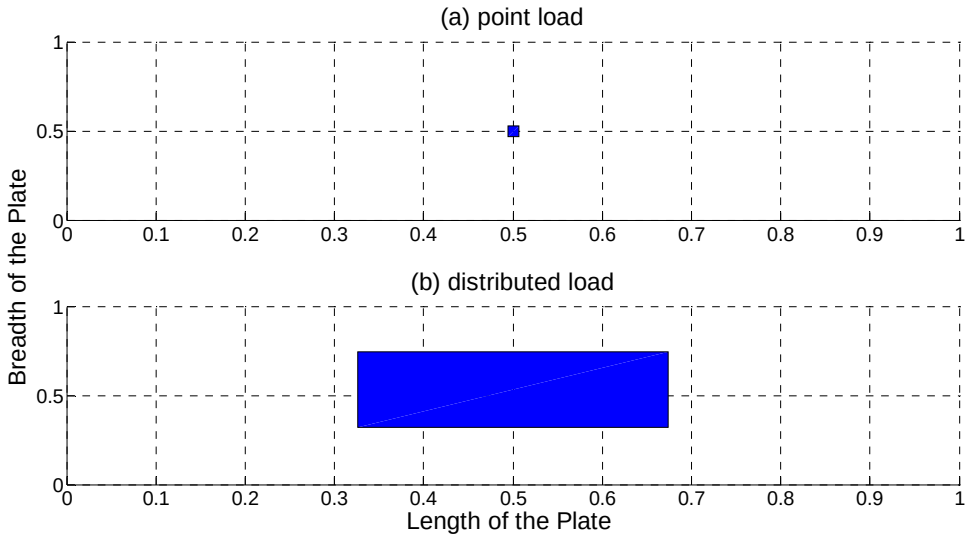

Figure 4.26: Spatial distribution of the pressure on the plate, (a) pressure is concentrated at the center of the plate, and (b) pressure is distributed over an area (a/3*b/3) of the plate i.e. 1/9th of the plate area.

The numerical simulation was carried out with the time step of $2.6*10^{-5}$ sec and Figs. 4.27 and 4.28 show the deflection and von Mises stress at the center of the plate over time. Fig. 4.25 shows that in this kind of time profile pressure drops very quickly from maximum to mimimum and after this phase of pressure excitement, plate starts to vibrate with its natural frequency. It can be seen that point loading also excites some higher order vibration frequencies but this type of spatial distirbution of the load is highly improbable.

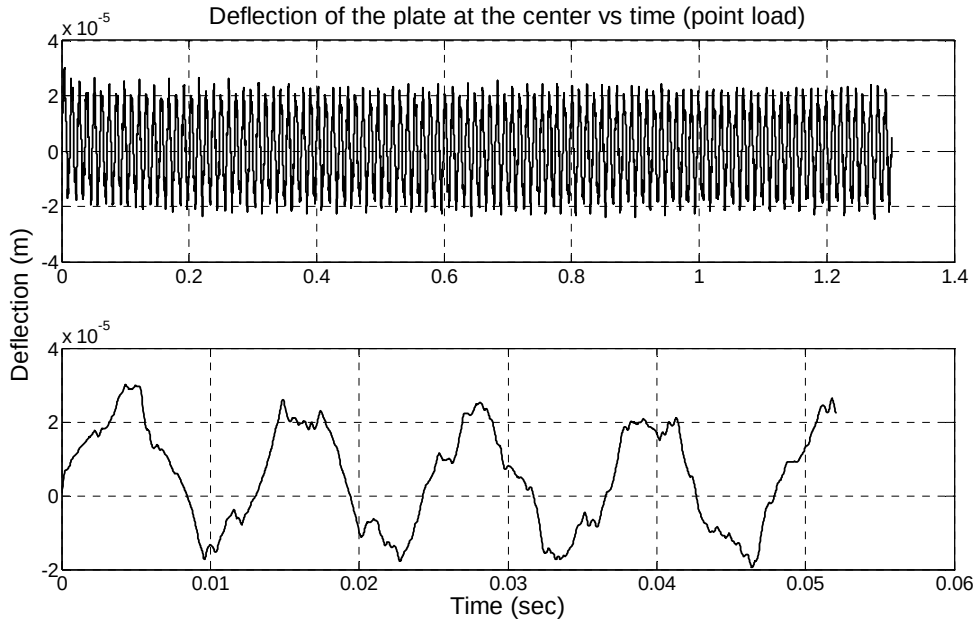

Figure 4.27: Deflection of the center of the plate vs. time. a = 1m, b = 1m, h = 1cm, time step = 2.6*10-5 sec. Maximum slamming pressure = 70 kPa with Wagner's type time profile at the center of the plate shown in Fig. 4.26(a).

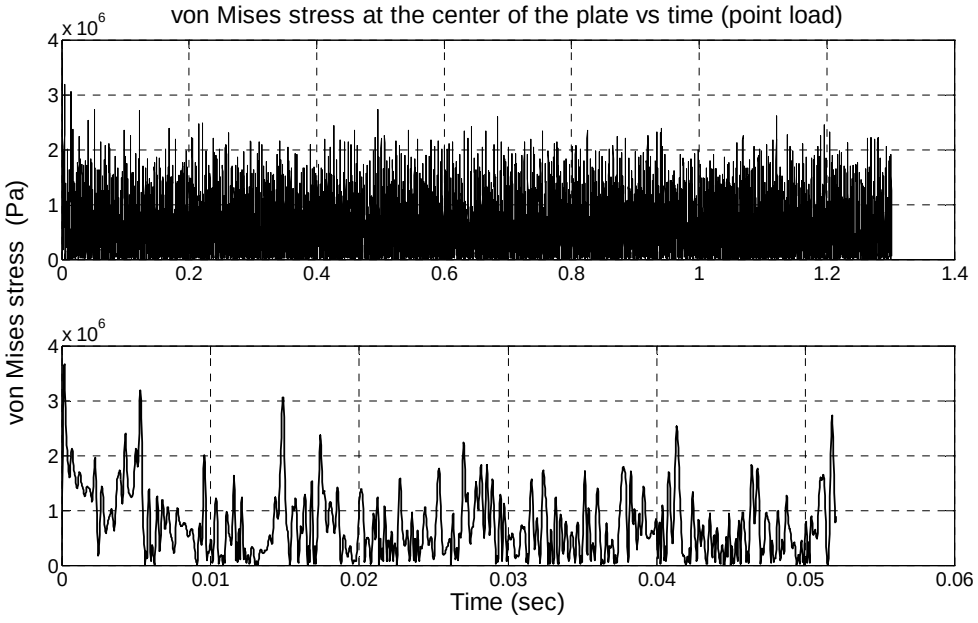

Figure 4.28: von Mises stress of the center of the plate vs. time. a = 1m, b = 1m, h = 1cm, time step = 2.6*10-5 sec. Maximum slamming pressure = 70 kPa with Wagner's type time profile at the center of the plate shown in Fig. 4.26(a).

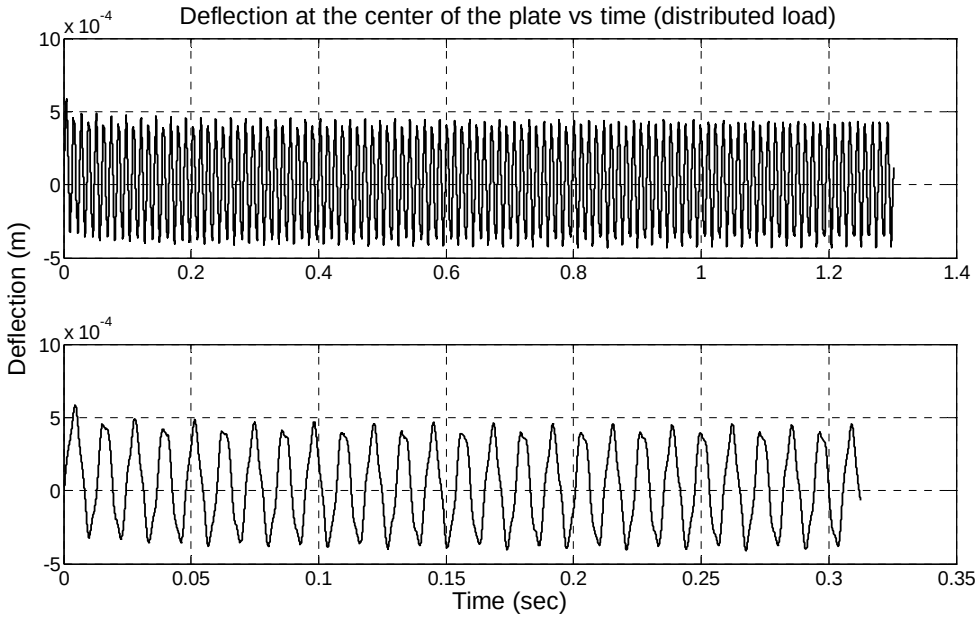

Figure 4.29: Deflection of the center of the plate vs. time. a = 1m, b = 1m, h = 1cm, time step = 2.6*10-5 sec. Maximum slamming pressure = 70 kPa with Wagner's type time profile distributed over a part of the plate shown in Fig. 4.26(b).

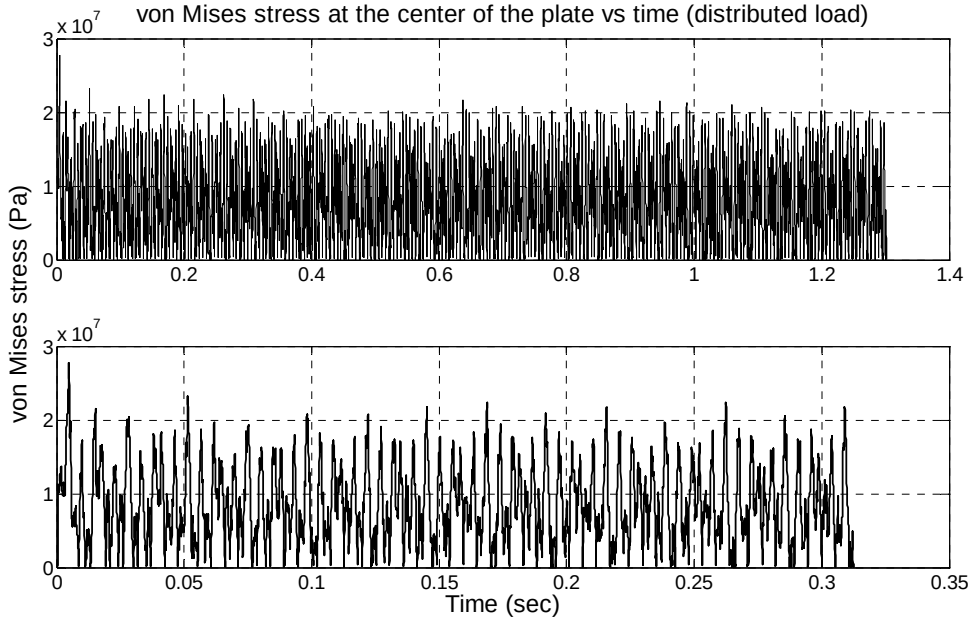

Figure 4.30: von Mises stress at the center of the plate vs. time. a = 1m, b = 1m, h = 1cm, time step = $2.6*10^{-5}$ sec. Maximum slamming pressure = 70 kPa with Wagner's type time profile distributed over a part of the plate shown in Fig. 4.26(b).

Figs. 4.29 and 4.30 show the deflection and von Mises stress at the center of the palate over time. It can be observed that distributed pressure results in higher stresses and deflection, while the plate vibrates in a smoother profile as compared to the point loading case, Fig. 4.27. This model of spatial distribution is more practical because wave slamming occurs over an area of the plate.

(ii) time profile observed in experiments

In real life scenarios, wet-deck slamming is not one time phenomenon. Wet-deck slamming occurs repeatedly, especially in rough seas. In order to simulate the real life scenario, we combine the design pressure with intermittent spike function as shown below with recurrence relating to ship's wave encounter frequency.

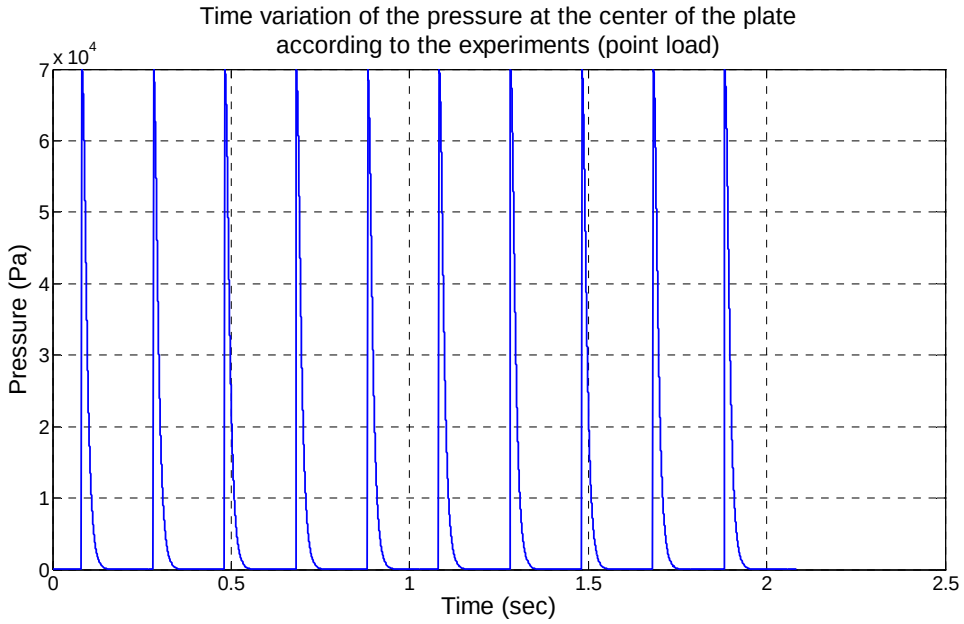

Figure 4.31: Time variation of the design pressure similar to experimental profile given in [92]

It has been observed in the experiments that wet-deck slamming takes a delta function formulation i.e. pressure reaches to a high value in a very short span of time. It's

not easy to simulate delta function numerically, so, to overcome this problem a spike function formulation is adopted. The spike function is expressed as in Xin and Wong [89]:

$$P(t) = P_{max} \sum_{i=1}^{M} \left[\cosh\left(\frac{t - t_i}{\epsilon} \right) \right]^{-1} \tag{4.6}$$

where, P_{max} is the maximum design pressure and ϵ is the width of spike function. Spike is center at $t = t_i$ and it can be applied after an interval of time to obtain a train of slamming pressure spikes, as shown in Fig. 4.31.

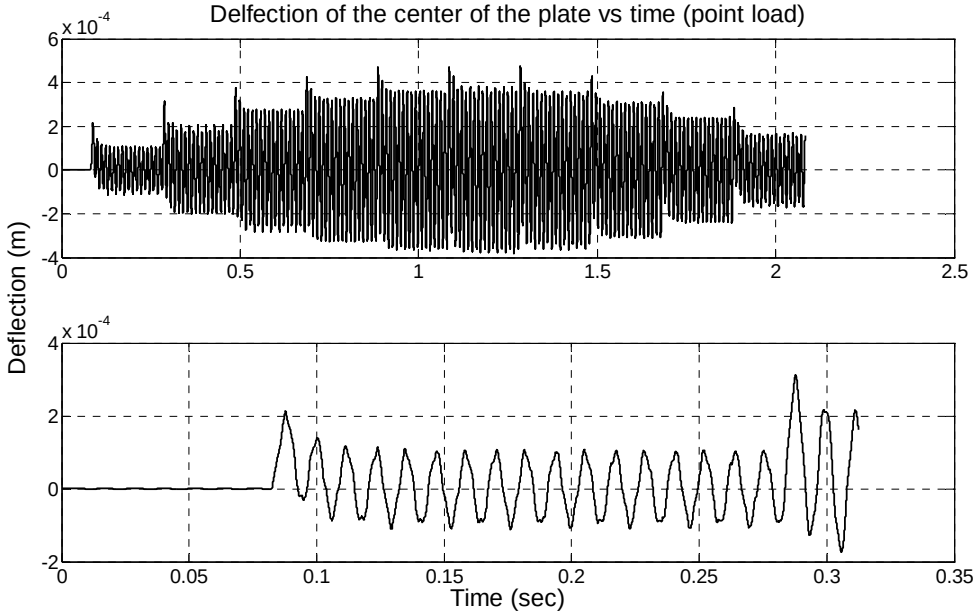

Figure 4.32: Deflection of the center of the plate vs. time. a = 1m, b = 1m, h = 1cm, time step = $2.6*10^{-5}$ sec. Maximum slamming pressure = 70 kPa with periodic spike at the center of the plate shown in Fig. 4.26(a).

Spike type loading is applied on isotropic plate as a point load as well as a distributed load. Plate's geometrical and material characteristics are kept same as previous section of Wagner's type loading results. Figs. 4.32 and 4.33 show the

deflection and von Mises stress at the center of the isotropic plate over time, respectively, due to point loading while Figs. 4.34 and 4.35 depict the deflection and von Mises stress at the center due to distributed loading. It is seen that the distributed pressure, results in larger amplitude of vibrations and stresses. Periodic spike type loading results in the development of larger stresses as compared to Wagner's type loading. In Fig. 4.35, it can be seen that at several instants von Mises stress at the center of the plate surpasses the yield stress limit. This kind of repeated behavior can lead to the structural failure of the plate panels.

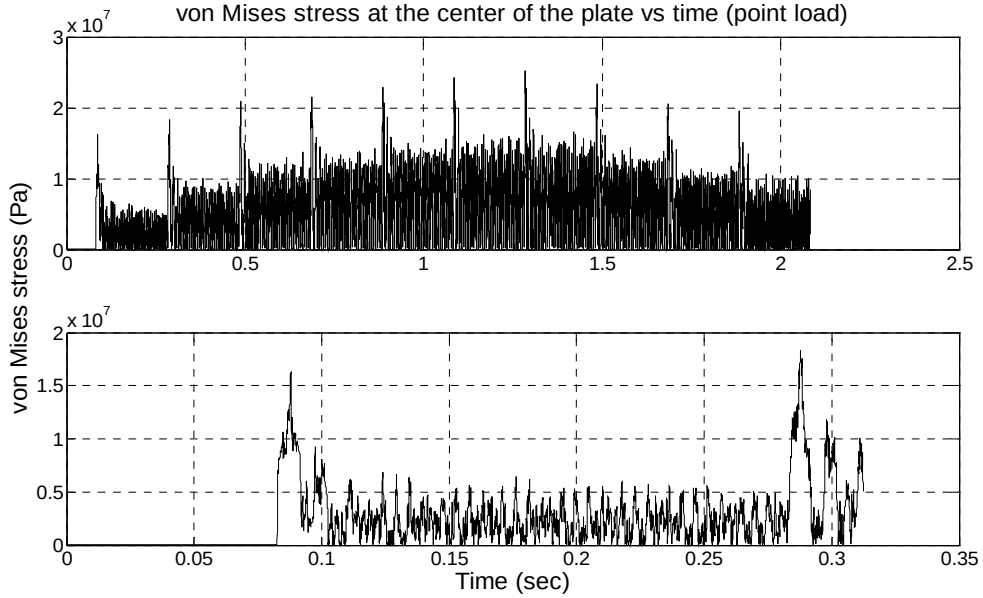

Figure 4.33: von Mises stress at the center of the plate vs. time. a = 1m, b = 1m, h = 1cm, time step = $2.6*10^{-5}$ sec. Maximum slamming pressure = 70 kPa with periodic spike at the center of the plate shown in Fig. 4.26(a).

As already discussed ABS provides only an estimated value of wet-deck slamming pressure. Next section of results is obtained by implementing the Wagner's theory, discussed in Chapter 2.

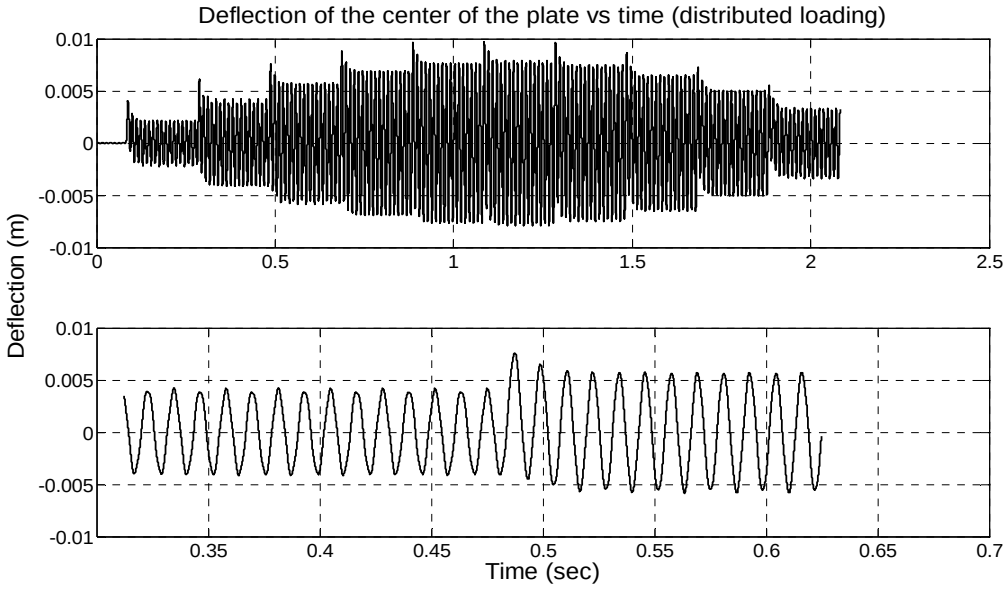

Figure 4.34: Deflection of the center of the plate vs. time. a = 1m, b = 1m, h = 1cm, time step = $2.6*10^{-5}$ sec. Maximum slamming pressure = 70 kPa with periodic spike distributed over an area of the plate shown in Fig. 4.26(b).

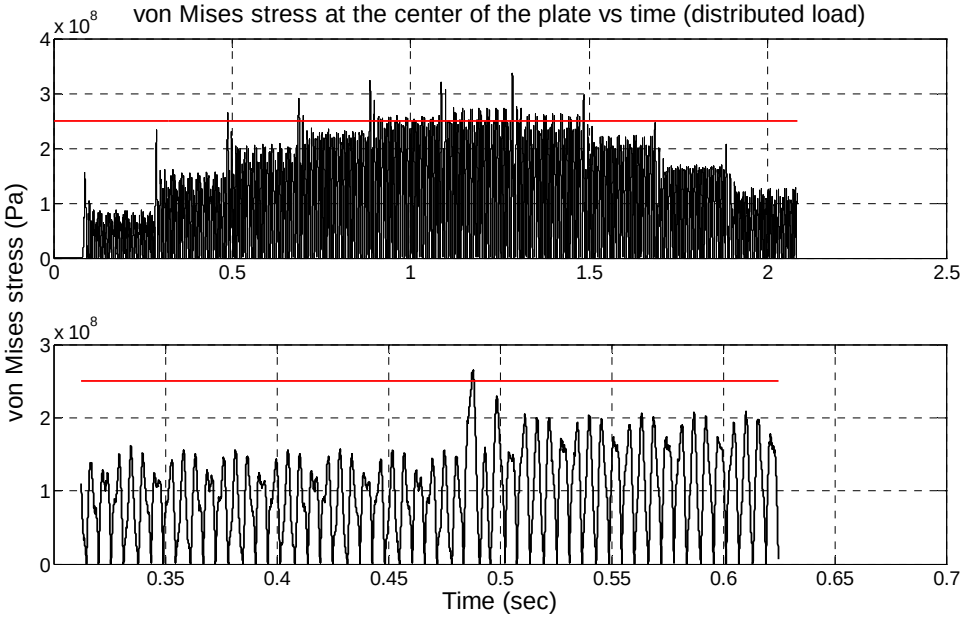

Figure 4.35: von Mises stress at the center of the plate vs. time. a = 1m, b = 1m, h = 1cm, time step = $2.6*10^{-5}$ sec. Maximum slamming pressure = 70 kPa with periodic spike distributed over an area of the plate shown in Fig. 4.26(b).

4.2.3 Slamming Pressure using Wagner's slamming model

Wagner's slamming model provides the slamming pressure varying in both space and time. Till this point, ABS design slamming pressure was applied on the rectangular isotropic plates to obtain the plate's deformation and stresses. Spatial distributions were kept unchanged throughout the simulation over two types of time profiles, wager's type and periodic spike type. This section illustrates the vibration characteristics of isotropic plate subject to variable, in both space and time, slamming pressure. Plate characteristics are kept same as the previous sections, i.e. length of the plate = 1m, breadth of the plate = 1m, thickness of the plate = 1cm and modulus of elasticity = 200GPa. Two cases of wet-deck slamming are discussed here in this section, (i) wet-deck hitting a paraboloid wave form, and (ii) wet-deck hitting a sinosoidal wave form.

(i) Of paraboloidal surface form:

The wet-deck is assumed to hit paraboloidal wave with a constant velocity V, where paraboloid is of the form $\eta_b(x, y) = 0.5\frac{x^2+y^2}{R}$. R, which provides the steepness of the wave, is taken as 3m in the simulations. Fig. 4.37 shows the pressure spatial distribution over the plate at time instant t=5 ms.

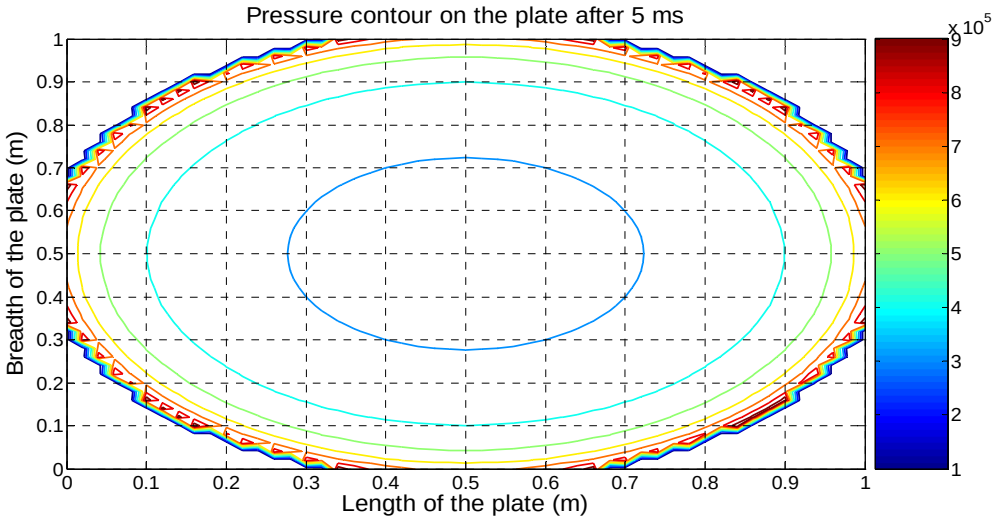

Figure 4.36: Slamming pressure distribution over the plate when falling on the parabolid wave form.

As we can see that maximum pressure is observed at the outer contact points of fluid and the plate while pressure minimizes at the center of the plate as time elapses. This trend matches with published results of beam-wave crest slamming, Faltinsen [56]. Simulations are carried out for two cases of velocities, 1m/s and 2m/s. Figs. 4.37 and 4.38 correspond to velocity of 1 m/s and show the deflection and von Mises stress at the center of the plate, respectively. In this case, stress remains under the yield stress limit but for the case of V=2m/s, stress surpasses the yield stress limit which is shown in Fig. 4.40.

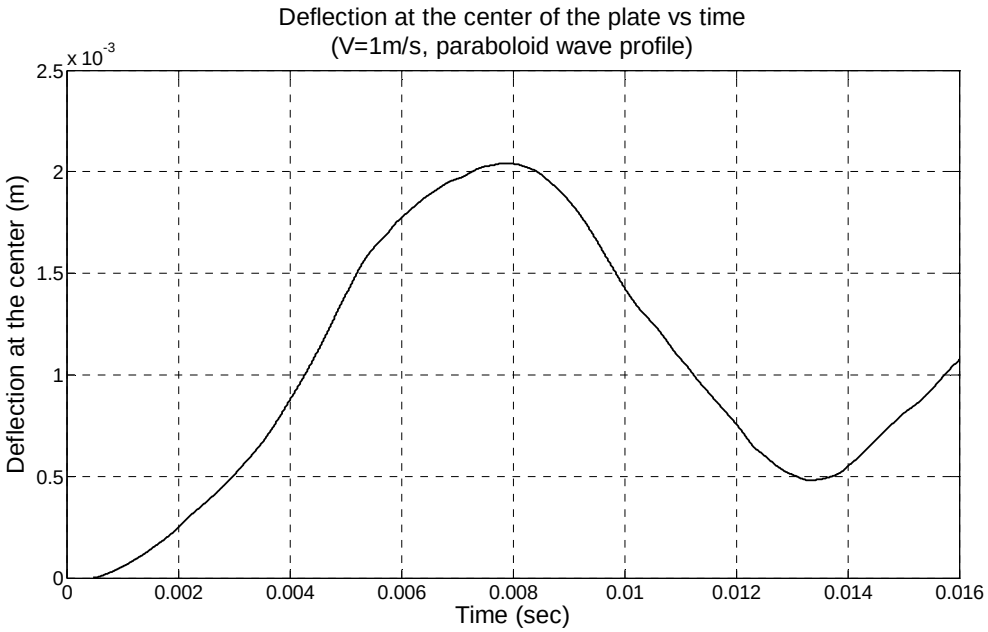

Figure 4.37: Deflection of the center of the plate over a time span. a = 1m, b = 1m, h = 1cm. Plate dropping on the paraboloid wave profile with velocity 1m/s.

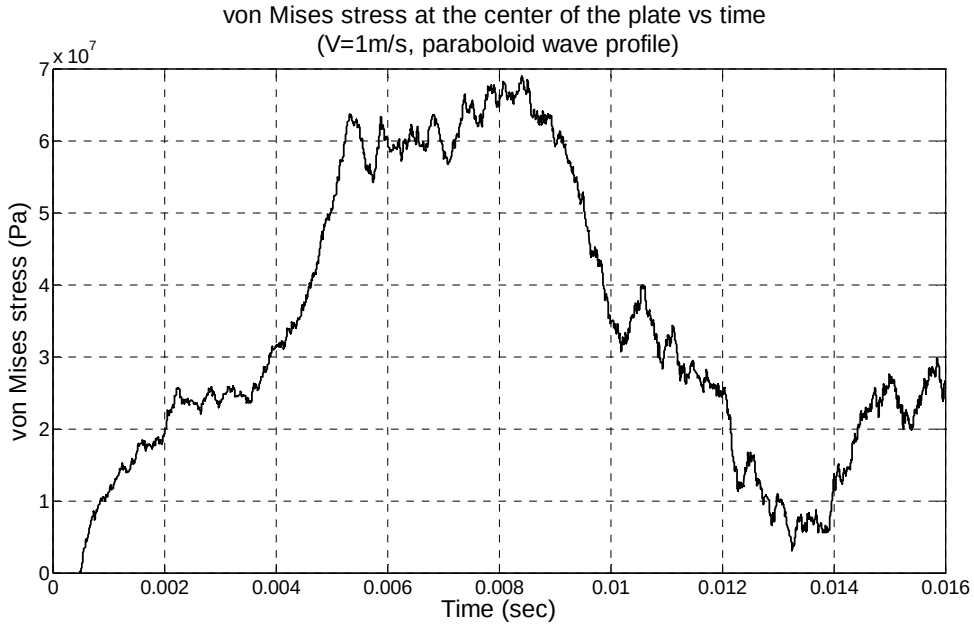

Figure 4.38: von Mises stress at the center of the plate over a time span. a = 1m, b = 1m, h = 1cm. Plate dropping on the paraboloid wave profile with velocity 1m/s.

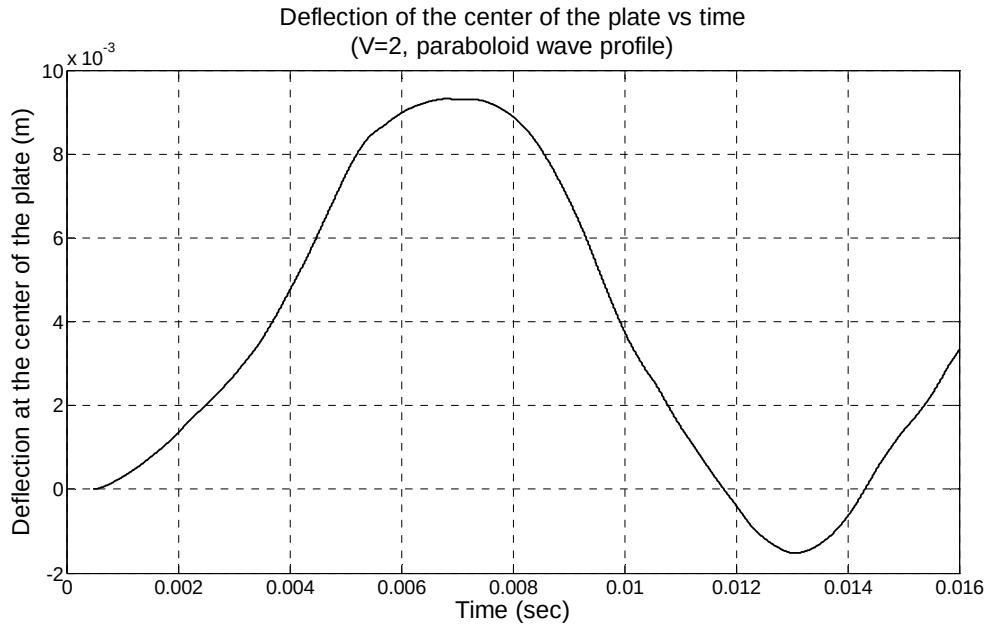

Figure 4.39: Deflection of the center of the plate over a time span. a = 1m, b = 1m, h = 1cm. Plate dropping on the paraboloid wave profile with velocity 2m/s.

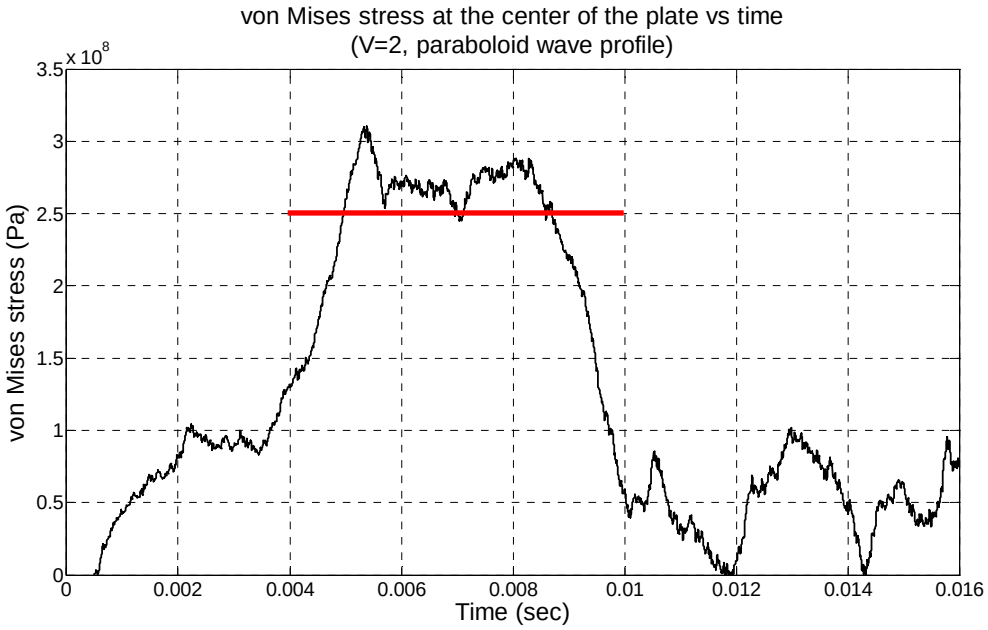

Figure 4.40: von Mises stress at the center of the plate over a time span. a = 1m, breadth b = 1m, h = 1cm. Plate dropping on the paraboloid wave profile with velocity 2m/s.

(ii) Of long-crested sinusoidal surface profile

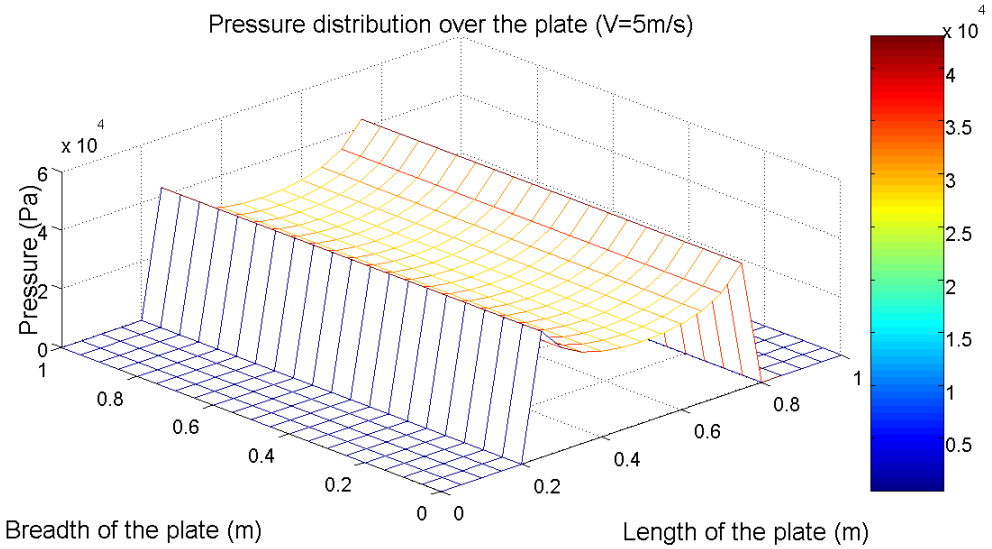

Figure 4.41: Slamming pressure distribution over the plate after 19 ms when falling on the sinusoidal wave form.

This section illustrates the phenomenon of wet-deck slamming when the wet-deck hits the sinusoidal wave with different water entering velocities. Wave is assumed to be long crested in y-direction and Fig. 4.41 shows the instantaneous slamming pressure distribution over the plate after 19 ms. The wave is assumed to be steep wave and ratio H/λ is taken as 1/7 with wave height as 5m. The wave number and time period of the wave is determined using the wavelength as obtained from the ratio.

Wet-deck hitting a sinusoidal wave profile corresponds to the real environment scenario. Figs. 4.42 and 4.43 show the deformation and von Mises stress distribution at the center of the plate over time when wet-deck enters into the water with velocity of 5 m/s. Real scenario of wet-deck slamming shows that the parabolic wave impact was

overdetermining the stress distribution over the plate. Similarly, Figs. 4.44 and 4.45 show the same when the water entering velocity increases to 10 m/s.

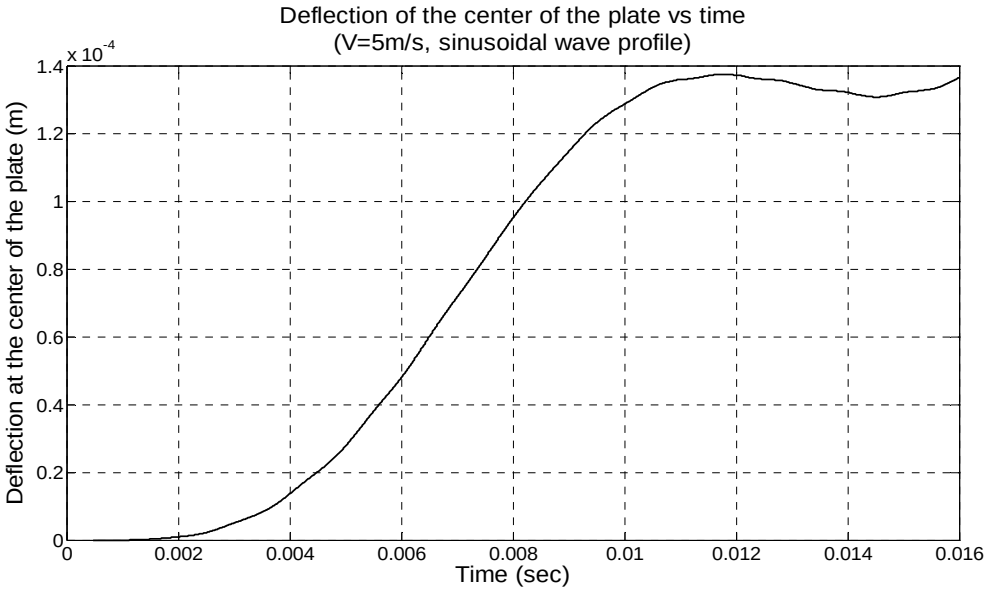

Figure 4.42: Deflection of the center of the plate over a time span. a = 1m, b = 1m, h = 1cm. Plate dropping on the sinusoidal wave profile with velocity 5m/s.

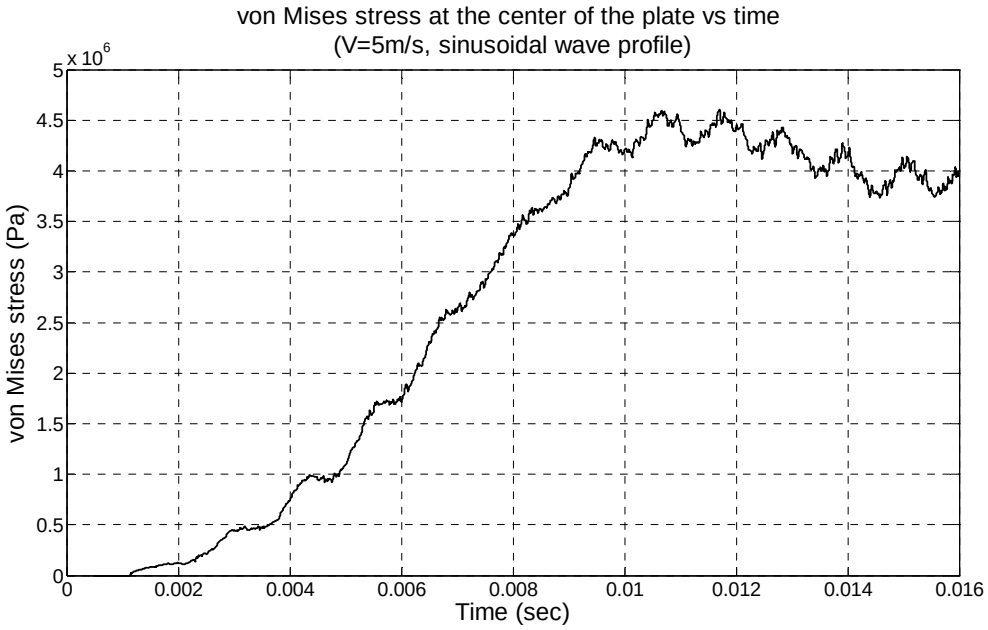

Figure 4.43: von Mises stress at the center of the plate over a time span. a = 1m, b = 1m, h = 1cm. Plate dropping on the sinusoidal wave profile with velocity 5m/s.

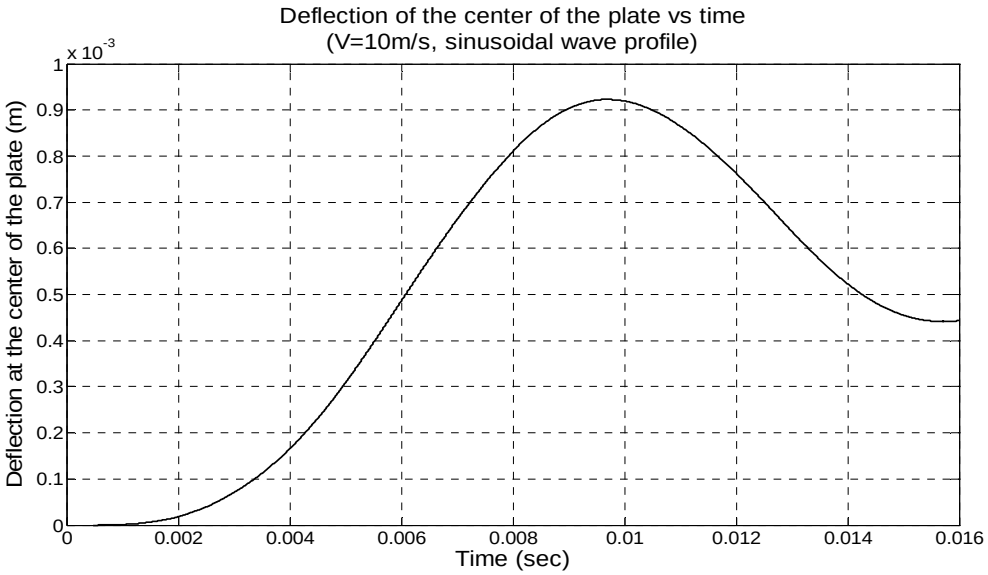

Figure 4.44: Deflection of the center of the plate over a time span. a = 1m, b = 1m, h = 1cm. Plate dropping on the sinusoidal wave profile with velocity 10m/s.

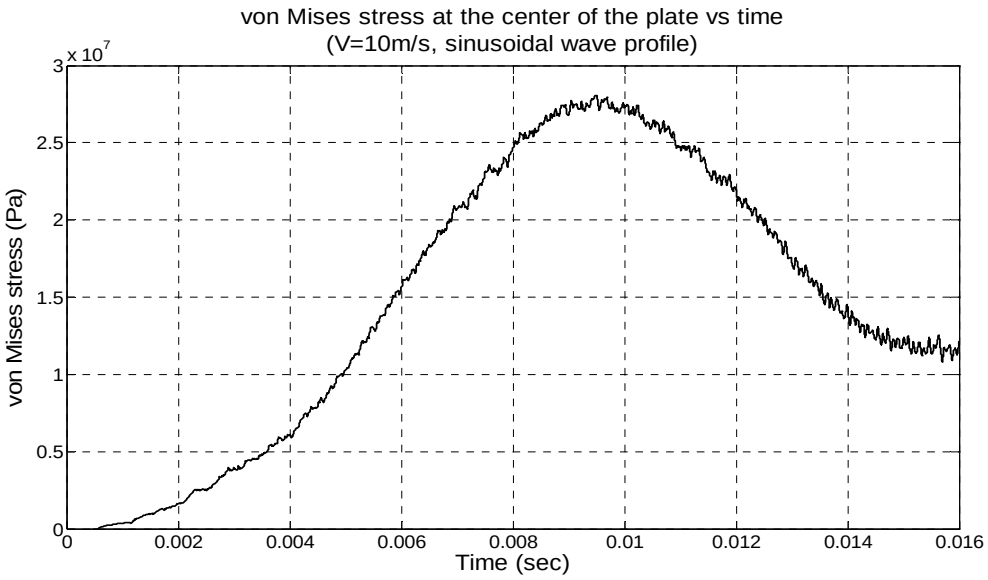

Figure 4.45: von Mises stress at the center of the plate over a time span. a = 1m, b = 1m, h = 1cm. Plate dropping on the sinusoidal wave profile with velocity 10m/s.

This concludes the study of effect of various slamming loads on linear isotropic plates. Next sections illustrate the vibration physics and stresses on the isotropic plate using nonlinear vibration theory and the effect of material damping.

4.3 Non-linear Vibration Analysis of Isotropic Plates in Time Domain

This section is based on the determination of nonlinear vibrations and stresses of isotropic plates under various kinds of wave loading. The formulation of non-linear plate theory has already been discussed in Chapter 3, and the governing equations for the nonlinear vibration were presented. Rewriting Eqn. 3.42;

$$D\left(\frac{\partial^4 W}{\partial x^4}+2\frac{\partial^4 W}{\partial x^2\partial y^2}+\frac{\partial^4 W}{\partial y^4}\right)+\rho\frac{\partial^2 W}{\partial t^2}+2\rho\gamma_d\frac{\partial W}{\partial t}$$

$$=P+h\frac{\partial^2 F}{\partial y^2}\frac{\partial^2 W}{\partial x^2}+h\frac{\partial^2 F}{\partial x^2}\frac{\partial^2 W}{\partial y^2}-2h\frac{\partial^2 F}{\partial x\partial y}\frac{\partial^2 W}{\partial x\partial y} \qquad (4.6)$$

$$\frac{\partial^4 F}{\partial x^4}+2\frac{\partial^4 F}{\partial x^2\partial y^2}+\frac{\partial^4 F}{\partial y^4}=E\left[\left\{\frac{\partial^2 W}{\partial x\partial y}\right\}^2-\frac{\partial^2 W}{\partial x^2}\frac{\partial^2 W}{\partial y^2}\right]$$

where, F is the airy stress function and P is the loading. Eqns. 4.6 is solved consecutively at each time step to solve for the deformation W under various types of fluid loading. For non-linear vibrations of isotropic plate, following types of loading will be used:

(i) Distributed design slamming pressure obtained using ABS rules with Wagner's type of time variation,

(ii) Distributed design slamming pressure obtained using ABS rules with spike time function,

(iii) Slamming pressure obtained using Wagner's slamming model.

4.3.1 Distributed design slamming pressure with Wagner's type of time variation

Plate dimensions are kept same as linear case, i.e. length of the plate = 1m, breadth of the plate = 1m, thickness of the plate = 1 cm, design pressure amplitude = 70 *kPa.* The pressure is assumed to be distributed over a part of plate as shown in Fig.4.27 and time variation profile is taken similar to Wagner's slamming time variation profile $f(t) = \frac{1}{\sqrt{t}}$.

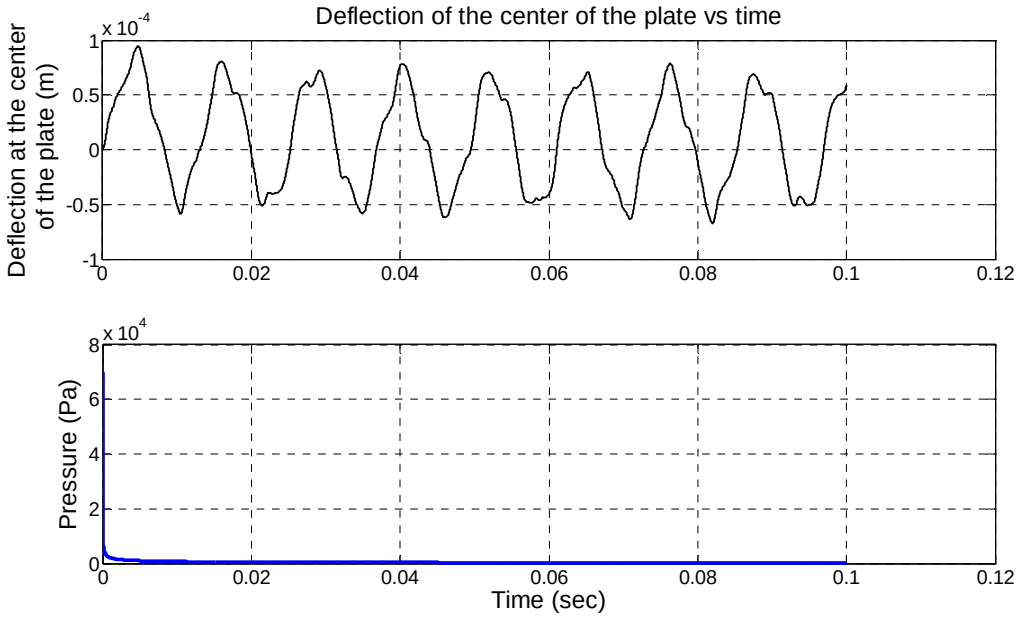

Figure 4.46: Deflection of the center of the plate over a time span. a = 1m, b = 1m, h = 1cm, Maximum slamming pressure = 70 kPa with Wagner's type time profile and distributed over a part of the plate shown in Fig. 4.26(b).

Fig. 4.46 shows the deflection at the center of plate which is less as compared to the linear one, Fig. 4.30. This reduction in the amplitude of the deformation is mainly due to the internal stresses developed in the plate. Few fluctuations can be observed from the time history of deflection. Nonlinearity of the plate can be a reason behind this

phenomenon as it excites the higher vibration modes of the plate. The time variation of von Mises stress at the center is shown in Fig. 4.47.

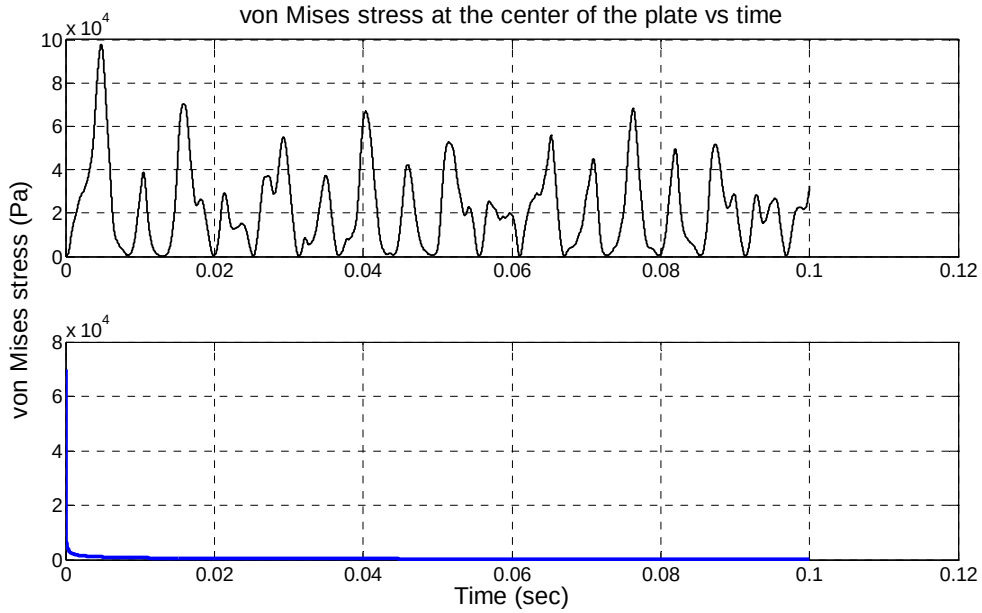

Figure 4.47: von Mises stress at the center of the plate over a time span. a = 1m, b = 1m, h = 1cm, Maximum slamming pressure = 70 kPa with Wagner's type time profile and distributed over a part of the plate shown in Fig. 4.26(b).

4.3.2 Distributed design slamming pressure with spike time variation

A periodic slamming function Eqn. 4.6 is applied to obtain the effect of repeated slamming. Based on the different encounter frequencies, two sets of results have been obtained. A ship is assumed to be moving with a constant velocity of 40 knots which encounters the ocean waves at time period of 3 sec and 1.5 sec. It is taken as an assumption that every wave, which hits the wet-deck, exerts a slamming pressure of 70kPa. Fig. 4.48 shows the deflection of the center of the plate, which is again lower than the linear case. Fig. 4.49 illustrates the von Mises stress at the center of the plate. It is observed that after the impact of the second spike, the amplitude of the free vibration

of the plate is increased which leads to the higher amplitude of the stress which can also be observed from Fig. 4.49.

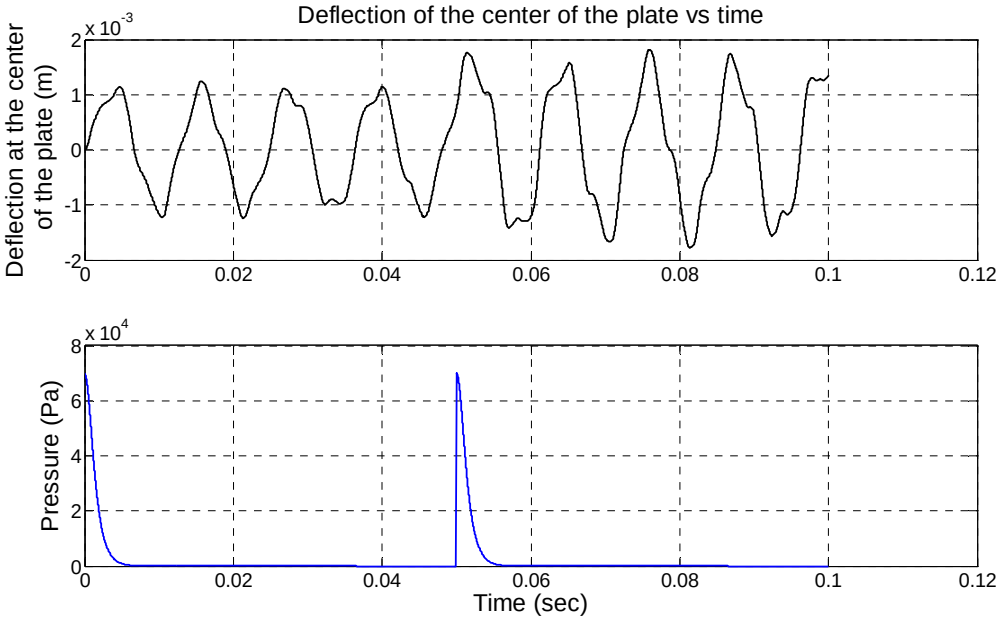

Figure 4.48: Deflection of the center of the plate over a time span. a = 1m, b = 1m, h = 1cm, Maximum slamming pressure = 70 kPa with time profile as spike function and distributed over a part of the plate shown in Fig. 4.26(b).

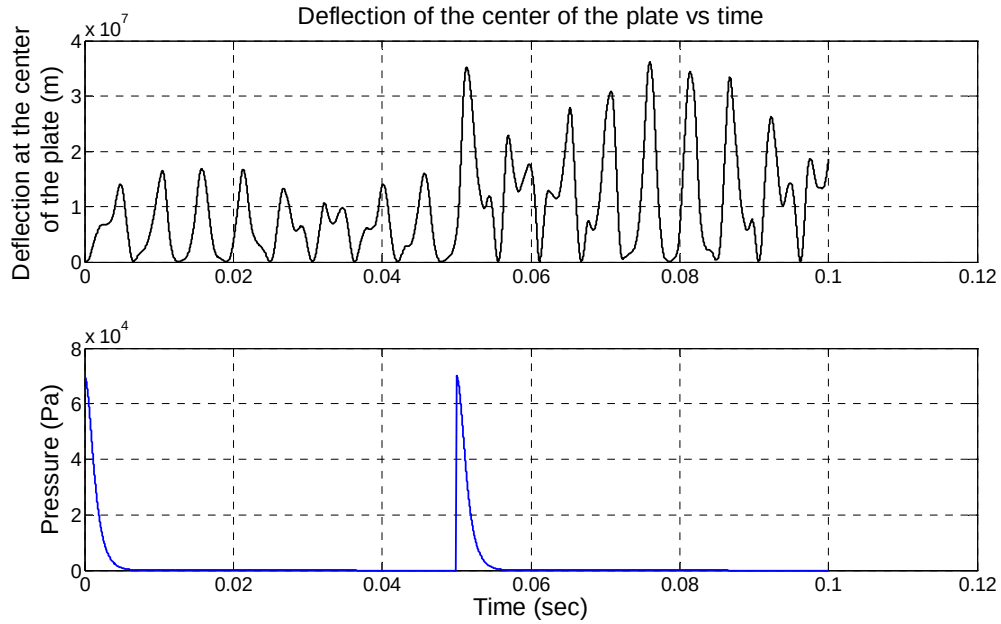

Figure 4.49: von Mises stress at the center of the plate over a time span. a = 1m, b = 1m, h = 1cm, Maximum slamming pressure = 70 kPa with time profile as spike function and distributed over a part of the plate shown in Fig. 4.26(b).

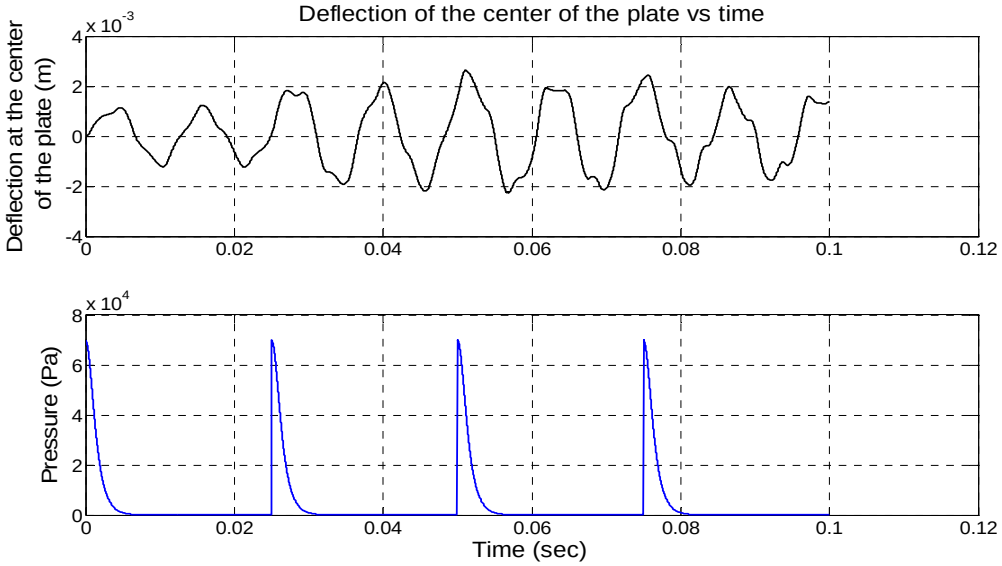

Figure 4.50: Deflection of the center of the plate over a time span. a = 1m, b = 1m, h = 1cm, Maximum slamming pressure = 70 kPa with time profile as spike function and distributed over a part of the plate shown in Fig. 4.26(b).

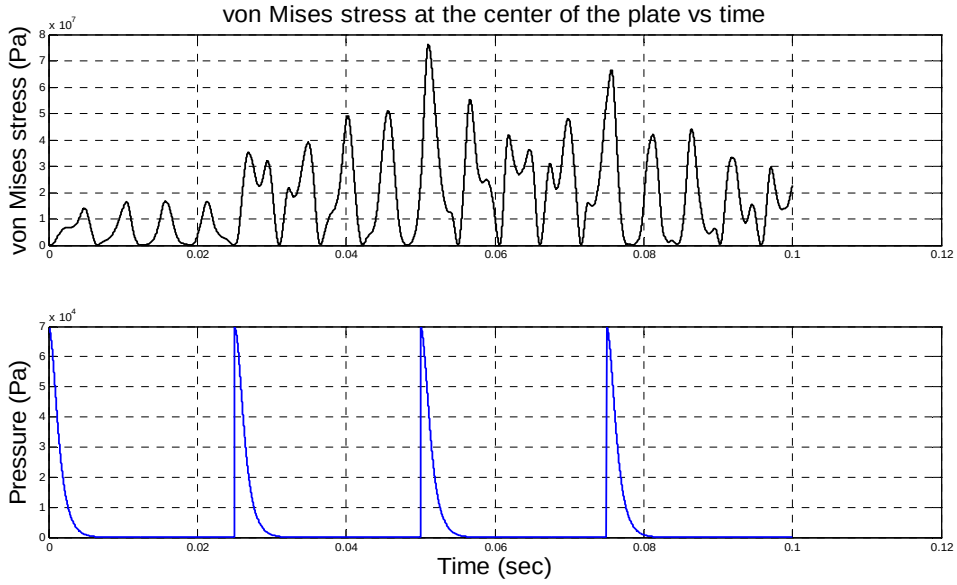

Figure 4.51: von Mises stress at the center of the plate over a time span. a = 1m, b = 1m, h = 1cm, Maximum slamming pressure = 70 kPa with time profile as spike function and distributed over a part of the plate shown in Fig. 4.26(b).

Here, the deflection, Fig. 4.50, and von Mises stress, Fig. 4.51, at the center of the plate are obtained using the wave time period of 1.5 sec. With the longer chain of such events, flexural vibrations can create larger stress amplitude.

4.3.3 Slamming pressure using Wagner's slamming model

Next two sections are based on the nonlinear vibration analysis of isotropic plates which are subjected to slamming loads obtained using Wagner's theory. As already mentioned, Wagner's slamming model provides the instantaneous slamming pressure on the plate. This slamming pressure reaches the maximum at the contact point of the fluid and the plate. Two types of wave profiles, (i) paraboloid and sinusoidal, are considered here to determine the slamming pressure in the event of plate water entry.

(i) Paraboloidal surface

It is assumed that the plate is hitting a paraboloid wave form $\eta_b(x, y) = 0.5\frac{x^2+y^2}{R}$. R is fixed at 3m while performing the simulations. Spatial distribution of the slamming pressure over the plate at 5 ms can be seen in Fig. 4.36.

Fig. 4.52 and 4.54 show the deflection of the center of the plate at impact velocities 1m/s and 2 m/s, respectively. The vibration profiles are same as the linear case except the difference in the maximum amplitude. It can be deducted from the figures that the deflection of at the center is not too much but the stress developed due to the impact pressure is at a higher side, which can be seen in Figs. 4.53 and 4.55, respectively.

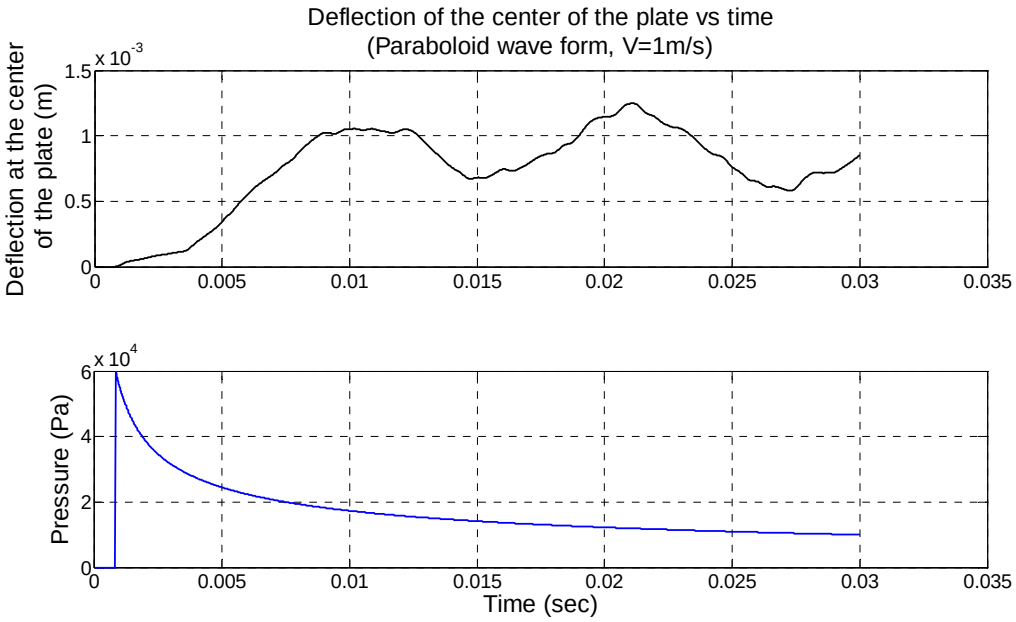

Figure 4.52: Deflection of the center of the plate over a time span. a = 1m, b = 1m, h = 1cm. Plate dropping on the paraboloid wave profile with velocity 1m/s.

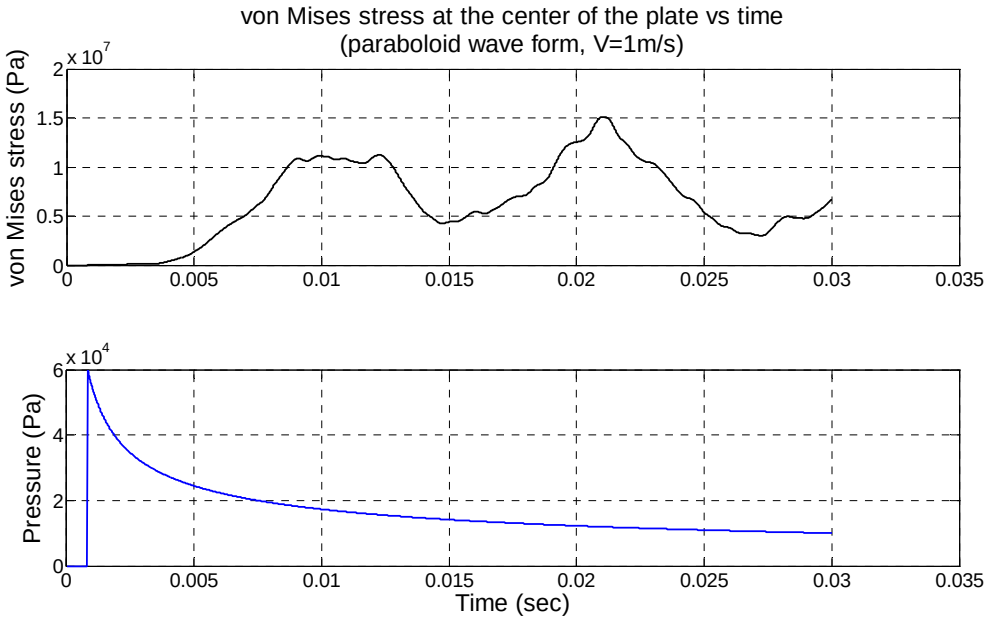

Figure 4.53: von Mises stress at the center of the plate over a time span. a = 1m, b = 1m, h = 1cm. Plate dropping on the paraboloid wave profile with velocity 1m/s.

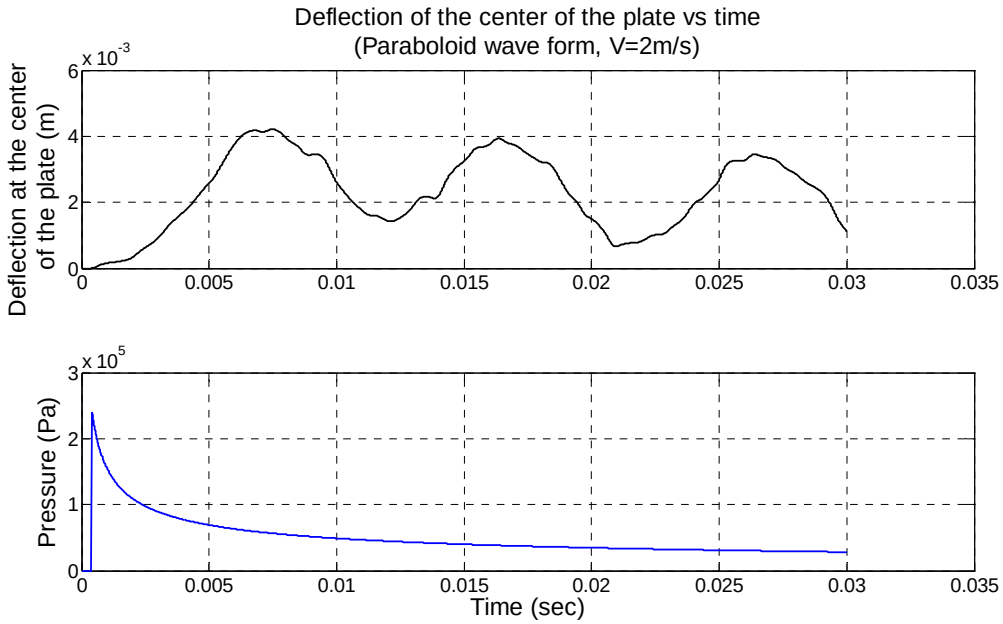

Figure 4.54: Deflection of the center of the plate over a time span. a = 1m, b = 1m, h = 1cm. Plate dropping on the paraboloid wave profile with velocity 2m/s.

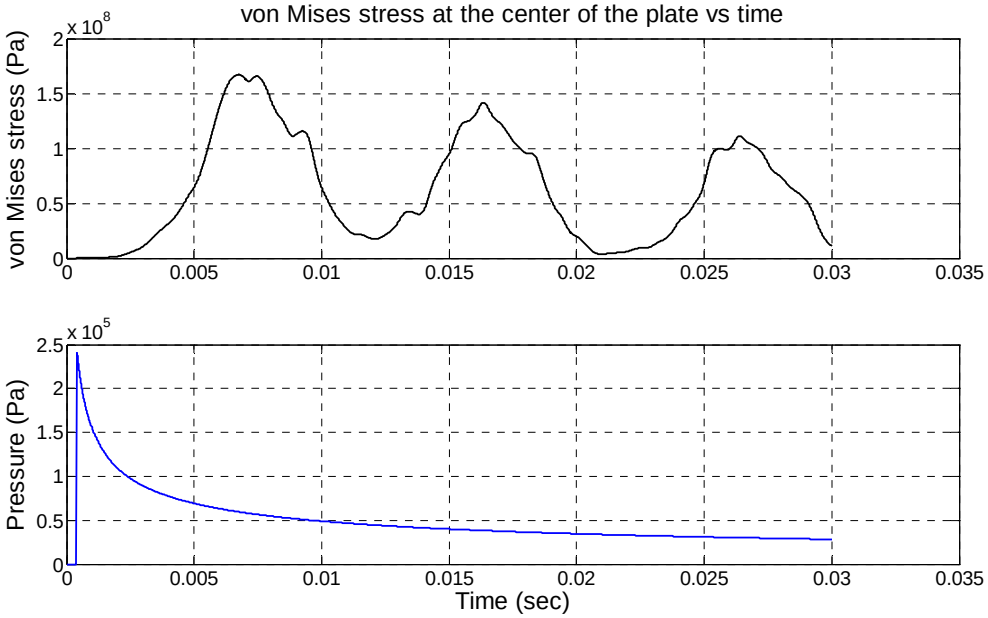

Figure 4.55: von Mises stress at the center of the plate over a time span. a = 1m, b = 1m, h = 1cm. Plate dropping on the paraboloid wave profile with velocity 2m/s.

(ii) Sinusoidal wave

In this section, the slamming pressure is determined for the event of the plate hitting a sinusoidal wave profile. The pressure distribution over the plate can be seen in Fig. 4.42. It shows that the maximum pressure occurs at the intersection point of fluid and structure. The ocean wave is considered as a long crested steep wave in y-direction. Ratio H/λ is taken as 1/7, Newman [21], with the wave height H as 5m. Using this information of step waves, wave number and wave time period were obtained.

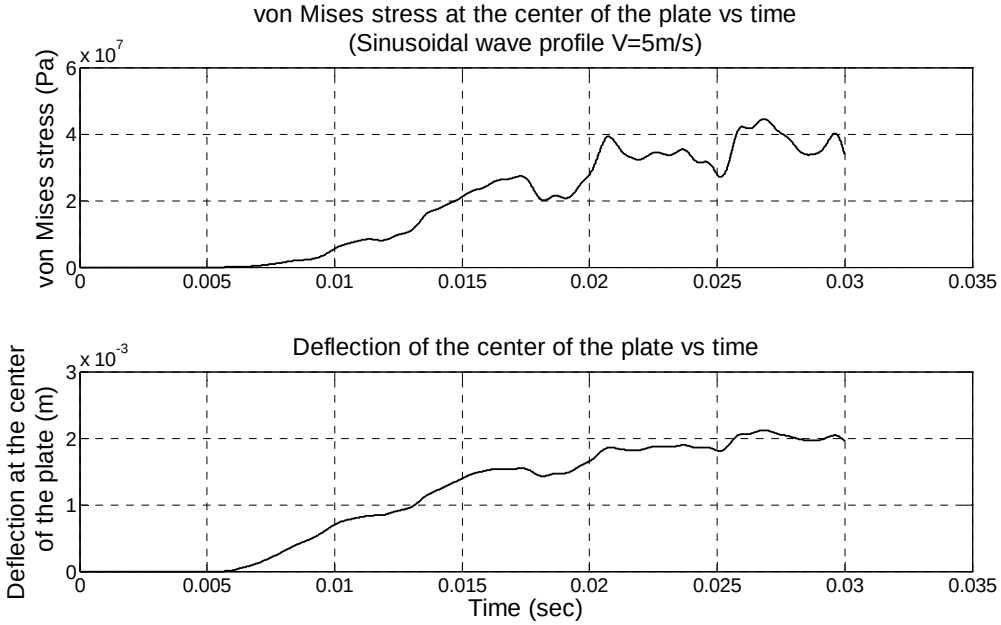

Figure 4.56: von Mises stress and deformation at the center of the plate over a time span. a = 1m, b = 1m, h = 1cm. Plate dropping on the sinusoidal wave profile with velocity 5m/s. wave height = 5m, H/λ = 1/7.

Figs. 4.56 and 4.57 show the Deflection and von Mises stress at the conter of the plate over time at 5m/s and 10m/s impact velocities, respectively. At the lower impact velocity 5 m/s, the deflection and stresses remain under the permissible limit, whereas at

higher impact velocity 10 m/s, there is no significant change in the deflection of the plate, but a significant change in stresses is noticed.

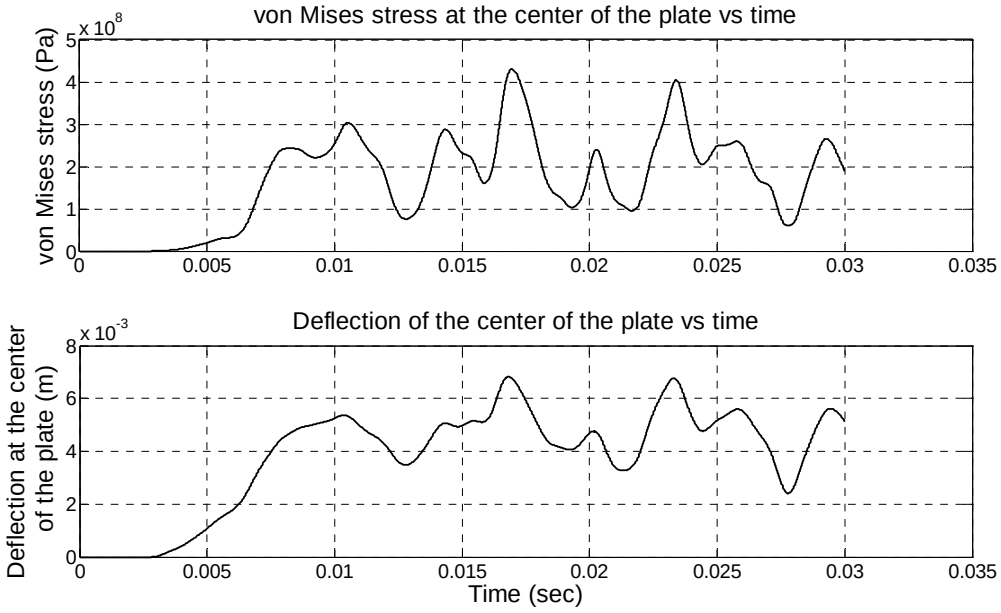

Figure 4.57: von Mises stress and deformation at the center of the plate over a time span. a = 1m, b = 1m, h = 1cm. Plate dropping on the sinusoidal wave profile with velocity 10m/s. wave height = 5m, $H/\lambda = 1/7$.

This high shift in stress is due to the dynamic nature of the plate, as it was previously observed that for small dynamic deflection stresses can exceed the limit. This same reason can cause this phenomenon to lead the structure to yield failure, as observed in Fig. 4.57.

4.4 Effect of material viscous damping

In this section, the effect of material viscous damping is analyzed. The equation for linear damped isotropic plate vibration can be written as;

$$\frac{\partial^4 W(x,y,t)}{\partial x^4} + 2\frac{\partial^4 W(x,y,t)}{\partial x^2 \partial y^2} + \frac{\partial^4 W(x,y,t)}{\partial y^4} + 2\rho_p \gamma_d \frac{\partial W}{\partial t} - \frac{\rho_p}{D}\frac{\partial^2 W(x,y,t)}{\partial t^2} = q(x,y) \tag{4.7}$$

where, γ_d is the material viscous damping coefficient, which is equal to 0.002 for steel.

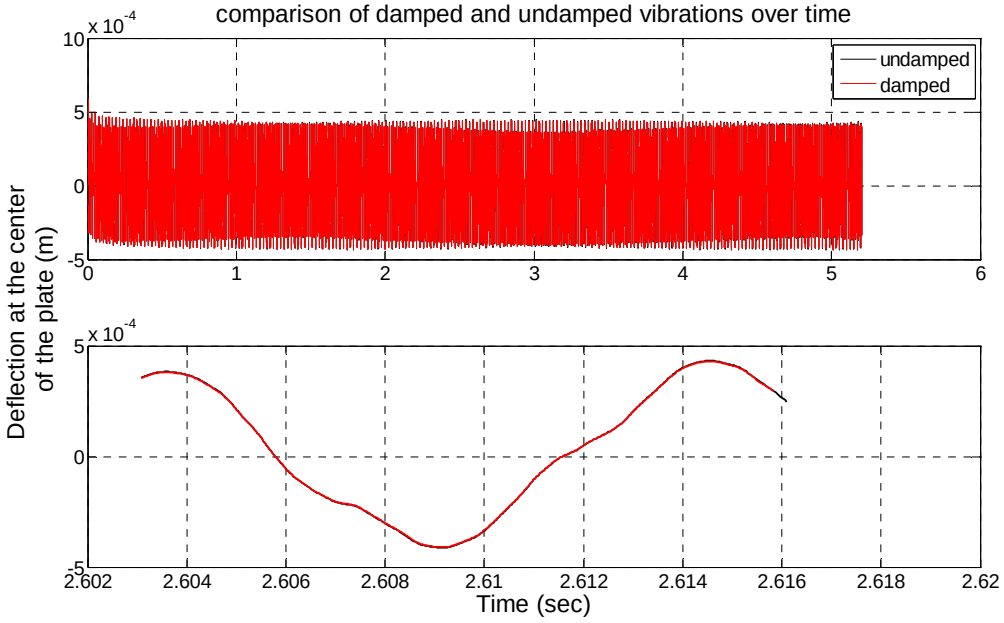

Figure 4.58: deformation at the center of the plate over a time span. a = 1m, b = 1m, h = 1cm. design slamming pressure=70kPa, wagner's type time variation.

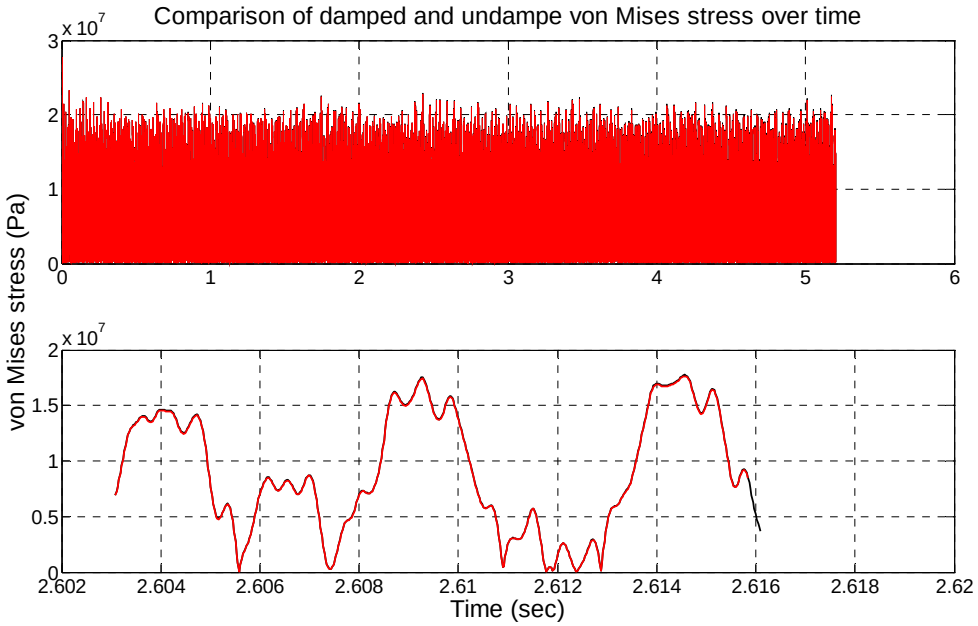

Figure 4.59: von Mises stress at the center of the plate over a time span. a = 1m, b = 1m, h = 1cm. design slamming pressure=70kPa, Wagner's type time variation.

An isotropic plate, length 1m, breadth 1m, thickness 1cm, is tested to determine the effect of material viscous damping. It can be observed from Figs. 4.58 and 4.59 that the material damping does not have any significant effect on the deflection and the stress over the plate so the damping is not included in the simulations.

In this Chapter, we had examined the response characteristics of isotropic plates subject time-harmonic Froude-Krylov and transient slamming wave forces. The effect of radiating wave forces has been ignored. That including radiation forces is considered in the next chapter. Isotropic plates were assumed to be clamped on the boundaries, because of the stiffeners. The low-frequency motion of the stiffener, or for that matter of the ship hull, is assumed to be more governed by hydrostatic restoring force than by that of elasticity.

5. RESULTS: VIBRATIONS OF A STIFFENED PLATE

This chapter presents the behavior of stiffened plates under various types of fluid loading, such as regular ocean wave load, slamming loads based on ABS wave slamming model and slamming loads based on Wagner's theory. Stiffened plates of the ship hull/wet-deck is modeled as an orthotropic plate because similar to the orthotropic plates, a stiffened plate also has different rigidities in orthogonal directions, which arise because of the stiffeners. Governing equation of stiffened/orthotropic plate vibrations, Eqn. 3.48, has already been discussed in Chapter 3. Eqn. 3.48 is then solved for the pressures specified above.

In this section, two locations, (i) wet-deck, (ii) ship hull bottom, on the twin hull ships have been studied for the stress and deflection analysis of the hull panels subjected to wave slamming loads. ABS rules and Wagner's formula are used to determine the pressure distribution on the wet-deck plating and for the hull plating. Pressure distribution is obtained using the Wagner's theory for hull's water entry (slamming problem) and the pressure distribution obtained by Ananthakrishnan [55] for the forced hull oscillations (radiation problem).

5.1 Vibration/stress analysis of wet-deck plate panels

Wet-deck slamming is of great concern in twin hull ship design. To do the stress analysis of the wet-deck, two methods have been adopted to determine the slamming pressure, (i) slamming method based on ABS rules, and (ii) Wagner's method.

5.1.2 Method based on ABS rules

A twin-hull ship of length L_W=48.5 m and displacement 346500 kg is taken as an example for the present results. It is assumed that the twin hull ship is moving forward with a speed of 35 knots and the significant wave height is H_s=3.25 m at certain sea-state. The formulation of the design slamming pressure has already been discussed in Chapter 2. Using the formulation for the given ship data, we obtain the following results;

Transverse Spacing s_t= 5 m

Longitudinal Spacing s_l= 0.65 m

Length of the plate a= 5m

Breadth of the plate b= 2m

Thickness of the plate h= 6.75mm

Design Slamming Pressure P_{wd}= 78.6 kN/m^2

Design pressure is assumed to be distributed oven a part of plate as shown in Fig. 5.1. The time profile used here corresponds to Wagner's type as well as periodic spike type profile. Wagner's type time profile follows $f(t) = \frac{1}{\sqrt{t}}$ type profile and spike function is expressed as Eqn. 4.6.

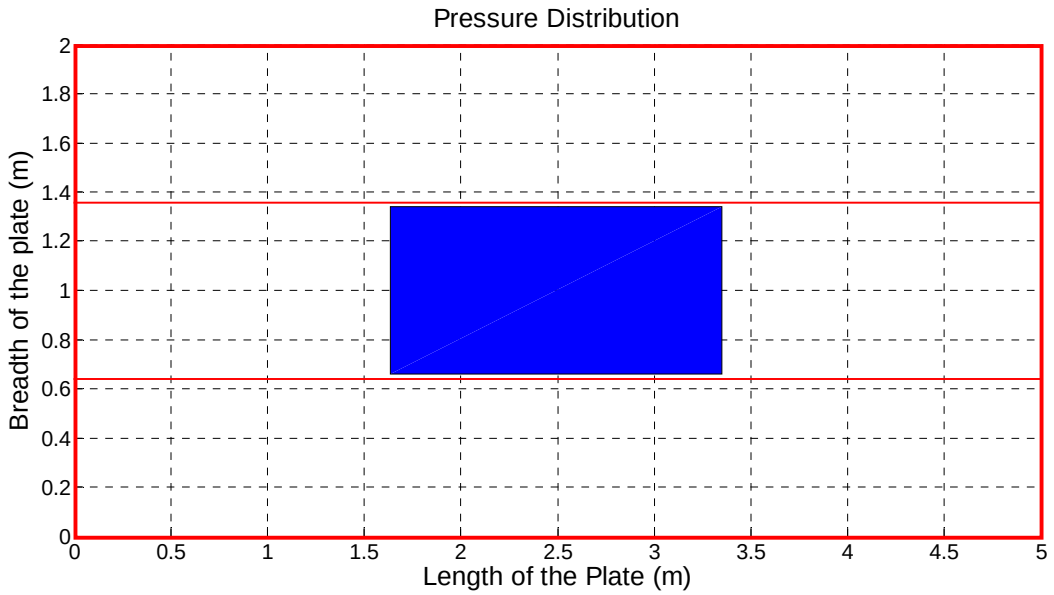

Figure 5.1: Spatial distribution of the pressure on plate. a=5m, b=2m, and h=1cm. Red colored lines show the locations of the stiffeners on the plate.

Fig. 5.2 shows the deflection of the center of the wetdeck plate under the ABS design slamming pressure load. It can be seen that Wagner type time profile does not create any large deformation in the beginning of the simulation. As we can see from Fig. 5.3 that the stress developed due to this type of time profile remains well below the yield stress limit. To observe the near practical effect of the wet-deck slamming, periodic spike type loading results are presented. In order to better represent real life input in the assumptions, we tried to connect wave encounter frequency to the number of spikes hitting the wet-deck per second.

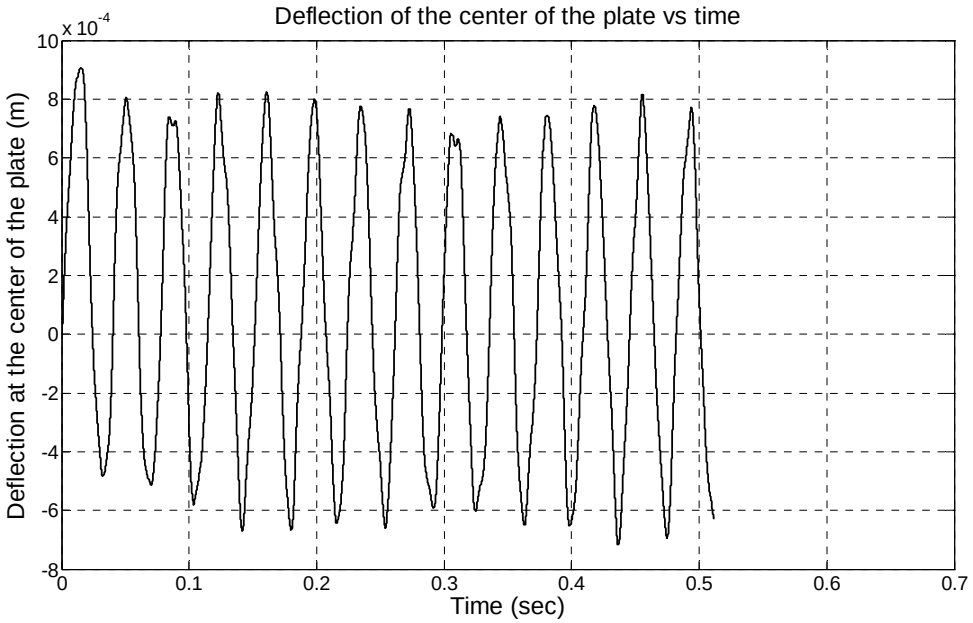

Figure 5.2: Deflection of the center of the wet-deck plate over a time span. a = 5m, b = 2m, h = 1cm, design pressure = 78kPa, Wagner type time profile

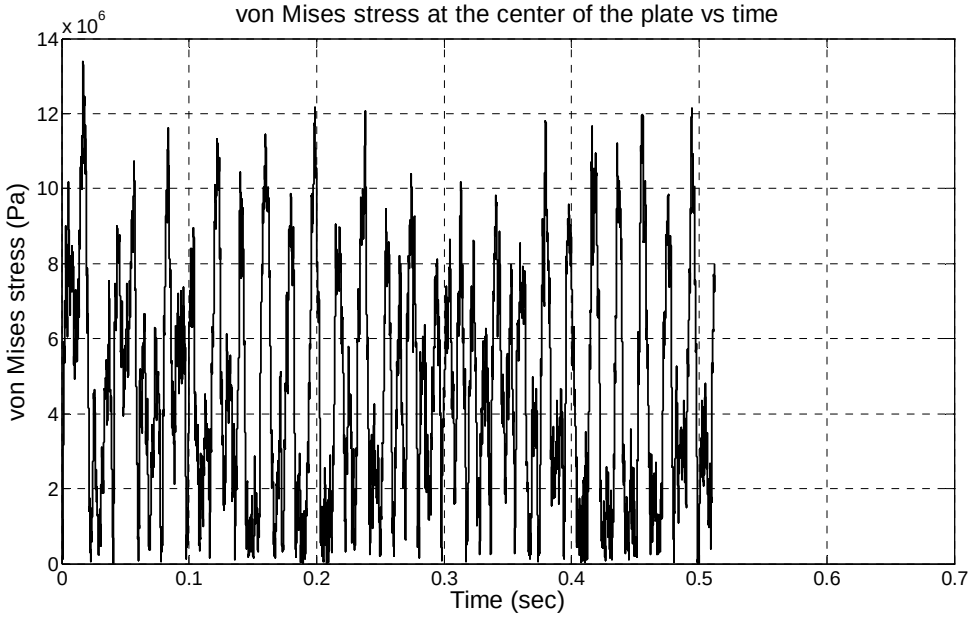

Figure 5.3: von Mises stress at the center of the wet-deck plate over a time span. a = 5m, b = 2m, h = 1cm, design pressure = 78kPa, Wagner type time profile

If ship moves with the speed of V, then the encounter frequency can be expressed as;

$$\omega_{encounter} = \omega - \frac{\omega V^2 \cos\theta}{g} \tag{5.1}$$

where, $\omega_{encounter}$ is the wave encounter frequency and θ is the wave heading angle. It has been assumed that the ship is moving in head sea, hence θ can be taken as 180^o , and the wet-deck is hitting every wave crest in the process. Design slamming pressure is kept constant throughout the wet-deck slamming event

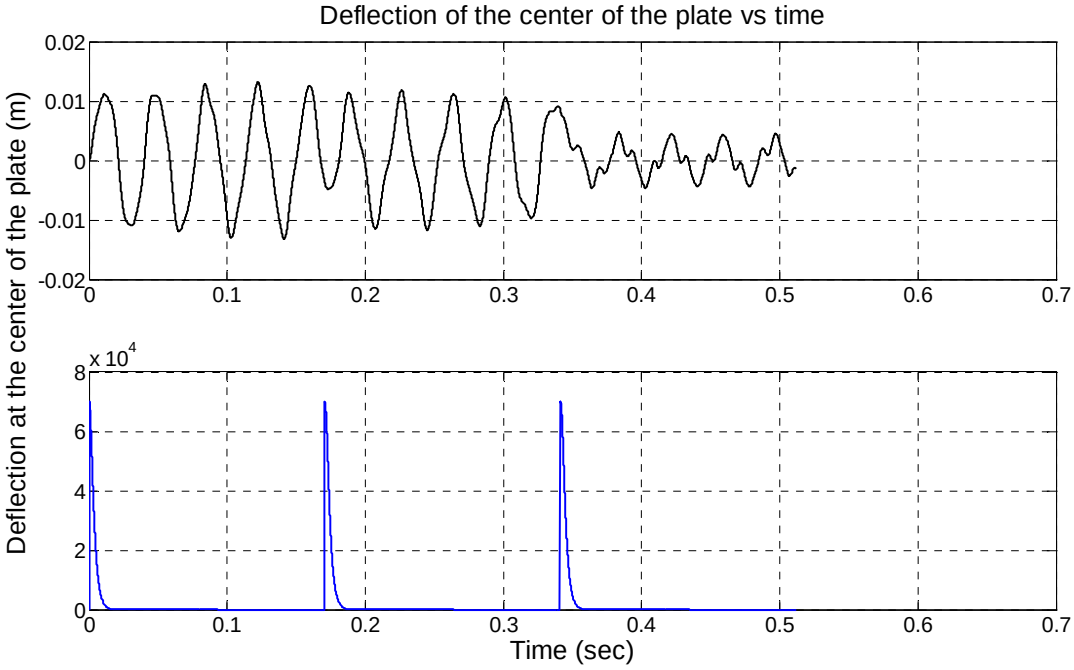

Figure 5.4: Deflection of the center of the wet-deck plate over a time span. a = 5m, b = 2m, h = 1cm, design pressure = 78kPa, periodic spike time profile, wave time period = 5sec

The deformation at the center of the stiffened plate is shown in Fig. 5.4 while Fig. 5.5 shows the von Mises stress variation over time at the center of the plate. The wave time period is selected as 5secs. It can be observed from Fig. 5.5 that due to periodic

spike, loading stress approaches very close to the yield stress limit, and it is highly probable thatthe former can surpass the later as time progresses.

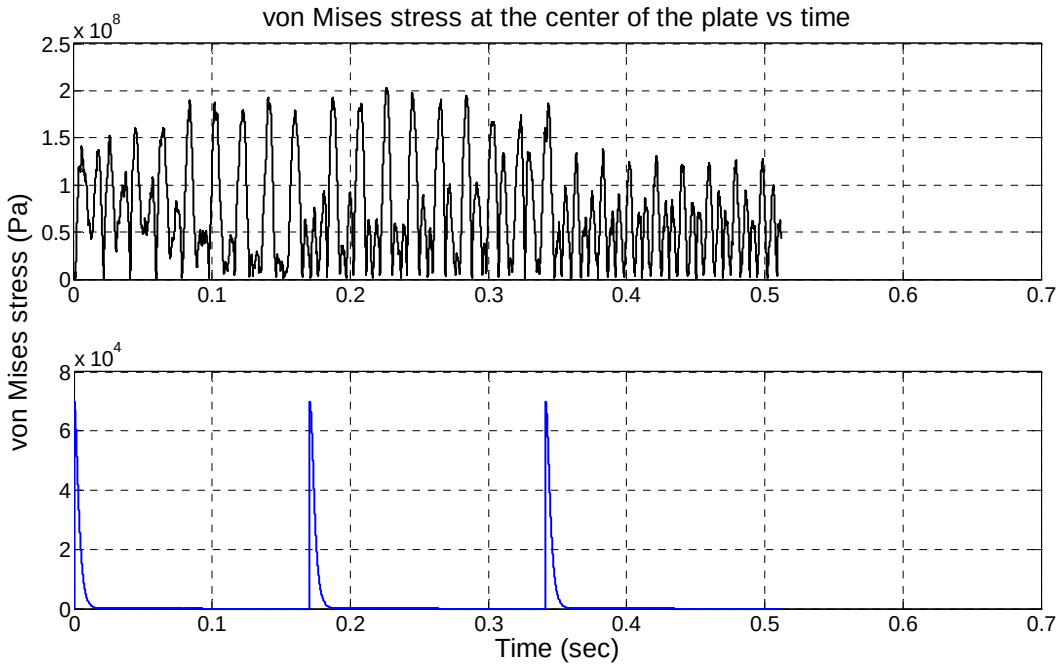

Figure 5.5: von Mises stress at the center of the wet-deck plate over a time span. a = 5m, b = 2m, h = 1cm, design pressure = 78kPa, periodic spike time profile, wave time period = 5sec

To analyze the effect of more frequent waves, wave time period is reduced to 3 sec. Fig. 5.6 and 5.7 show the deformation and von Mises stress at the center of the plate. It is observed that if the period of plate vibrations and loading period are out of phase then stress can be reduced over time, but in case, both periods are in phase then it can result into higher amplitude vibrations and stress distribution at the center.

Next the effect of slamming pressure obtained using Wagner's theory of plate and wave crest impact, will be discussed.

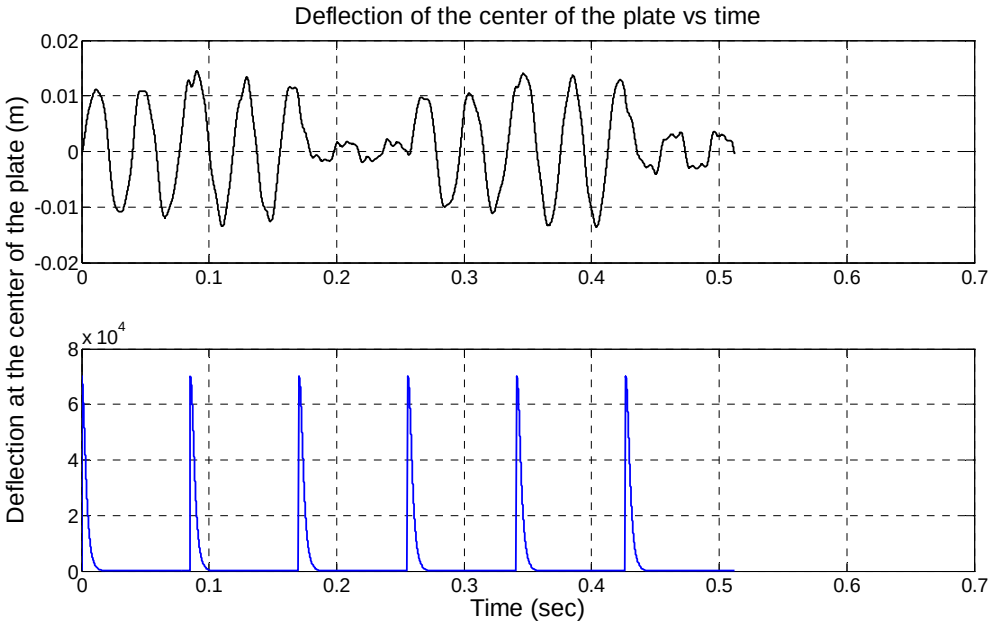

Figure 5.6: Deflection of the center of the wet-deck plate over a time span. a = 5m, b = 2m, h = 1cm, design pressure = 78kPa, periodic spike time profile, wave time period = 3sec

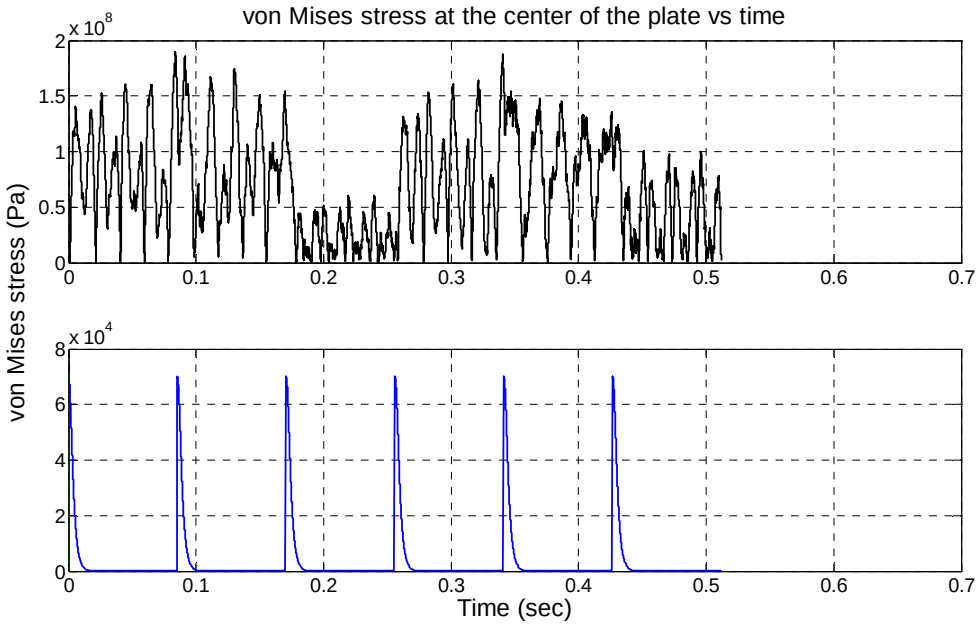

Figure 5.7: von Mises stress at the center of the wet-deck plate over a time span. a = 5m, b = 2m, h = 1cm, design pressure = 78kPa, periodic spike time profile, wave time period = 3sec

5.1.2 Wagner's slamming model

In this section, results are obtained for two types of wave profiles, (i) paraboloid wave profile, and (ii) sinusoidal wave profile. Figs. 5.8-5.11 are based on the slamming pressure obtained using paraboloid form and Figs. 5.12-5.15 are obtained for the sinusoidal wave profile.

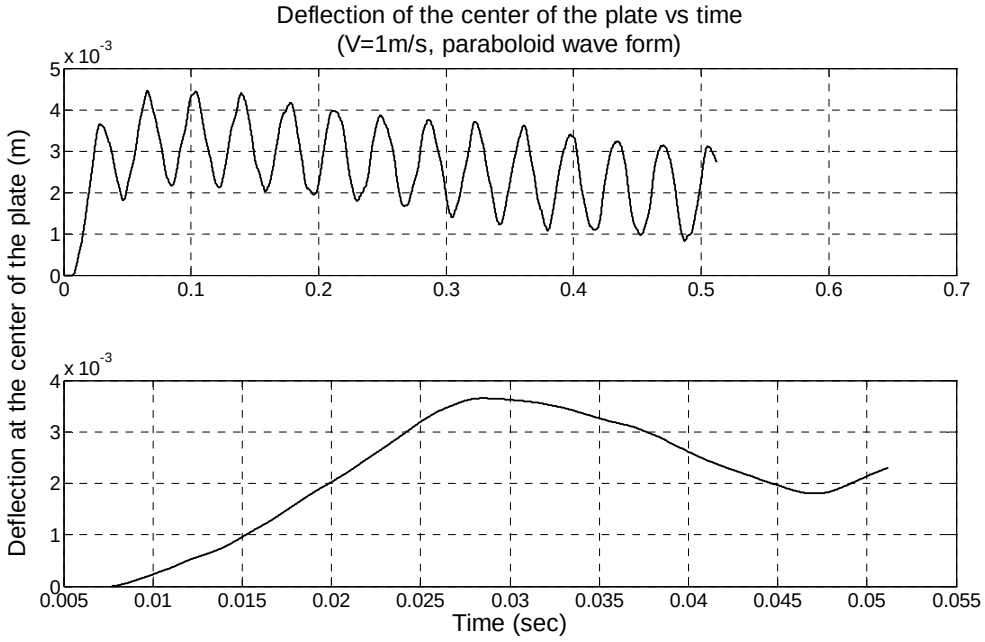

Figure 5.8: Deflection of the center of the wet-deck plate over a time span. a = 5m, b = 2m, h = 1cm, paraboloid wave profile R = 3m, impact velocity V=1m/s

Fig. 5.8 and 5.9, show the deflection of the stiffened plate element and the von Mises stress distribution at the center of the plate over time. Plate deflection mainly follows the pressure profile but natural vibrations along the path cause fluctuations in the stresses. Sometimes these fluctuations in the stresses can surpass the yield stress limit, 250 *MPa*. Hence, the study of elastic nature of the plates or hull girder provides the accurate estimates.

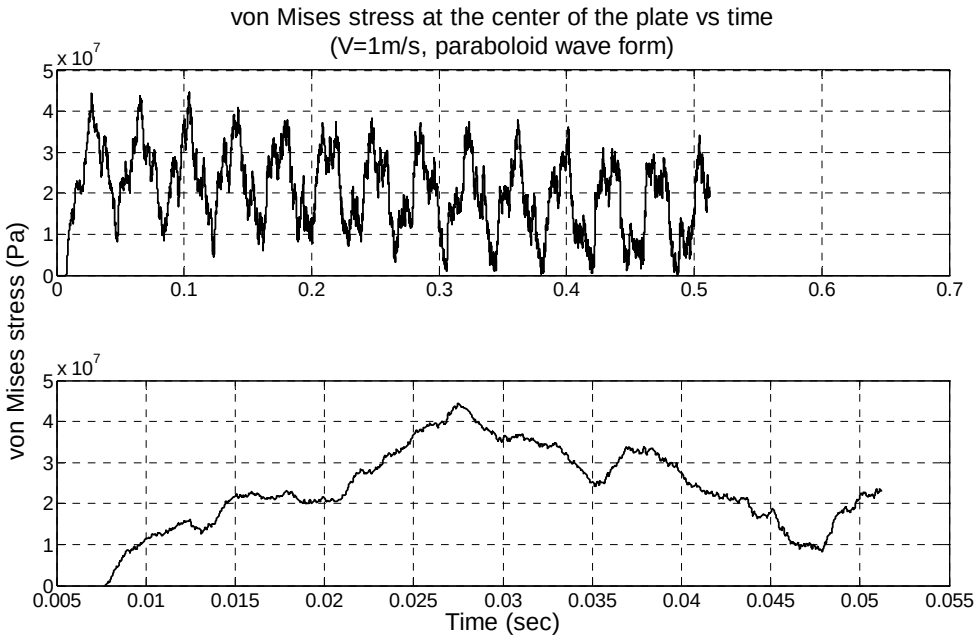

Figure 5.9: von Mises stress at the center of the wet-deck plate over a time span. a = 5m, b = 2m, h = 1cm, paraboloid wave profile R = 3m, impact velocity V=1m/s

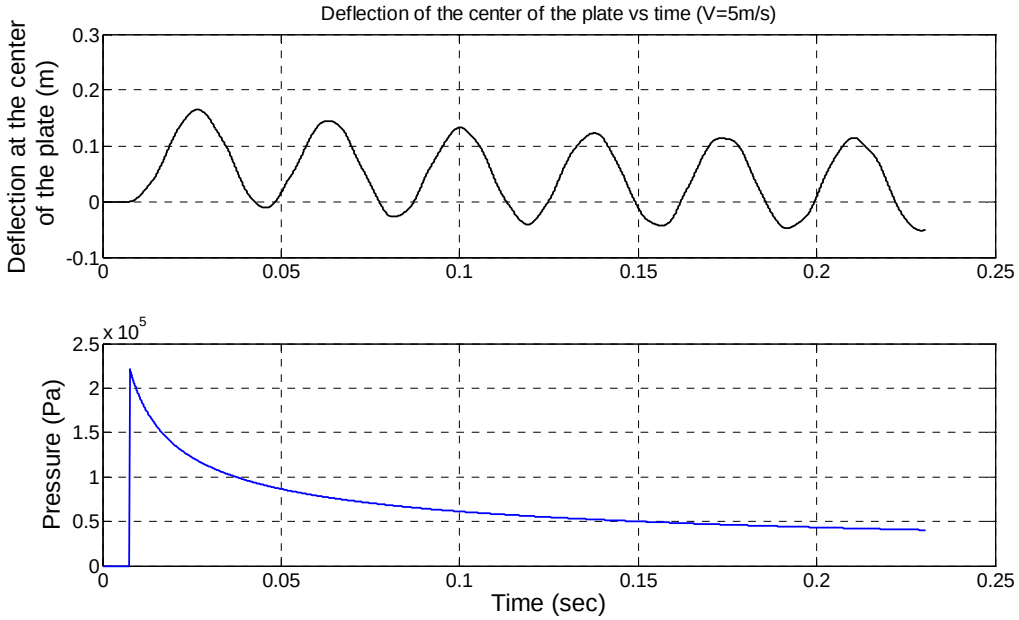

Figure 5.10: Deflection of the center of the wet-deck plate over a time span. a = 5m, b = 2m, h = 1cm, paraboloid wave profile R = 3m, impact velocity V=5m/s

Next, the plate is assumed to be hitting the paraboloid wave profile at the velocity of 5 m/s. The deflection of the center of the plate is shown in Fig. 5.10 and von Mises stress distribution is depicted in Fig. 5.11.

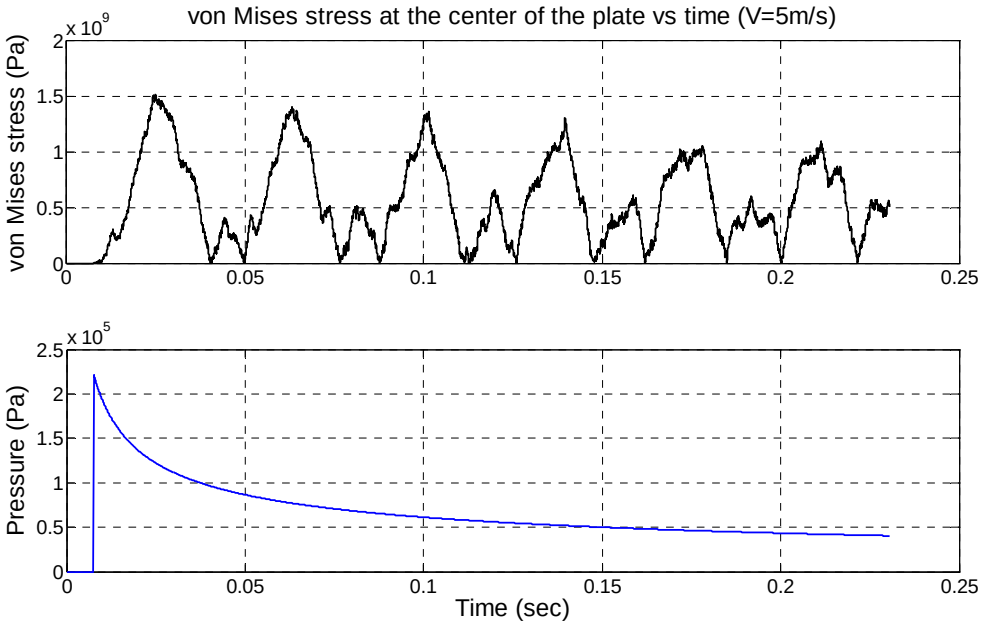

Figure 5.11: von Mises stress at the center of the wet-deck plate over a time span. a = 5m, b = 2m, h= 1cm, paraboloid wave profile R = 3m, impact velocity V=5m/s

On camparing Figs. 5.9 and 5.11, It can be deduced that at high water entering velocities, the stresses on the wet-deck plates can go above the yield stress limit frequently. As we have seen earlier, paraboloid form of the wave is also responsible for producing larger amplitude of the stress.

Now, wet-deck plate element is examined under the slamming forces which are produced by the slamming type interaction of wet-deck and sinusoidal wave form. Von Mises stress analysis has been carried out along with the determination of the plate vibrations. Deflection of the plate under different impact velocities, 1m/s and 5m/s, are

shown in Figs. 5.12 and 5.14, respectively. Stress generated due to the impact velocity of 1m/s is shown in Fig. 5.13. This stress is smaller as compared to the one with impact velocity of 5 m/s, Fig 5.15.

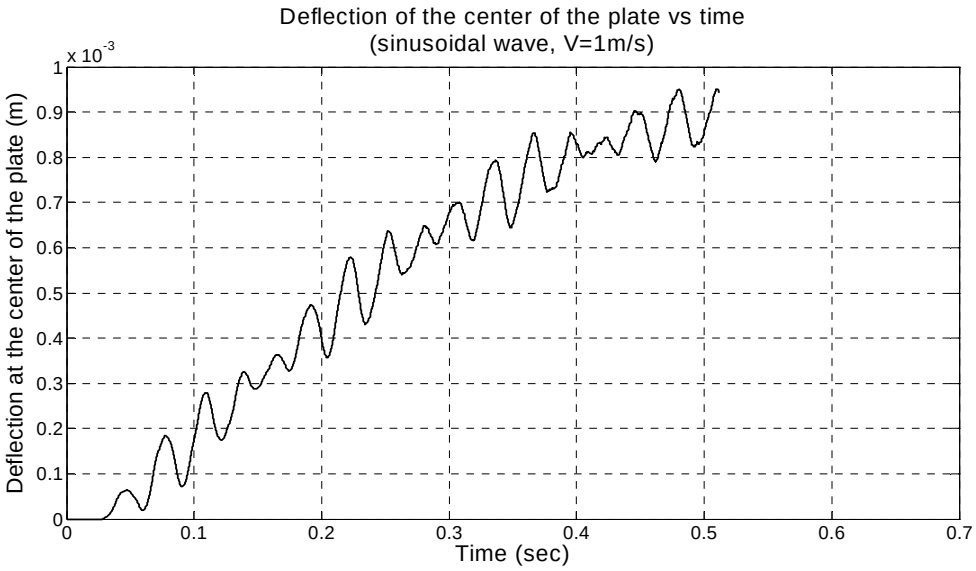

Figure 5.12: Deflection of the center of the wet-deck plate over a time span. a = 5m, b = 2m, h = 1cm, sinusoidal steep wave H/λ = 1/7, H=3m, impact velocity V=1m/s

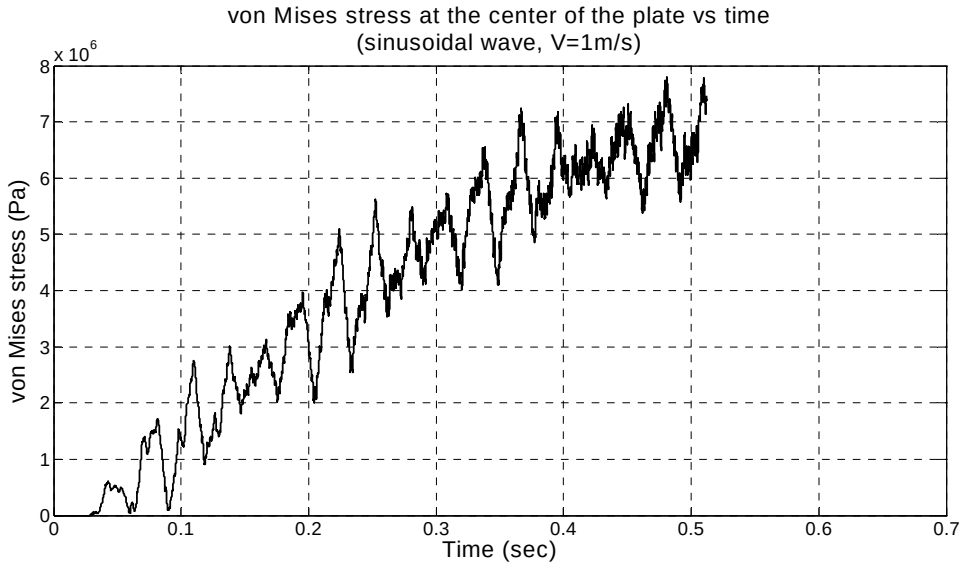

Figure 5.13: von Mises stress at the center of the wet-deck plate over a time span. a = 5m, b = 2m, h = 1cm, sinusoidal steep wave H/λ = 1/7, H=3m, impact velocity V=1m/s

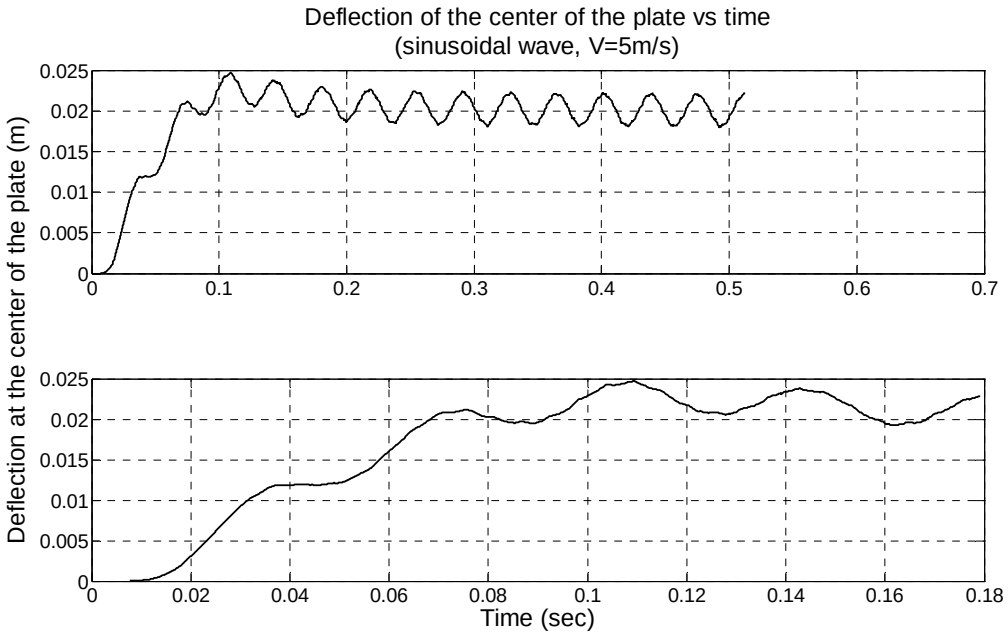

Figure 5.14: Deflection of the center of the wet-deck plate over a time span. a = 5m, b = 2m, h = 1cm, sinusoidal steep wave H/λ = 1/7, H=3m, impact velocity V=5m/s

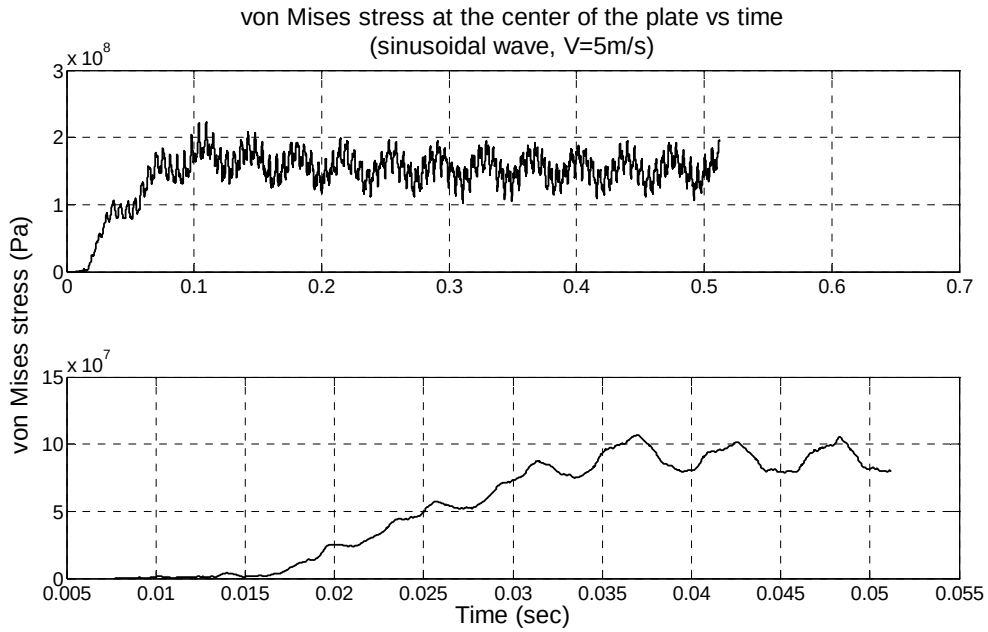

Figure 5.15: von Mises stress at the center of the wet-deck plate over a time span. a = 5m, b = 2m, h = 1cm, sinusoidal steep wave H/λ = 1/7, H=3m, impact velocity V=5m/s

This concludes the analysis of the stress on the wet-deck of a twin hull ship which were obtained using ABS design formula and Wagner's theory of slamming. The results conclude that higher amplitude of the slamming load generated free vibrations of higher amplitude, which can lead the structure stresses to exceed the yield stress limit. It was observed that at certain impact velocities and periodicities of the wet-deck slamming events could lead to structural failure. These findings can be used to reform the empirical formula of design slamming pressure.

5.2 Vibration/stress analysis of hull plate panels

So far we have illustrated the vibration and stress analysis of wet-deck under various types of slamming loads. Now, in this section, we will discuss the effect of slamming and regular loads on the hull plate. Slamming loads have been determined using the wedge drop formulation provided by Wagner, Flatinsen [56], with the effect of the jet spray provided by Peseux et al [87]. Regular wave loads were determined by using the work of Anathakrishnan [55], where a twin hull rectangular body is in oscillating heave motion. Pressure at the bottom is determined due to forced oscillations and later this pressure is used with the wave excitation force in equation of stiffened plate vibration, Eqn. 3.48, to obtain stresses and deflection of the hull bottom plate.

5.2.1 Wedge entering in the calm water with downward velocity V

The formulation of determining the slamming pressure on water entering wedge has already been discussed in Chapter 3. Here the wedge is assumed to descend with a constant velocity V throughout the entire entering process. The stiffeners spacing has

been taken according to Luo et al [80]. The plate and stiffeners material is selected to be steel which has the modulus of elasticity as $200*10^9$ *GPa* and shear modulus as $80*10^9$ *GPa*. Fig. 5.16 shows the new hull plate element with length = 2.88m, breadth = 1.8m and thickness = 0.003m. Longitudinal stiffeners are placed at a gap of 0.18 m and transverse stiffeners spacing is 0.48 m. The tip of the hull is at y-axis so when wedge starts entering the water, slamming pressure builds up at the tip and then travels constantly through the plate as wedge continues entering into the water.

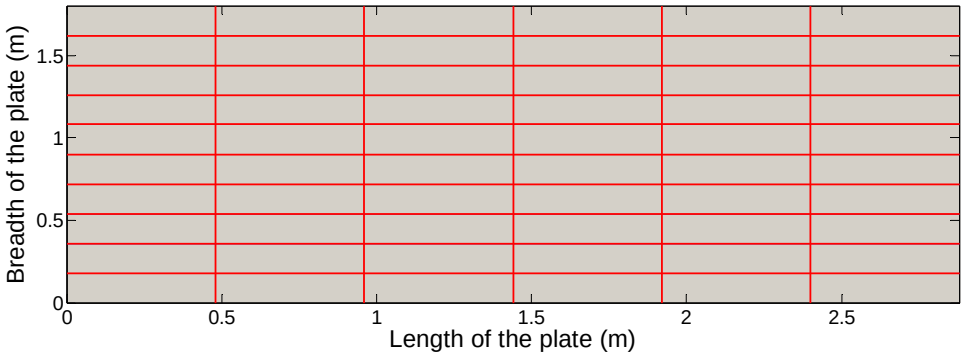

Figure 5.16: Hull plate sketch. a=2.88m, b=1.8m and h=0.003 m. Red colored lines show the stiffeners locations on the plate.

In the event of wedge entry into the fluid domain, the keel (y axis of above figure) first into the fluid i.e. wetted surface start from the y-axis to the right most end of the plate. During wedge emersion, high slamming pressures occur at the contact line of fluid and the plate. Two simulations are done in this section which corresponds to the dead-rise angle of the wedge, (i) 15^o, and (ii) 22^o. High values of slamming pressure are recorded for the lower dead-rise angle of the wedge.

Figs. 5.17-5.20 correspond to the first case of dead-rise angle as 15^o. The wedge water entry velocity is kept same at 5 m/s and assumed to be unchanged during the

slamming event. Deflection, stress in x-direction, and von Mises stress are plotted at the center of the plate in Fig. 5.17-5.19. Lower part of each figure shows the pressure variation over time at the center of the plate.

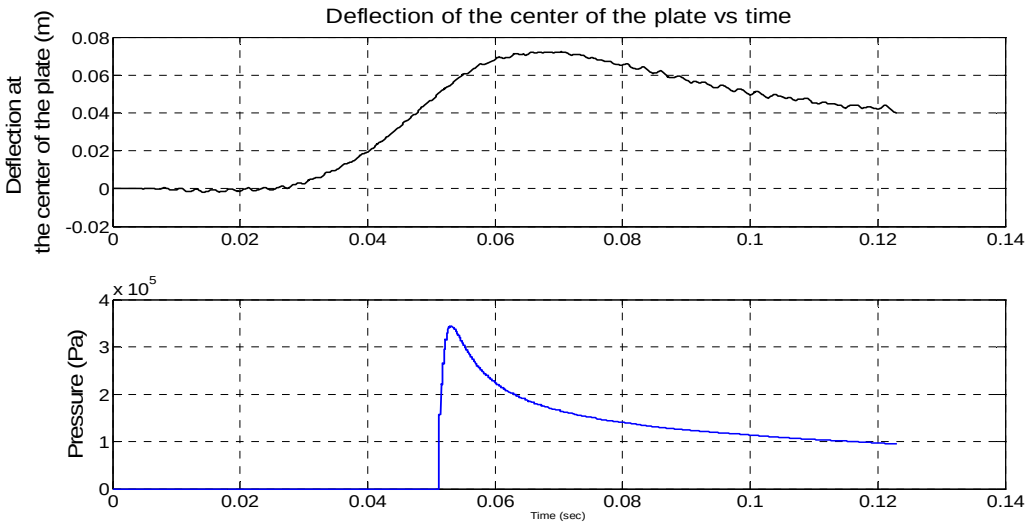

Figure 5.17: Deflection at the center of the hull plate over a time span. a = 2.88m, b = 1.8m, h = 0.003m, dead-rise angle 15o and impact velocity V = 5m/s

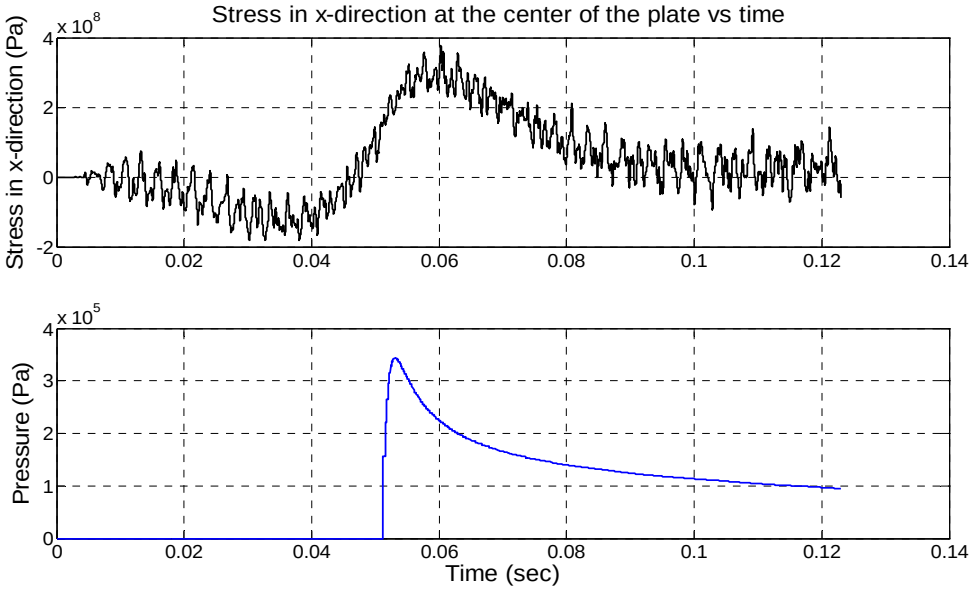

Figure 5.18: Stress in x-direction at the center of the hull plate over a time span. a = 2.88m, b = 1.8m, h = 0.003m, dead-rise angle 15o and impact velocity V = 5m/s

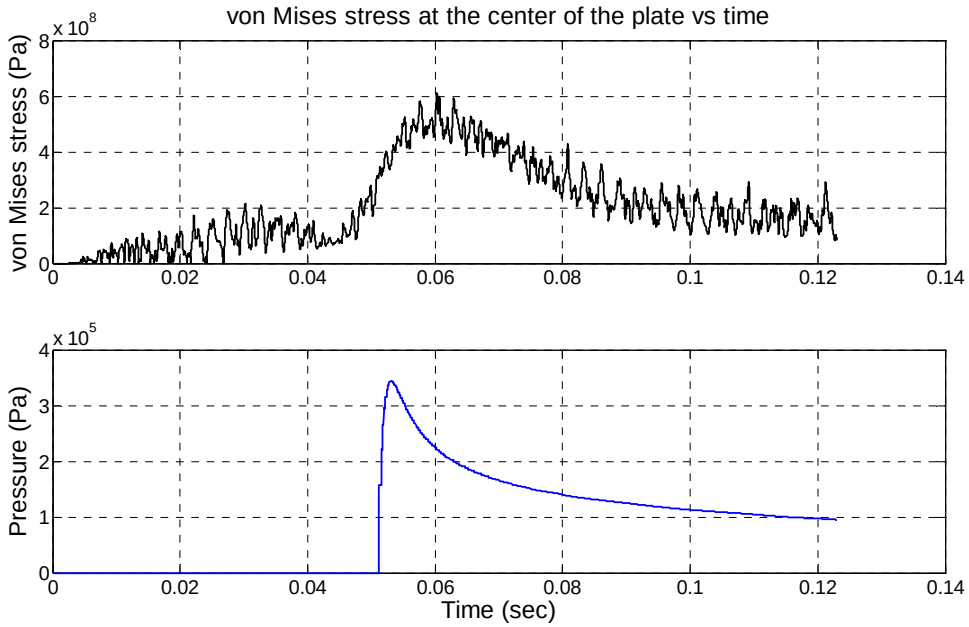

Figure 5.19: von Mises at the center of the hull plate over a time span. Length of the plate a = 2.88m, breadth of the plate b = 1.8m, thickness of the plate h = 0.003m, dead-rise angle 15o and impact velocity V = 5m/s

It can be seen that the deflection, Fig. 5.17, does not have large amplitude of the natural vibration of the plate, but fluctuations in von Mises stress are recorded which surpass the yield stress limit.

Fig. 5.20 shows the von Mises stress time distribution at the tip of the wedge. High value of the slamming pressure is recorded when the wedge just starts entering into the fluid domain and it remains above the permissible limit of the stress.

Next four figures, from Fig. 5.21 to 5.24, correspond to the wedge with dead-rise angle of 22^{o}, which show the deflection, stress in x-direction and von Mises stress at the center of the plate and von Mises stress at the tip of the plate, respectively. This specific value of the dead-rise angle is chosen for performing a validation using the results from the experiments conducted by Luo et al [80].

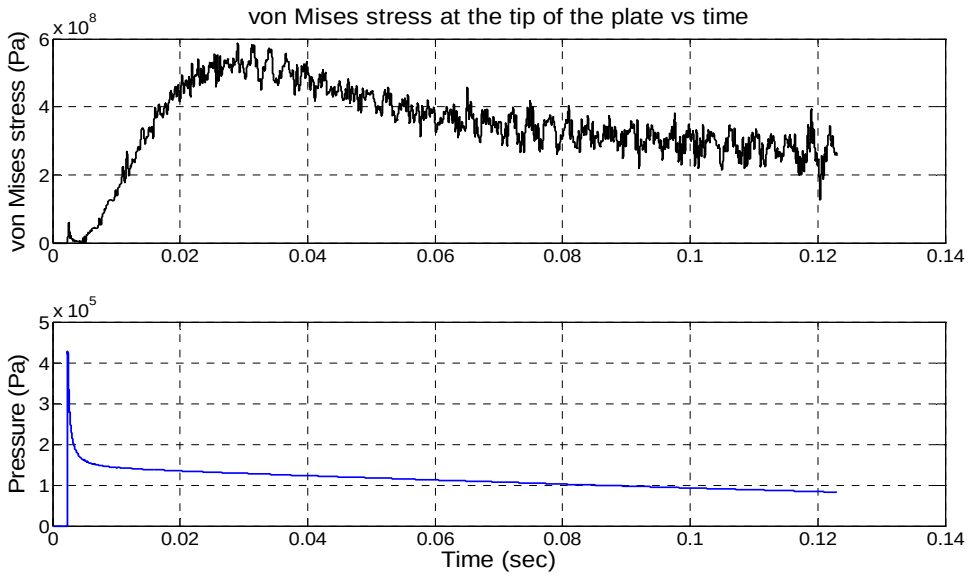

Figure 5.20: von Mises stress at the tip of the hull plate over a time span. Length of the plate a = 2.88m, breadth of the plate b = 1.8m, thickness of the plate h = 0.003m, dead-rise angle 22o and impact velocity V = 5m/s

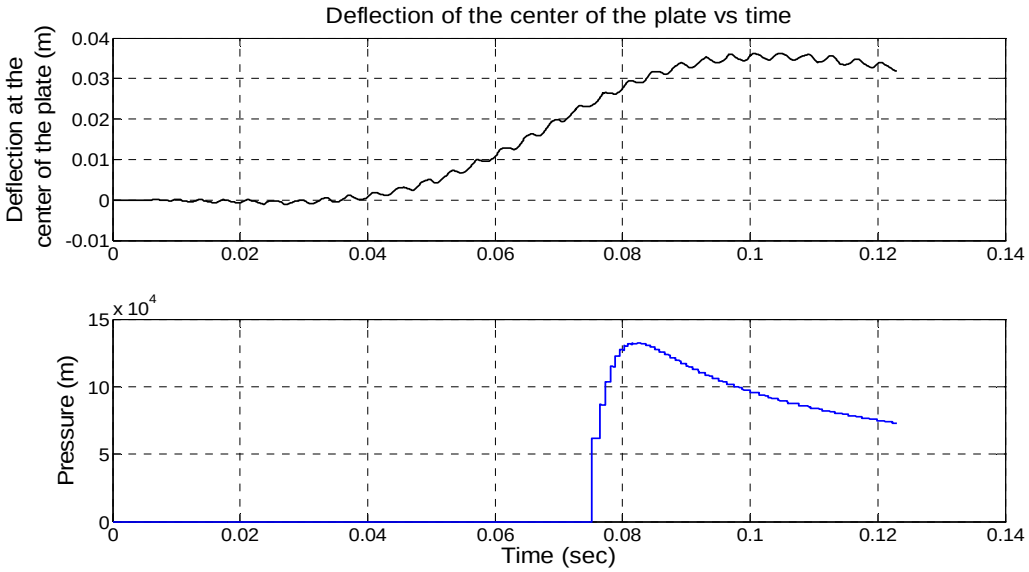

Figure 5.21: Deflection at the center of the hull plate over a time span. a = 2.88m, b = 1.8m, h = 0.003m, dead-rise angle 22o and impact velocity V = 5m/s

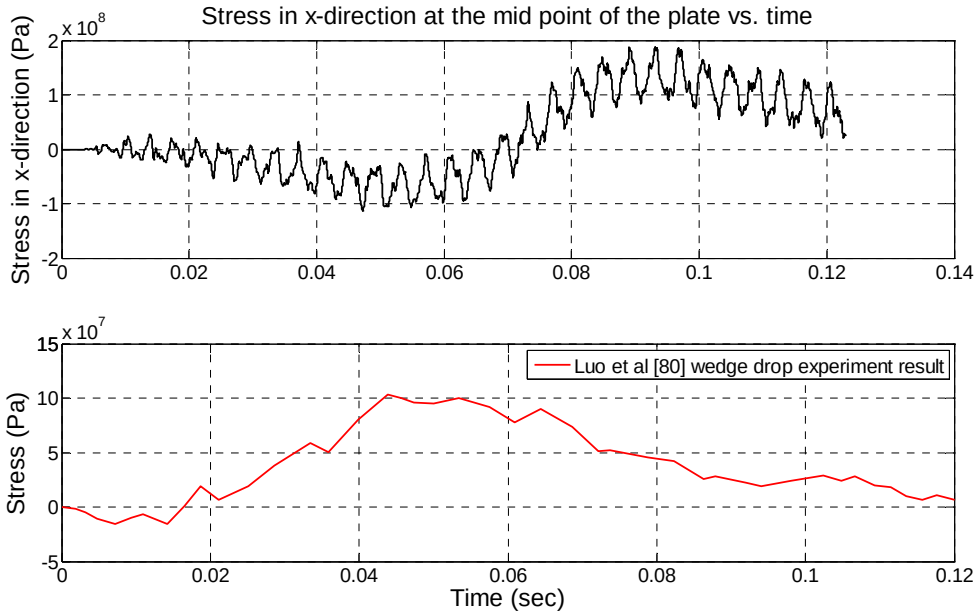

Figure 5.22: Stress in x-direction at the center of the hull plate over a time span. a = 2.88m, b = 1.8m, h = 0.003m, dead-rise angle 22^{o} and impact velocity V = 5m/s

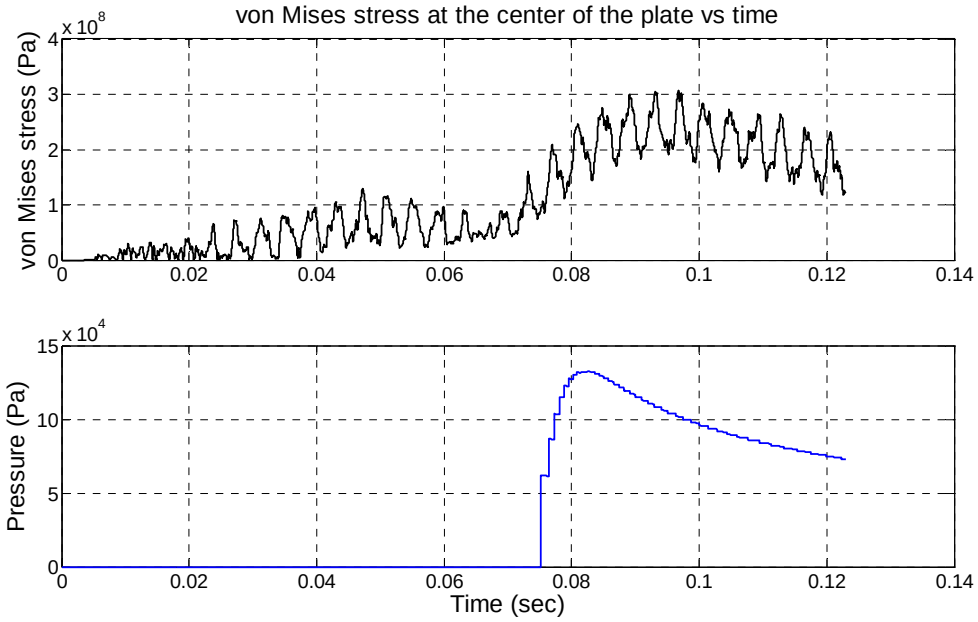

Figure 5.23: von Mises stress at the center of the hull plate over a time span. a = 2.88m, b = 1.8m, h = 0.003m, dead-rise angle 22o and impact veloicty V = 5m/s

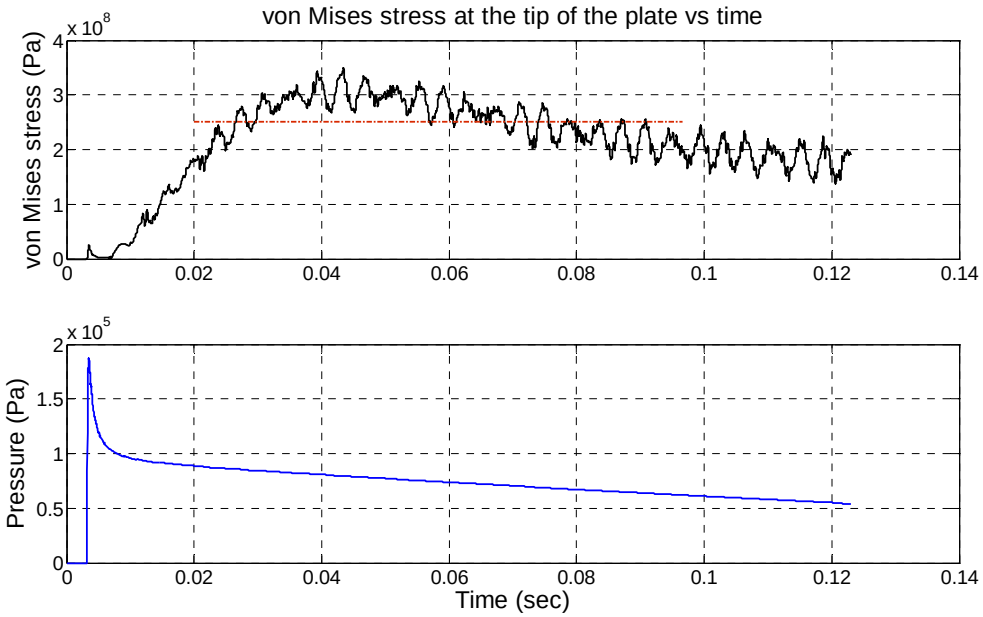

Figure 5.24: von Mises stress at the tip of the hull plate over a time span. Length of the plate a = 2.88m, breadth of the plate b = 1.8m, thickness of the plate h = 0.003m, dead-rise angle 22o and impact velocity V = 5m/s

In Fig. 5.22, the comparison has been made with the wedge drop experimental results obtained by Luo et al [80]. Amplitudes of the stress match with each other but time histories do not compare well, a possible reason for which could be is the fact that in the experiments the wedge is dropped and therefore entry velocity may not be constant with respect to as assumed in the present calculations. Nevertheless, the present calculation is able to determine the primary quantity of design concern, namely the amplitude of the stresses as shown in Fig. 5.25 below with reasonable accuracy.

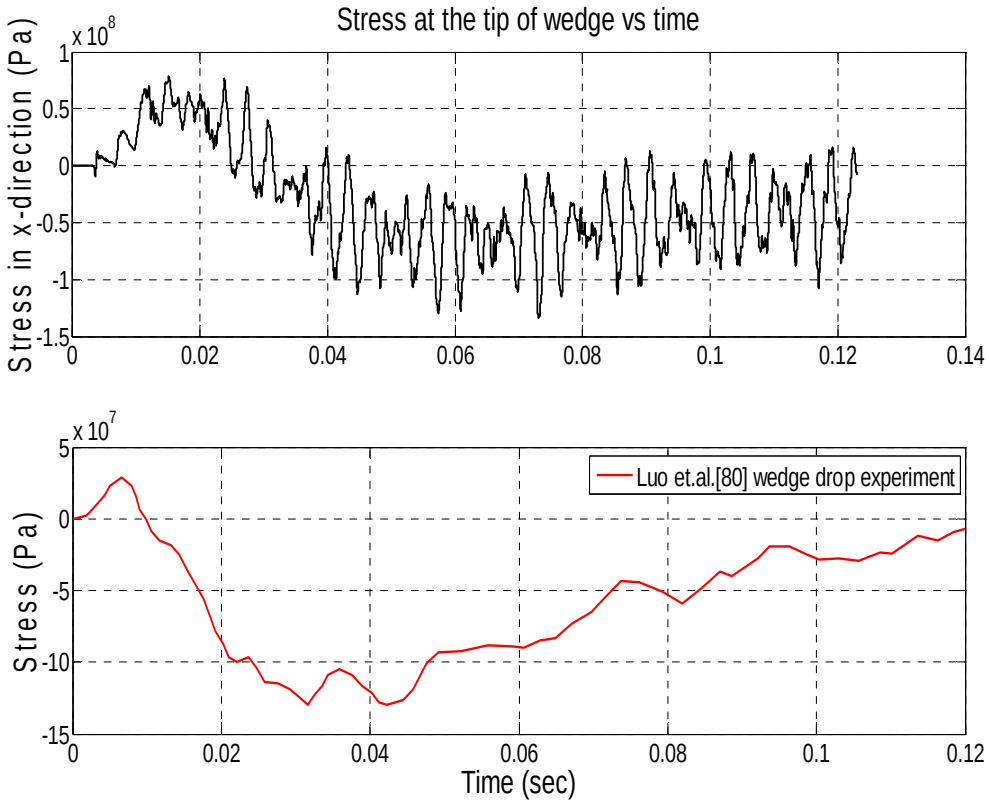

Figure 5.25: Stress in x-direction at the tip of the hull plate over a time span. a = 2.88m, b = 1.8m, h = 0.003m, dead-rise angle 22o and impact velocityty V = 5m/s

Next we consider a twin hull undergoing the heaving motion and determine the vibration of a bottom plate. The effect of wave excitation force and the radiation force on the bottom plate of the hull will be presented here.

5.2.2 Twin hull under forced heave oscillations

This part of results discusses the effect of wave excitation force on the bottom of an oscillating wedge in vertical direction (heave). Fig. 5.25 shows the sketch of oscillating wedge and the location of the hull plate element.

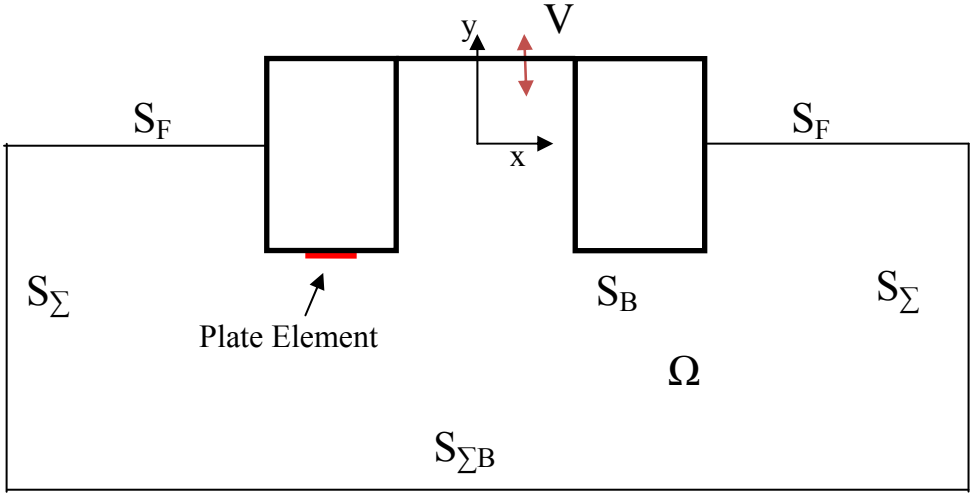

Figure 5.26: Sketch of the twin hull barge under going the forced heaving motion.

Boundary representation has already been shown in Chapter 2. Here the focus is on the bottom plate element which is shown in Fig. 5.25. The equation of the stiffened plate vibrations Eqn. 3.48, can be rewritten with the pressure terms as;

$$D_x \frac{\partial^4 W(x,y,t)}{\partial x^4} + 2H \frac{\partial^4 W(x,y,t)}{\partial x^2 \partial y^2} + D_y \frac{\partial^4 W(x,y,t)}{\partial y^4} - \rho_p \frac{\partial^2 W(x,y,t)}{\partial t^2} = P_{exc} + P_{radiation} \tag{5.2}$$

where, P_{exc} is the wave excitation pressure, which is modeled using Froude-Krylov incident wave force and $P_{radiation}$ is the radiation pressure acting on the plate which in the present work is taken to be that due to body oscillation and not translation. The justification could be that wave resistance may not contribute significantly to the

vibration of a bottom plate, even though the wave resistance potential may affect the wave radiation potential due to oscillation. Diffraction force due to incident waves has been ignored in this study and radiation pressure can be expressed in terms of added mass and damping, Newman [21];

$$P_{radiation} = A_{22}\dot{V}_2 + B_{22}V_2 \tag{5.3}$$

where, subscript *2* represents the heave motion, A_{22} is the heave added mass coefficient per unit area, and B_{22} is the damping coefficient per unit area. V_2 and $\dot{V}_2$ represent the periodic body velocity and acceleration, respectively.

Damping coefficient B_{22} is equal to the average work done against the pressure over one cycle. This assumption is true for the single mode of oscillations [21]. The expression can be written as;

$$\overline{P_{radiation}V_2} = B_{22}\overline{V_2^{\,2}} \tag{5.4}$$

Above expression provides the damping coefficient and it can be used in Eqn. 5.3 to obtain the value of added mass coefficient. Using V_2 as $V_2 = \varsigma_2 e^{-i\omega t}$, where ω is the oscillation frequency and ς_2 is the heave amplitude. $P_{radiation}$ can be written as follows;

$$P_{radiation} = -A_{22}\varsigma_2\omega^2 e^{-i\omega t} - B_{22}i\omega\varsigma_2 e^{-i\omega t} \tag{5.5}$$

Linear wave excitation force does not depend on the radiation of the body, and even the added mass and damping are independent of incident wave characteristics. The wave exciting force is taken to be that as Froude-Krylov force at the frequency corresponding to that of the heave motion and with unit incident wave amplitude. Using Eqn. 5.5, the equation for vibration can be solved for the plate vibration response;

$$Z^* = \frac{P^*_{exc}}{(\rho_P + A_{22}\varsigma_2)\omega^2 - iB_{22}\omega + K^4} \tag{5.6}$$

where, superscript "*" represents only spatial distribution and *K* depends on the plate restoring force terms, i.e. rigidities.

The radiation pressure, Ananthakrishnan [55], is obtained for two radiation frequencies. One corresponds to the slosh resonance frequency, i.e resonant movement of water between the twin hulls, and the other is at regular frequency without any resonance effect.

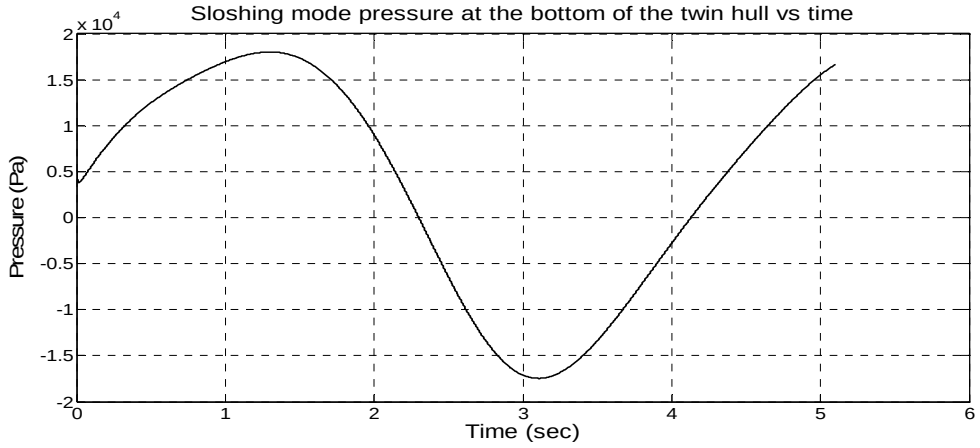

Figure 5.27: Radiation pressure at the bottom of the demihull at sloshing mode frequency σ=1.5336 rad/sec, beam of the demi hull = 5m, amplitude of oscillations = 0.5 m, draft = 2.5m

Fig. 5.27 shows the radiation pressure distribution at the bottom of the hull over time. This radiation pressure is then applied to Eqn. 5.2 along with the wave excitation force of unit amplitude. The deflection and von Mises stress at the center of the bottom plate are shown in Figs. 5.28 and 5.29, respectively. It is observed that the deformation has two principal modes of vibration; one belongs to the wave pressure and the other to the natural frequency of the stiffened plate. These frequencies can be seen in the power spectrum of the time history of deflection, Fig. 5.30.

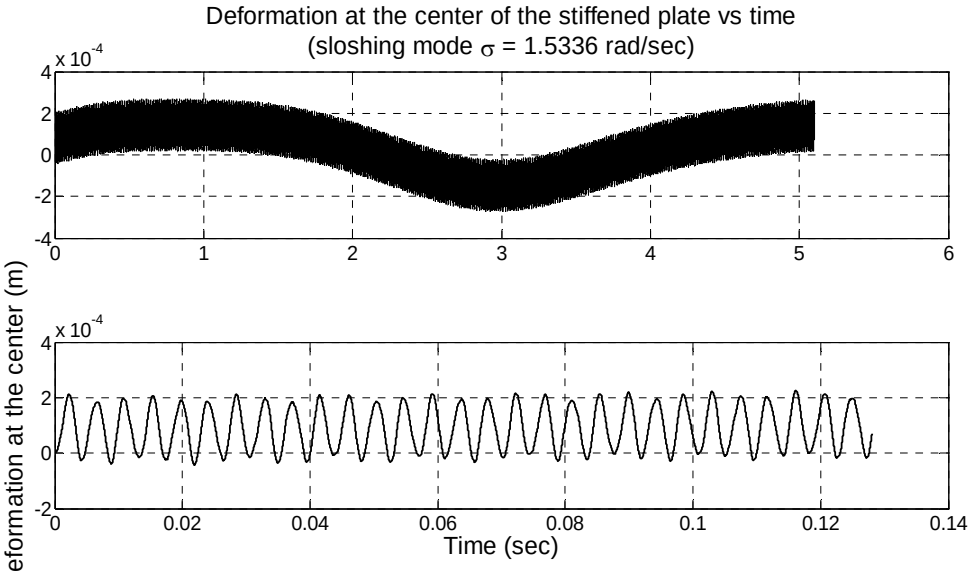

Figure 5.28: deformation at the center of the bottom plate of demi hull over a time span. a = 2.88m, b = 1.8m, h = 0.003m, sloshing mode frequency σ=1.5336 rad/sec, beam of demi hull = 5m, amplitude of oscillations = 0.5 m, draft = 2.5m

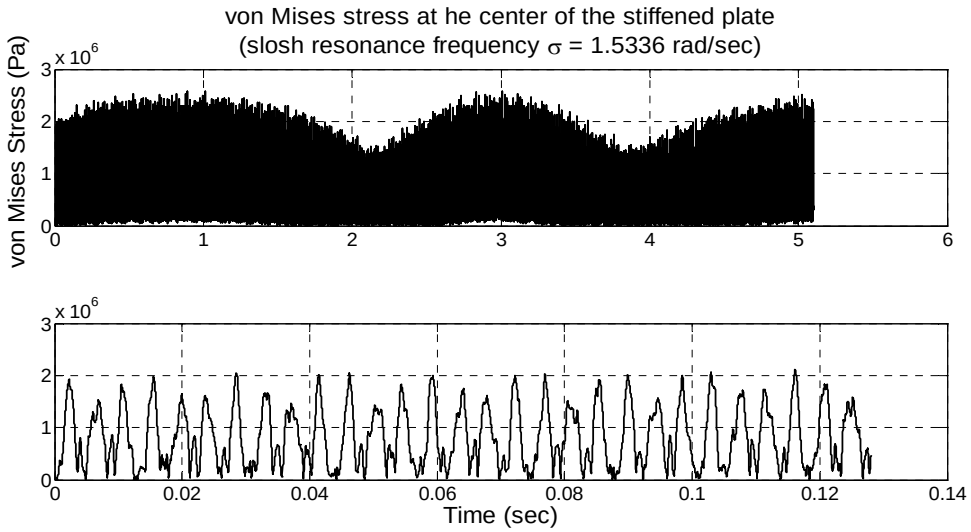

Figure 5.29: von Mises stress at the center of the bottom plate of demi hull over a time span. a = 2.88m, b = 1.8m, h = 0.003m, sloshing mode frequency σ=1.5336 rad/sec, beam of demi hull = 5m, amplitude of oscillations = 0.5 m, draft = 2.5m

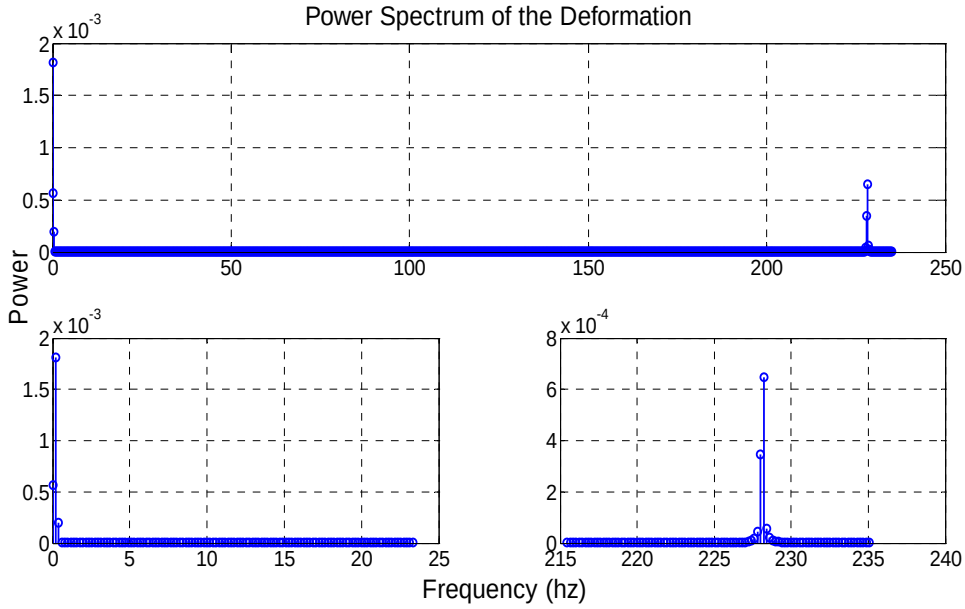

Figure 5.30: Power spectrum of the deflection of the plate. Second peak @ 228 rad/sec corresponds to the plate's natural vibration frequency

The power spectrum of the deformation of the plate shows two major components of frequencies - first one is located at the frequency of wave force while the second peak shows the frequency of natural vibration of the stiffened plate.

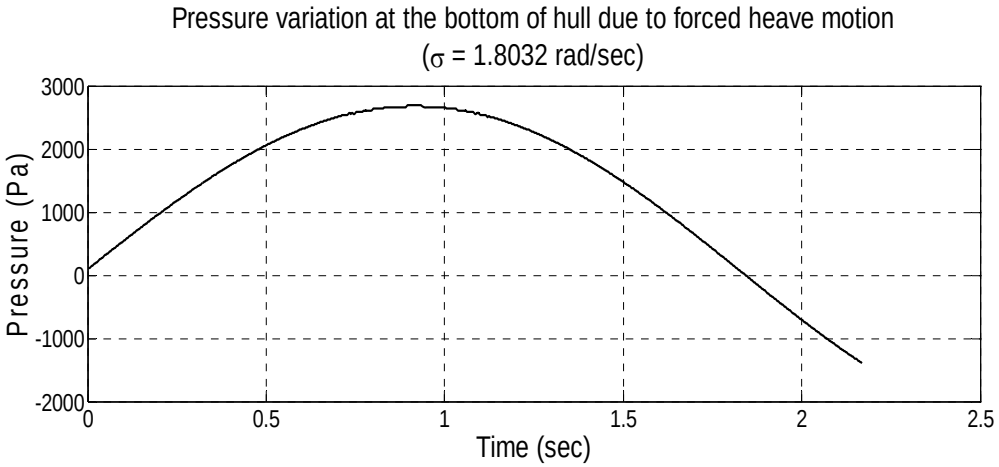

Figure 5.31: Radiation pressure at the bottom of the demihull at a regular (non-resonant) mode frequency σ=1.8032 rad/sec, beam of demi hull = 5m, amplitude of oscillations = 0.5 m, draft = 2.5m

Second case of the hull vibration corresponds to the regular frequency. Fig. 5.31 shows the time variation of radiation pressure at the bottom of the hull. This pressure is then applied to the stiffened plate, dimensions are specified above, and stress analysis along with the deflection of the plate are carried out which are shown in Figs. 5.32 and 5.33.

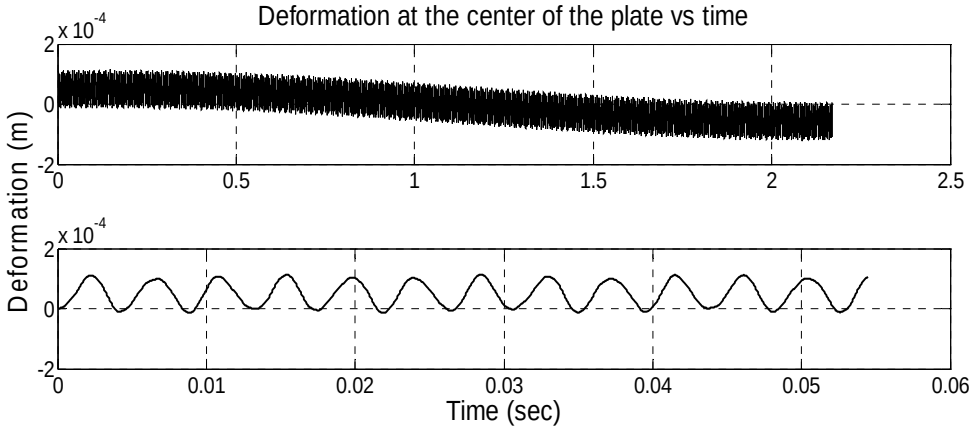

Figure 5.32: deformation at the center of the bottom plate of demi hull over a time span. a = 2.88m, b = 1.8m, h = 0.003m, regular (non-resonant) frequency σ=1.8032 rad/sec, beam of demi hull = 5m, amplitude of oscillations = 0.5 m, draft = 2.5m

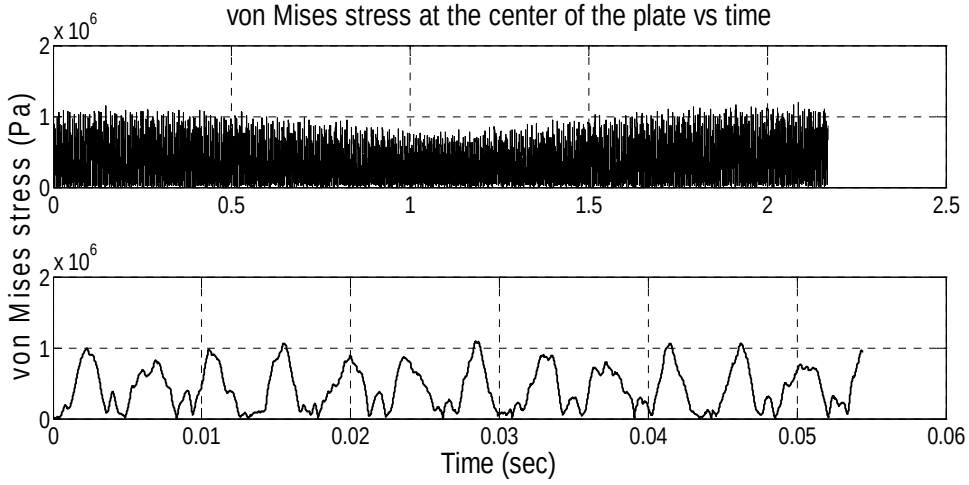

Figure 5.33: von Mises stress at the center of the bottom plate of demi hull over a time span. a = 2.88m, b = 1.8m, h = 0.003m, a regular (non-resonant) frequency σ=1.8032 rad/sec, beam of demi hull = 5m, amplitude of oscillations = 0.5 m, draft = 2.5m

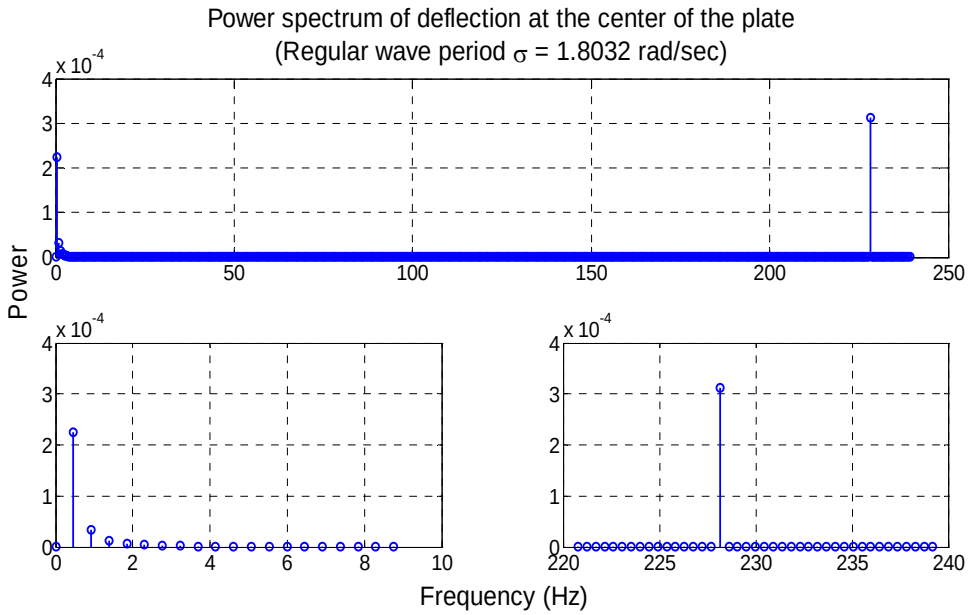

Figure 5.34: Power spectrum of the deflection of the plate. Second peak @ 228 rad/sec corresponds to the plate's natural vibration frequency

Fig. 5.34 shows the power spectrum of the deformation of the plate. First peak corresponds to the wave force frequency and second peak corresponds to the plate's natural frequency which is same as the one in Fig. 5.30.

In the above calculations, the heave motion amplitude and incident wave amplitude values were taken to be independent of each other. Considering the relation between the incident wave and heave motion response per linear transfer function;

$$Z_R^* = \frac{P_{exc}^*}{\rho g A_w + i\sigma B_{22} - (m + A_{22})\omega^2} \tag{5.6}$$

where, Z_R^* is the rigid body heave response of the ship and m is mass per unit length of the ship hull girder.

We find the wave amplitude corresponding heave motion amplitude of 0.5 m at 1.8 rad/s to be A = 2.75. Since the relation used for the Froude-Krylov force is a linear function

of wave amplitude, the plate vibration results presented in Fig. 5.28 were to be multiplied by a factor of 2.75 for the correct plate vibration.

In this chapter, we have determined the effect of slamming pressure on the hull as well as the effect of wave excitation pressure and radiation pressure on the bottom of twin hull. It is observed that in a few cases of slamming the stress goes above the yield stress limit which can be of concern for naval architects.

6. WHIPPING ANALYSIS OF SL7 CONTAINER SHIP

Hydroelastic effects are significant in the response of the structure while moving with high forward speed. The analysis of these hydroelastic effects can be categorized into two parts, (i) springing analysis, and (ii) whipping analysis with the former corresponding to time-harmonic wave forces and the latter to the transient slamming force. In this chapter, we present the results for the whipping as it is more prone to structural failure. The added mass effect is not taken into consideration in the transient analysis. A 280 m long SL7 class containership is used for the whipping analysis and the principal particulars of the ship are tabulated below:

Paratmeter	**Value**
Length between perpendiculars (m)	280
Breadth (m)	32
Draught (m)	9.95
Displacement (t)	50,500
Block Coefficient	0.585
Moment of inertia amidships (m^4)	350
Forward Speed (knots)	25

Table 6.1: Main specifications of SL-7 class container ship.

The longitudinal mass and moment of inertia distribution is given in Figs. 6.1 and 6.2, respectively. Springing analysis has been done for two sea-states and deflection and vertical bending moment RAOs are determined.

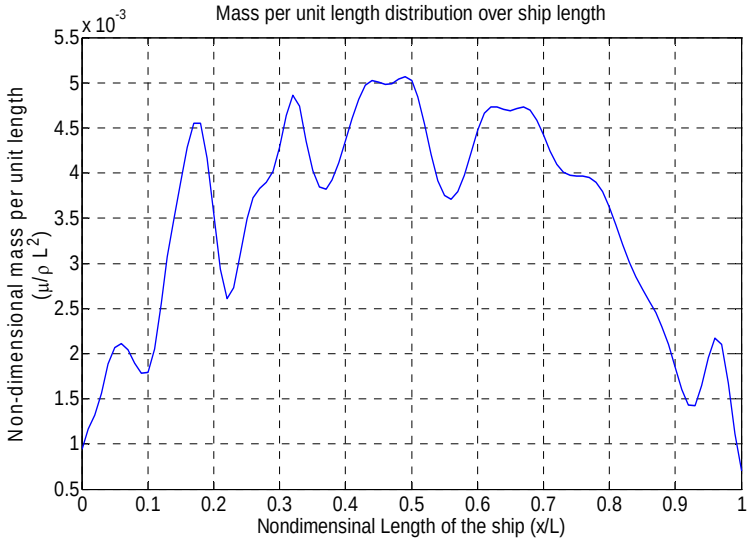

Figure 6.1: Non-dimensional mass distribution of the SL-7 class containership

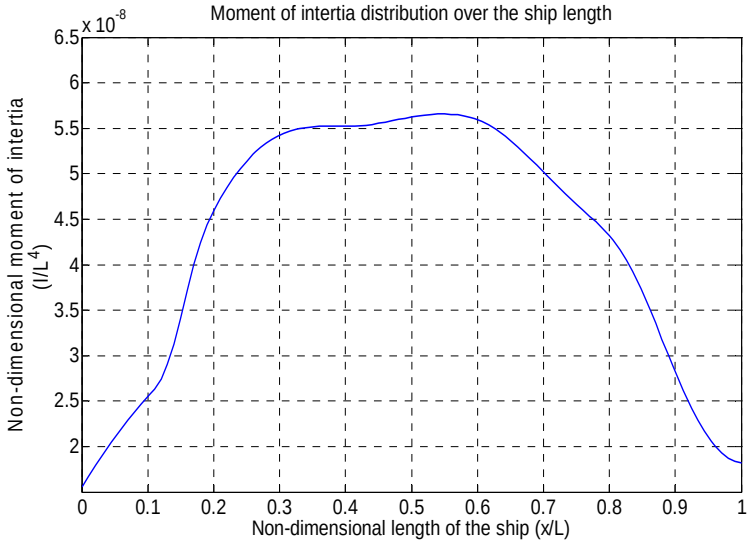

Figure 6.2: Non-dimensional moment of inertia distribution over the ship length

Whipping analysis of the SL-7 type container ship is done for the periodic spike loading, which is shown in the Fig. 4.31. The spike loading is applied to the forward one third of the ship length and it can be observed that the frequent slam loads excite the higher modes of hull vibrations.

Figs. 6.3 and 6.4 show the time history of vertical bending moment of the ship while moving with the speed of 25 knots.

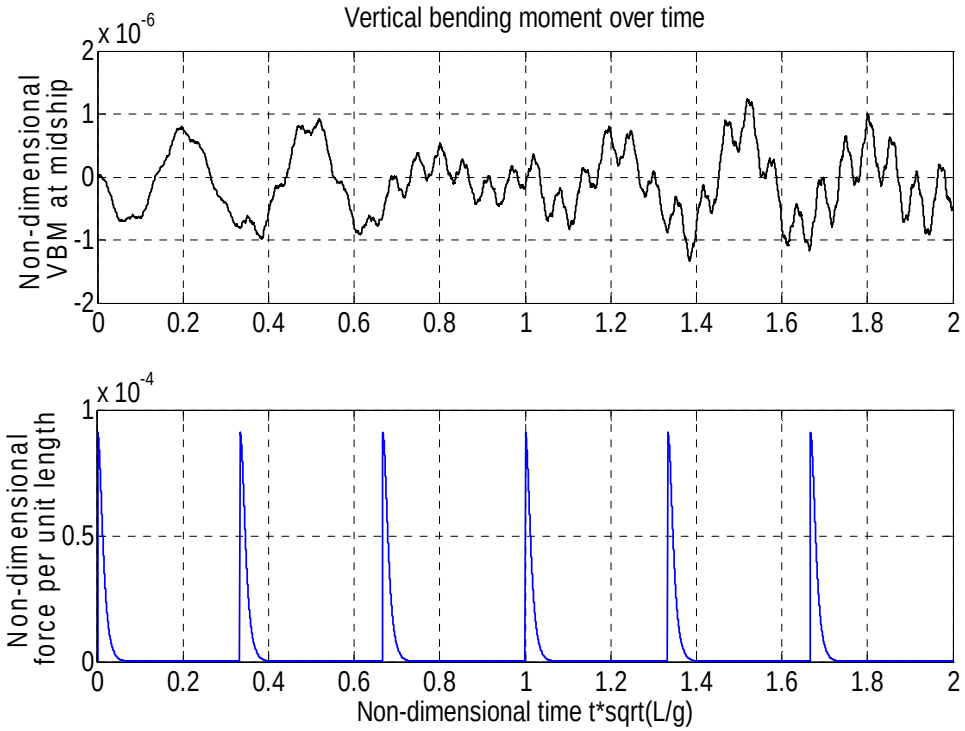

Figure 6.3: Time history of vertical bending moment under spike loading. Ship speed= 25knots

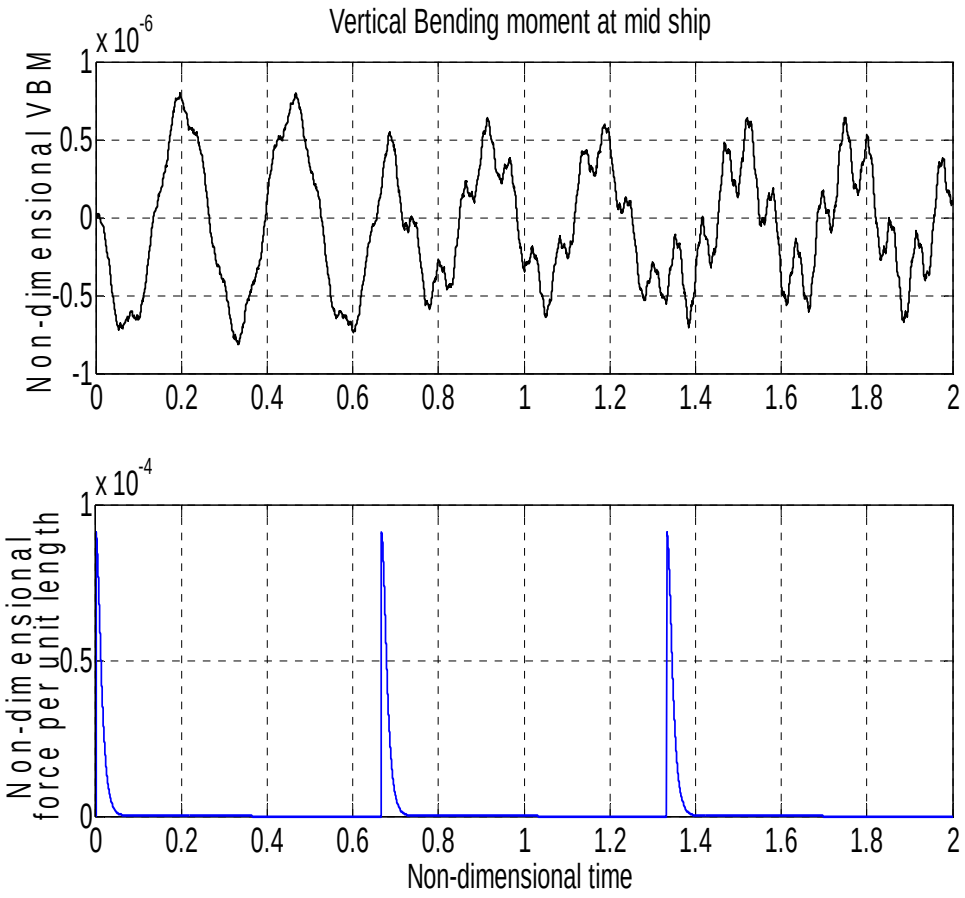

Figure 6.4: Time history of vertical bending moment under less frequent spike loading. Ship speed = 25 knots

By an order of magnitude, for the bending moment given in the above figures the bending stress on the deck (or bottom) of the SL7 is estimated to be $O(10^6)$ [Pa] which is sufficiently less the yield stress of steel 250 x 10^6 [Pa].

More thorough analysis can be done by using for example the finite element model of the ship, but above results provide a preliminary insight of the whipping effects on the ship. It can be concluded from the results that the whipping effects can be prominent at large forward speeds which in turn will cause frequent slamming events.

7. CONCLUSION AND FUTURE RESEARCH RECOMMENDATIONS

The dissertation, which involves the consideration of both hydrodynamics and structural mechanics, has modeled and analyzed the vibrations of ship hull and plates due to regular waves and in extreme events such as wave slamming which is a concern for structural failure. Depending on the parameter values and cases, wave forces were determined using classical theories as that of Froude and Krylov and Wagner as well as numerical and empirical methods. In particular, the nonlinear wave forces due to large amplitude waves and slamming, are determined using numerical methods, Wagner's theory and ABS design classification rules. The dissertation has considered a wide range of plate theories to model ship hull plate vibrations including large deformations, plate stiffeners and material damping. Robust numerical algorithms are to analyze the hull and plate vibrations. Transient as well as steady-state results are obtained for a large number of cases and range of wave and structural parameters. Results obtained compare well with experimental results, including as that in the extreme case of wedge drop and entry into water. Stresses (primary and von Mises) are obtained and compared with the yield stress as a possible indicator of structural failure. It may be added that structural failure is an extensive subject in itself meriting a separate focused research.

With the experience gained in the present research, the author would recommend following topics and approaches for future research:

- Consideration of full three-dimensional hydrodynamic analysis of ship hulls, including viscosity and turbulence modeling, to compute the wave forces. At present, there are standard software and codes such as ANSYS-CFX®, SHIP-IOWA® and OPENFOAM ® which seem to give reasonable estimates of wave forces. These commercial codes are however computationally demanding and more work is perhaps needed to accurately model free surface nonlinearity including viscous stresses and determine the wave slamming force.
- A full three-dimensional inviscid nonlinear boundary element code may be also developed to determine the wave slamming force on a ship which can be computationally more efficient than present 3D software and can better track the deforming wave surface.
- With regard to structural mechanics of the subject, the results may be used to strengthen or to develop models on structural failure criteria including that on fatigue failure.

As a future endeavor, the present algorithms, in particular of plate deformations, may be integrated into other models, for example as that used in finite-element models (such as that of Maki et al [79] and Ma [92]), used for ship structural and wave interactions.

APPENDIX A

FINITE DIFFERENCE SCHEME

This appendix expatiates the finite difference scheme which is used in solving the governing differential equation of the plate vibrations. Plate vibration equations are defined in both spatial and time domains and finite difference scheme is applied to both types of derivatives. Rewriting the governing differential equation for the vibrations of isotropic plate;

$$\frac{\partial^4 W(x,y,t)}{\partial x^4} + 2\frac{\partial^4 W(x,y,t)}{\partial x^2 \partial y^2} + \frac{\partial^4 W(x,y,t)}{\partial y^4} + 2\rho_p \gamma_d \frac{\partial W}{\partial t} - \frac{\rho_p}{D}\frac{\partial^2 W(x,y,t)}{\partial t^2} = q(x,y) \tag{A1}$$

As shown in Eqn. A1, there are three types of derivatives present in the equation, 4th order derivative term in space, 2nd order term in time, and 1st order term in time. This holds true for nonlinear plate theory and stiffened plate theory also.

Expansion of these derivative terms using the finite difference scheme is presented below for a given grid.

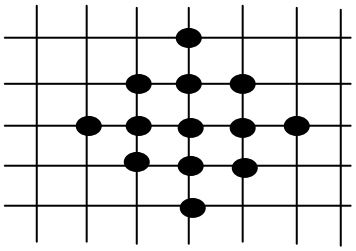

Figure A1: Spatial representation of the mesh which is generated on the plate.

Assuming that the central point is represented as the ordered pair (m, n), where *m* is numbering in x-direction and *n* is numbering in y-direction. So, the first point to the right of central point can be expressed as (m+1, n) and point to the left side as (m-1, n). Similarly, point above the central point can be expressed as (m, n+1) and the point below as (m, n-1). All the other points can be represented in the similar way. Expanded derivative now can be written as follows;

$$\frac{\partial^4 W}{\partial x^4} = \frac{1}{\delta x^4}\left(W^p_{m+2,n} + W^p_{m-2,n} - 4W^p_{m+1,n} - 4W^p_{m-1,n} + 6W^p_{m,n}\right)$$

$$\frac{\partial^4 W}{\partial x^2 \partial y^2} = \frac{1}{\delta x^2 \delta y^2}\left(W^p_{m+1,n+1} + W^p_{m+1,n-1} - 2W^p_{m+1,n} + W^p_{m-1,n+1} + W^p_{m-1,n-1} - 2W^p_{m-1,n} - 2W^p_{m,n+1} - 2W^p_{m,n-1} + 4W^p_{m,n}\right)$$

$$\frac{\partial^4 W}{\partial y^4} = \frac{1}{\delta y^4}\left(W^p_{m,n+2} + W^p_{m,n-2} - 4W^p_{m,n+1} - 4W^p_{m,n-1} + 6W^p_{m,n}\right)$$

$$\frac{\partial^2 W}{\partial t^2} = \frac{1}{\delta t^2}\left(W^{p+1}_{m,n} + W^{p-1}_{m,n} - 2W^p_{m,n}\right)$$

$$\frac{\partial W}{\partial t} = \frac{1}{\delta t}\left(W^{p+1}_{m,n} - W^{p-1}_{m,n}\right)$$

where, δx and δy are the mesh element lengths in x and y directions, respectively, and δt is the time step. Superscript *p* is the time representation so *p+1* represents the value at time next time step and *p-1* represents the value a time step before.

Boundary condition for each plate vibration equation is kept as clamped boundary condition. The mathematical representation of the boundary conditions is given as;

$$W = 0, \qquad \frac{\partial W}{\partial x} = 0 \quad at\ x = 0\ and\ a$$

$$W = 0, \qquad \frac{\partial W}{\partial y} = 0 \quad at\ y = 0\ and\ b$$

The application of the finite difference scheme on the boundary is different than when it is applied in the middle. Boundary conditions can be expanded using the finite difference method as;

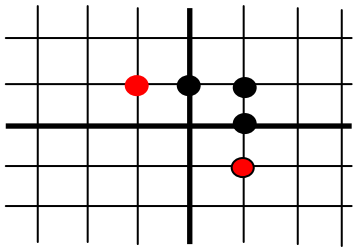

Figure A2: Spatial representation of the mesh which is generated on the plate, where bold lines are the axis and the plate is in 1st quadrant. The nodes, shown in 2nd and 4th quadrants, are the ghost nodes.

The expansion can be written as;

$$W^p_{m,n} = 0, \qquad W^p_{m-1,n} = W^p_{m+1,n} \quad at\ x = 0\ and\ a$$

$$W^p_{m,n} = 0, \qquad W^p_{m,n-1} = W^p_{m,n+1} \quad at\ y = 0\ and\ b$$

The finite difference expansion, for the nodes next to the boundary, can be modified using the above boundary conditions.

BIBLIOGRAPHY

1. Lamb, H., "Hydrodynamics," Dover Publication *(1932)*
2. Stoker, J. J, "Water waves: The mathematical theory with applications," *Wiley (1958)*
3. Wehausen, J., Laiton, E., "Surface waves," *Encyclopedia of Physics IX (1960) 446-778*
4. Ursell, F., "On the heaving motion of a circular cylinder on the free surface of a fluid," *Quarterly Journal of Mechanics and Applied Mathematics 2 (1949) 218-231*
5. Whitham, G. B., "Linear and nonlinear waves," *A Wiley Interscience Publication, New York (1974)*
6. Salvesen, N., Tuck, E. O., Faltinsen, O., "Ship motions and sea loads", *Trans. SNAME (1978) 250-287*
7. Doctors, L. J., Beck, R. F., "Numerical aspects of the Newmann-Kelvin problem", *Journal of ship Research 31 (1987) 1-13*
8. Frank, W., "The heave damping coefficients of bulbous cylinder", *Journal of Ship Research 11 (1967) 151-153*

9. Yeung, R. W., "A singularity-distribution method for free-surface flow problems with an oscillating body", *Ph.D. dissertation, University of California, Berkeley, 1973*

10. King, B., "Time domain analysis of wave exciting forces on ships and bodies," *PhD dissertation, University of Michigan (1987)*

11. Clement, A., "A discrete time model of transient hydrodynamics Green function," *7th workshop on water waves and floating bodies, Val de Revil (1992)*

12. Beck, R. F., Liapis, S., "Transient motions of floating bodies at zero forward speed," *Journal of Ship Research 31 3 (1987) 164-176*

13. McIver, M., "An example of non-uniqeness in the two-dimensional linear water wave problem", *Journal of Fluid Mechanics 315 (1996) 257-266*

14. McIver, M., "Trapped modes supported by submerged obstacles", *Proceedings of Royal Scociety London A 456 (2000) 1851-1860*

15. Wehausen, J. V., "The motion of floating bodies," *Annual Review of Fluid Mechanics 3 (1971) 237-268*

16. Yeung, R. W., "Numerical Methods for free-surface flows", *Annual Review of Fluid Mechanics 14 (1982) 395-442*

17. Wehausen, J. V., "The wave resistance of ships," *Advances in Applied Mechanic 13 (1973) 93-245*

18. Ogilvie, T. F., "Singular perturbation problems in ship hydrodynamics," *Advances in Applied Mechanics 17 (1977) 92-187*

19. Dean, R. G., Dalrymple, R. A., "Water wave mechanics for engineers and scientists," *Advanced Series on Ocean Engineering, World Scientific Publication*

20. Yeung, R. W., Ananthakrishanan, P., "Solution of nonlinear water-wave and wave body interaction problems using a new boundary-fitted coordinates method," *Proceedings of the 4th International Conference on Water Waves and Floating Bodies, Norway (1989) 269-274*

21. Newman, J. N., "Marine hydrodynamics", *The MIT Press, Cambridge, 1977*

22. Yeung, R. W., "A hybrid integral equation method for time harmonic free surface flows", *Proceedings of the 1st International Conference of Numerical Ship Hydrodynamics, Gaithersburg, Md. (1975) 581-608*

23. Longuet-Higgins M. S., Cokelet, E. D., "The deformation of steep waves on water: I. A numerical method of computation", *Proceedings of Royal Society, London A 350 (1976) 1-26*

24. Dommermuth, D. G., Yue, D. K. P., "Numerical simulations of nonlinear axisymmetric flows with a free surface", *Journal of Fluid Mechanics 178 (1987) 195-219*

25. Grosenbaugh, M. A., Yeung, R. W., "Nonlinear bow flows – An experimental and theoretical investigation", *Proceedings of the 17th symposium on Naval Hydrodynamics, The Hague, Netherland (1988) 195-214*

26. Timoshenko, S., Woinowsky-Krieger, S., "Theory of Plates and Shells," *McGraw-Hill Book Company , Inc. New York (1959)*

27. Ventsal, E., Krauthammer, T., "Thin Plates and Shells: theory, analysis, and applications," *Marcel Dekker, Inc. New York (2001)*

28. Vladimir, S., "Dynamics of elastic systems," *PhD Dissertation, New York University, New York (1998)*

29. Vladimir, S., "Dynamics of elastic systems," *PhD Dissertation, New York University, New York (1998)*

30. Hirt, C., Nichols, B., "Volume of fluid (VOF) method for the dynamics of free boundaries," *Journal of Computational Physics 39 (1981) 201*

31. Deardorff, J. W., "Convective velocity and temperature scales for the unstable planetary boundary layer and Rayleigh convection," *J. Atmos. Sci. 27 (1972) 1211-1213.*

32. Colagrossi, A., Landrini, M., Tulin, M. P., "Near shore bore propagation and splashing processes: gridless simulations," *Proceedings of 6th International Workshop on Wave Hind-casting and Forecasting, Monterey (2000)*

33. Ananthakrishnan, P., "Surface waves generated by a translating two-dimensional body: Effects of viscosity," *PhD Thesis, Department of Naval Architecture and Offshore Engineering, University of California at Berkeley (1991)*

34. Ananthakrishnan, P., "Heave oscillations of a submerged vertical cylinder in a viscous fluid," *International Journal of Offshore and Polar Engineering 8(3) (1998) 173-181*

35. Ananthakrishnan, P., "Radiation hydrodynamics of a floating vertical cylinder in a viscous fluid," *Journal of Engineering Mechanics 125(7) (1999) 836-847*

36. Nichols, B. D., Hirt, C. W., R. S. Hotchkiss, "SOLA-VOF: A solution algorithm for transient fluid flow with multiple free boundaries," *Los Alamos National Lab Resport LA (1980)*

37. Hirt, C. W., Nichols, B. D., "Volume of fluid (VOF) method for the dynamics of free boundaries," *Journal of Computational Physics 39 1 (1981) 201-225*

38. Puaut, C., "Hydrodynamic analysis of an underwater body including free surface effects," *PhD dissertation, Florida Atlantic University (2001)*

39. Saout, O., "Computation of hydrodynamic coefficients and determination of dynamic stability characteristics of an underwater vehicle including free surface effect," *PhD dissertation, Florida Atlantic University (2003)*

40. Vinayan, V., "Boundary integral analysis of nonlinear diffraction forces on a submerged body," *PhD dissertation, Florida Atlantic University (2003)*

41. Koo, W., Kim, M. H., "fully nonlinear wave-body interactions with fully submerged dual cylinders", *Proceedings of the thirteenth (2003) International offshore and polar engineering conference, Honolulu, hawaii*

42. Koo, W., Kim, M. H., "Freely floating-body simulation by a 2D fully nonlinear numerical wave tank", *Ocean Engineering 31(2004) 2011-2046*

43. Koo, W., Kim, M. H., "Fully nonlinear wave-body interactions with surface-piercing bodies", *Ocean Engineering 34(2007) 1000-1012*

44. Tarafdar, S., Suzuki, K., "Computation of wave-making resistance of a catamaran in deep water using a potential based panel method", *Ocean Engineering 34 (2007) 1892-1900*

45. Tarafdar, S., Suzuki, K., "Numerical calculation of free-surface potential flow around a ship using the modified Rankine source panel method", *Ocean Engineering 35 (2008) 536-544*

46. McIver, P., Evans, D. V., "Approximation of wave forces on cylinder arrays," *Applied Ocean Research 6(2) (1984) 101-107*

47. Linton, C. M., Evans, D. V., "The interaction of waves with arrays of vertical circular cylinders," *Journal of Fluid Mechanics 215 (1990) 549-569*

48. Spring, B. H., Monkmeyer, P. L., "Interaction of plane waves with vertical cylinders," *Proceedings of 14th Conference on Coastal Engineering, ASCE (1974) 1828-1847*

49. Evans, D. V., Porter, R., "Near-trapping waves by circular arrays of vertical cylinders," *Applied Ocean Research 19 (1997) 83-99*

50. Maniar, H. D., Newman, J. N., "Wave diffraction by a long array of cylinders," *Journal of Fluid Mechanics 339 (1997) 309-330*

51. Newman, J. N., "Wave effects of multiple bodies," *Hydrodynamics in Ship and Ocean Engineering, RIAM, Kyushu University (2001) 3-26*

52. McIver, P., McIver, M., "Trapped modes in the water-wave problem for a freely floating structure," *Journal of Fluid Mechanics 558 (2006) 53-67*

53. McIver, P., McIver, M., Zheng, J., "Excitation of trapped water waves by the forced motion of structures," *Journal of Fluid Mechanics 494 (2003) 141-162*

54. Ananthakrishnan, P., Chaffin, J., "Inviscid and viscous flow analysis of multihull ships under forced oscillations in a free surface," *Proceedings of the VIII International Conference on Hydrodynamics, Nantes, France (October 2008)*

55. Ananthakrishnan, P., "Effects of viscosity and free surface nonlinearity on the wave motion generated by an oscillating twin hull," *submitted for the 31st Intl. Conf. on Ocean, Offshore and Arctic Engineering, Brazil (2012)*

56. Flatinsen, O. M., "Hydrodynamics of high speed marine vehicles," *Cambridge University Press, New York (2005)*

57. Sun, H., Faltinsen, O. M., " Water Impact of horizontal circular cylinders and cylindrical shells", Applied Ocean Research 28 (2006) 299-311

58. Wu, G. X., Sun, H., He, Y. S., "Numerical simulation and experimental study of water entry of a wedge in free fall motion", Journal of Fluids and Structures 19 (2004 277-289

59. Wu, G. X., "Numerical Simulation of water entry of twin edges", *Journal of Fluids and Structures 22 (2006) 99-108*

60. Xu, G. D., Duan, W. Y., Wu, G. X., "Numerical simulation of ablique water enrty of an asymmetrical wedge", *Ocean Engineering 35 (2008) 1597-1603*

61. Wu, G. X., Xu, G. D., Duan, W. Y., "A summary of water entry problem of a wedge based on the fully nonlinear velocity potential theory", *journal of Hydrodynamics (2010) 22(5) 859-864*

62. Massey, B.S., "Mechanics of Fluids-2nd Edition," *Van Nostrand Reinhold Co. London (1970)*

63. A. A. Korobkin, A. Iafrati, "Hydrodynamic loads during initial stage of floating body impact", *Journal of Fluids and Structures 21 (2005) 413-427*

64. A. Korobkin, R. Gueret, S. Malencia,"Hydroelastic coupling of beam finite element model with Wagner theory of water impact", *Journal of Fluids and Structures 22 (2006) 493-504*

65. ABS, "Guide for building and classing – High Speed Craft," *American Bureau of Shipping, New York (2001)*

66. Gorman, D. J, "Vibration analysis of plates by the superposition method," *World Scientific Publishing Co. Pte. Ltd, Singapore (1999)*

67. Gorman, D. J., "Free Vibration analysis of Completely Free Rectangular Plates by the Superposition-Gamerkin Method", *Journal of Sound and Vibration (2000) 237(5) 901-914*

68. Gorman, D. J., "Free in-plane vibration analysis of rectangular plates by the method of superposition", *Journal of Sound and Vibration 272 (2004) 831-851*

69. Yu, S. D., "Free and forced flexural vibration analysis of cantilever paltes with attached point mass" *Journal of Sound and Vibration 321 (2009) 270-285*

70. Andrianov, A. I., Hermans, A. J., "Hydroelasticity of a circular plate on water of finite and infinite depth", *Journal of Fluids and Structures 20 (2005) 719-733*

71. Andrianov, A. I., Hermans, A. J., "Hydroelastic Analysis of a plate of finite draft", *Applied Ocean Research 28 (2006) 313-325*

72. Senjanovic, I., Catipovic, I., Tomasevic, S., "Coupled horizontal and torsional vibrations of a flexible barge", *Engineering Structures 30 (2008) 93-109*

73. Senjanovic, I., Catipovic, I., Tomasevic, S., "Coupled flexural and torsional vibrations of ship-like girders", *Thin-Walled Structures 45 (2007) 1002-1021*

74. Senjanovic, I., Malenica, S., Tomasevic, S., "Investigation of ship hydroelasticity", *Ocean Engineering 35 (2008) 523-535*

75. Senjanovic, I., Malenica, S., Tomasevic, S., "Hydroelasticity of large container ships", *Marine Structures 22 (2009) 287-314*

76. Beskos, D. E., "Boundary element methods in mechanics", *Amsterdam Elsevier Science Publisher (1987)*

77. Lu, C. H., He, Y. S., Wu, G. X., "Coupled analysis of nonlinear interaction between fluid and structure during impact," *Journal of Fluids and Structures 14 (2000) 127-146*

78. Korobkin, A., Gueret, R., Malenica, S., "Hydroelastic coupling of beam finite element model with wagner theory of water impact," *Journal of Fluids and Structures 22 (2006) 493-504*

79. Maki, K. J., Lee, D., Troesch, A. W., Vlahopoulos, N., "Hydroelastic impact of a wedge-shaped body", *Ocean Engineering 38 (2011) 621-629*

80. Luo, H., Wang, H., Soares, C. G., "Numerical and experimental study of hydrodynamic impact and elastic response of one free-drop wedge with stiffened panles," *Ocean Engineering 40 (2012) 1-14*

81. Graff, K. F., "Wave motion in elastic solids," *Oxford University Press, New York, (1991)*

82. Kling, K. A., "Dynamic analysis of single and multi module platforms in waves," *Masters Thesis, Florida Atlantic University (2006)*

83. Mei, C. C., "Mathematical analysis in engineering," *Cambridge University Press (1997)*

84. Lewis, E. V., " Principles of naval architecture: second revision," *The Society of Naval Architects and Marine Engineers, NJ (1988)*

85. Kihara, H., "Numerical Modeling of flow in water entry of a wedge," *Proc. 19th International Workshop on Water Waves and Floating Bodies, Cortona, Italy March 28-31 (2004)*

86. Wu, J. H., Liu, A. Q., Chen, H. L., "Exact solutions for free-vibration analysis of rectangular plates using Bessel functions," *Journal of Applied Mechanics 74 (2007) 1247-1251*

87. Peseux, B., L. Gornet, Donguy, B., "Hydrodynamic impact: Numerical and experimental investigations," *Journal of Fluids and Structures 21 (2005) 277-303*

88. Zhao, R., Faltinsen, O. M., "Water entry of two-dimensional bodies," *Journal of Fluid Mechanics 246 (1993) 593-612*

89. Xin, T., Wong, H., "A Spike-function model of facets," *Materials Science and Engineering A364 (2004) 287-295*

90. Lin, W. M., Zhang, S., Weems, K., Jones, P., Meinhold, M., "Numerical simulation and validation study of wetdeck slamming on high speed catamaran," *9th International Conference on Numerical Ship Hydrodynamics, Ann Arbor, Michigan (2007) unclassified report*

91. Mei, C. C., Stiassnie, M., Yue, D. K. P., "Theory and applications of ocean surface waves: nonlinear aspects," *World Scientific Publishing Co. (2005)*

92. Ma, S., "Fluid structure interaction study of a multi-hull ship with composite sandwich structures,'' *PhD Dissertation, Florida Atlantic University (2012)*